Information Guidelines Explanatory Note

Subsidence associated with coal seam gas production

This document should be attributed as 'Leonardi C 2024. *Information Guidelines Explanatory Note: Subsidence associated with coal seam gas production*. Report prepared for the Independent Expert Scientific Committee on Unconventional Gas Development and Large Coal Mining Development through the Department of Climate Change, Energy, the Environment and Water, Commonwealth of Australia, 2024'.

On 15 December 2023, the *Nature Repair (Consequential Amendments) Act 2023* amended the EPBC Act to expand the IESC's remit to all unconventional gas developments. This publication was developed prior to these amendments of the EPBC Act commencing.

This publication is funded by the Australian Government Department of Climate Change, Energy, the Environment and Water. The views and opinions expressed in this publication are those of the authors and do not necessarily reflect those of the Australian Government or the Minister for the Environment and Water.

Acknowledgements

This document was finalised by the Independent Expert Scientific Committee on Unconventional Gas Development and Large Coal Mining Development (IESC) based on consideration of work commissioned by the Office of Water Science on behalf of the IESC in January 2022 through the Department of Climate Change, Energy, the Environment and Water, formerly known as the Department of Agriculture, Water and the Environment.

The main contributor to this work was Christopher Leonardi, who is substantively employed as an Associate Professor in the School of Mechanical and Mining Engineering at the University of Queensland (UQ). A/Prof Leonardi conducts research on various aspects of coal seam gas production, including subsidence, in collaboration with the UQ Centre for Natural Gas and its proponents (Santos Ltd, Arrow Energy Pty Ltd, Australia Pacific LNG Pty Ltd) and in accordance with the Australian Code for the Responsible Conduct of Research. The contributions of the following (in alphabetical order) are gratefully acknowledged: Sarah Brennand, Katarina David, Phil Hayes (IESC), Sebastian Hörning, Mohsen Masoudian, Travis Mitchell, Iain Rodger, Vanessa Salomao de Santiago, Wendy Timms (IESC), Jim Underschultz, Mohammadreza Zare Reisabadi, and Fengde Zhou. These contributions stem from past or ongoing research collaborations or employment at UQ.

This document was subject to independent peer review by Dr Peter Fokker from the Netherlands Organisation for Applied Scientific Research (TNO) and Emeritus Professor Joan Esterle (UQ). It was also revised after public stakeholder consultation.

Contact details

For information about this report or about the work of the IESC, please contact:

IESC Secretariat

Office of Water Science
Department of Climate Change, Energy, the Environment and Water
GPO Box 787
CANBERRA ACT 2601

The publication can be accessed at http://www.iesc.gov.au

Images

Front cover: McIntyre River | Location: Condamine catchment area | © Department of Climate Change, Energy, the Environment and Water (taken by staff)

All other images © Department of Climate Change, Energy, the Environment and Water unless specified otherwise.

Information Guidelines Explanatory Note

Subsidence associated with coal seam gas production

Overview

The role of the IESC

The Independent Expert Scientific Committee on Unconventional Gas Development and Large Coal Mining Development (IESC) is a statutory body under the *Environment Protection and Biodiversity Conservation Act 1999* (Cth) (EPBC Act). The IESC's key legislative functions are to:

- provide scientific advice to the Commonwealth Environment Minister and relevant state ministers on unconventional gas and large coal mining (LCM) development proposals that are likely to have a significant impact on water resources
- provide scientific advice to the Commonwealth Environment Minister on bioregional assessments (Commonwealth of Australia (CoA) 2018) of areas of coal seam gas (CSG) and LCM development
- provide scientific advice to the Commonwealth Environment Minister on research priorities and projects
- collect, analyse, interpret and publish scientific information about the impacts of unconventional gas and LCM activities on water resources
- publish information relating to the development of standards for protecting water resources from the impacts of CSG and LCM development
- provide scientific advice on other matters in response to a request from the Commonwealth or relevant state ministers.

On 15 December 2023, the *Nature Repair (Consequential Amendments) Act 2023* amended the EPBC Act to expand the IESC's remit to all unconventional gas developments. This publication was developed prior to these amendments of the EPBC Act commencing.

Further information on the IESC's role is on the IESC website.

The purpose of the Explanatory Notes

One of the IESC's key legislative functions is to provide scientific advice to the Commonwealth Environment Minister and relevant state ministers in relation to unconventional gas and LCM development proposals that are likely to have a significant impact on water resources.

The IESC outlines its specific information requirements in the IESC *Information Guidelines for proponents preparing coal seam gas and large coal mining development proposals* (IESC 2024) (the Information Guidelines). This information is requested to enable the IESC to formulate robust scientific advice for regulators on the potential water-related impacts of CSG and LCM developments.

For some topics, Explanatory Notes (ENs) have been written to supplement the IESC Information Guidelines, giving more detailed guidance to help the CSG and LCM industries prepare environmental impact assessments. These topics are chosen based on the IESC's experience of providing advice on over 150 development proposals.

ENs are intended to assist proponents in preparing environmental impact assessments. They provide tailored guidance and describe up-to-date, robust scientific methodologies and tools for specific components of environmental impact assessments of CSG and LCM developments. Case studies and practical examples of how to

present certain information are also discussed. ENs provide guidance rather than mandatory requirements. Proponents are encouraged to refer to issues of relevance to their particular project.

The aim of this EN is to present tailored guidance and robust scientific methodologies and tools for assessing the potential for and subsequent monitoring of subsidence associated with CSG production, and the EN is designed to be utilised across a range of regulatory regimes. Proponents are also encouraged to refer to specialised literature and engage with their relevant state regulators.

The IESC recognises that approaches, methods, tools and software will continue to develop. The Information Guidelines and ENs will be reviewed and updated as necessary to reflect these advances.

Legislative context

The EPBC Act states that water resources in relation to unconventional gas and LCM developments are a matter of national environmental significance.

A water resource is defined by the *Water Act 2007* (Cth) as:

> (a) surface water or ground water; or
>
> (b) a water course, lake, wetland or aquifer (whether or not it currently has water in it);
>
> and includes all aspects of the water resource (including water, organisms and other components and ecosystems that contribute to the physical state and environmental value of the resource).

Australian and state regulators who are signatories to the National Partnership Agreement seek the IESC's advice under the EPBC Act at appropriate stages of the approvals process for a unconventional gas or LCM development that is likely to have a significant impact on water resources. The regulator determines what is considered to be a significant impact based on the Significant Impact Guidelines 1.3 (CoA 2022).

Executive summary

Coal seam gas (CSG) production is currently taking place in Queensland and New South Wales, Australia, and it is possible that CSG production will occur in Australia for the next half a century. For both current and future production, the potential impacts of subsidence on adjacent industries, particularly agriculture, must be managed. This Explanatory Note outlines the analysis and monitoring tools that can be used to manage ongoing CSG activities and assess new projects in the context of subsidence.

Since publication of the last IESC report on CSG-induced subsidence in 2014, a number of independent sources have confirmed that CSG production does induce subsidence, but the magnitudes of surface elevation and slope change are relatively low. Satellite-borne interferometric synthetic aperture radar (InSAR) measurements indicate that most CSG-producing areas in the Surat and Bowen basins, and the smaller Camden Gas Project in New South Wales, have subsided less than 100 mm. In some areas the CSG-induced subsidence is of a similar order of magnitude as natural fluctuations, such as the shrinking and swelling of expansive clays, and so any impact of CSG operations needs to be considered in this context. Given that the magnitude of CSG-induced subsidence and differential settlement are both small and similar to natural fluctuations, the risk of impacts on infrastructure is low. Greatest attention must be given to locations that are sensitive to small changes in slope, such as flood-irrigated paddocks. However, there currently exists no evidence that CSG-induced subsidence has, or has the potential to, significantly alter surface drainage behaviour.

CSG-induced subsidence is driven by poromechanical compaction of coal and non-coal (i.e., rock) sedimentary layers in the subsurface, as well as desorption-induced shrinkage of the coal. Both mechanisms should be accounted for in future forecasts, noting that the degree to which shrinkage occurs in situ is an area of ongoing research. The quality of subsidence predictions is, consequently, dependent on the quality of predictions of water-gas transport and subsurface depressurisation. This is complicated by the stratigraphic complexity of, for example, the Walloon Coal Measures in the Surat Basin, where dozens of thin and laterally discontinuous coal seams are interleaved with layers of clastic rocks that can be significantly less permeable than the coal. Well-justified assumptions must be used to simplify such complex stratigraphy in analysis. Analytical and numerical approaches both have their place in the prediction of CSG-induced subsidence. The former can capture much broader length and time scales, while the latter can better accommodate stratigraphic heterogeneity and geological features, such as faults, and include more detailed material properties, leaving them well suited to hypothesis testing and benchmarking of analytical solutions.

InSAR has been demonstrated to be effective at monitoring basin-scale surface movement, of which CSG-induced subsidence is one part of the total signal. InSAR is not (yet) effective in areas prone to decorrelation (e.g., over areas of intensive cropping), where it is currently needed most. The deployment of light detection and ranging (LiDAR) or other levelling methods is recommended to complement InSAR in these areas, as they (LiDAR in particular) are well suited to capturing relative, as opposed to absolute, movement, which can be used to accurately determine changes in surface gradient.

The integrated use of monitoring and modelling for subsidence analysis and forecasting continues to advance around the world. The opportunity therefore exists to adopt some of these techniques for application related to CSG production. These include stochastic analysis, uncertainty quantification, inverse modelling, history matching, and geospatial data analysis. Finally, it should be recognised that there is uncertainty surrounding many of the drivers (e.g., stratigraphy, transport properties, mechanical properties) of CSG-induced subsidence. Some of this uncertainty is irreducible. In the past, uncertainty has been addressed by making conservative assumptions during the process of predicting potential future subsidence. This is not in the best interest of most, if not all, stakeholders, and so it is important that continued research and development (see Section 9) is leveraged to narrow the various windows of uncertainty.

Contents

1. Introduction

The production of coal seam gas (CSG) requires the extraction of associated water from the target formation to liberate methane that is adsorbed to the coal. Depressurisation of the subsurface leads to the compaction of geological units, a proportion of which can propagate to the surface, resulting in subsidence. An understanding of the magnitude and any risks of impacts associated with subsidence is of value to stakeholders including landholders, operators, local communities, and government regulators.

The Office of Water Science provides assistance to the Independent Expert Scientific Committee on Unconventional Gas Development and Large Coal Mining Development (IESC) in developing the IESC Information Guidelines. The guidelines outline to proponents and consultants the information requirements considered necessary to enable the IESC to provide robust scientific advice to government regulators on the water-related impacts of CSG and large coal mining development proposals. The IESC committed to the production of Explanatory Notes (ENs), which give more detailed background information on selected aspects of the guidelines. This EN addresses subsidence related to CSG production, while a companion document (Hebblewhite 2023) addresses underground coal mining.

The aim of this EN is to present tailored guidance and robust scientific methodologies and tools for assessing the potential for and subsequent monitoring of subsidence associated with CSG production. It has been prepared for a target audience of technical professionals commissioned to prepare environmental impact statements. Topics covered include:

- the production of CSG and the physical processes associated with compaction and subsidence
- national and international perspectives on subsidence, including the potential impacts of subsidence
- the prediction of subsidence, including parameter and model selection and the interpretation of results
- techniques for large-scale monitoring of subsidence in near real time
- Australian experience in the estimation and monitoring of subsidence related to CSG production.

At the time of writing (2023), complementary work on the potential for subsidence-induced impacts on farmland was being undertaken by the GasFields Commission Queensland (GasFields Commission Queensland 2023) and the Queensland Government's Office of Groundwater Impact Assessment (OGIA). Consequently, this EN does not cover topics related to:

- drainage rates of irrigated cropping land as a function of surface gradient
- impacts on crop productivity as a consequence of changes in drainage behaviour
- overland flow regimes and the dependence of dryland farming on them
- impacts on biodiversity and groundwater-dependent ecosystems
- the requirements for and preparation of environmental impact statements associated with CSG projects.

The production of CSG in Australia accelerated with the commencement of liquefied natural gas (LNG) export in 2014. There are no other comparable projects internationally that extract CSG at the same scale. In comparison to conventional oil and gas production, the Australian CSG industry is young and thus the scientific literature and technical documentation focused on CSG-induced subsidence is limited. However, the volume of monitoring data

(acquired from satellite and aircraft) continues to grow in terms of frequency and spatial extent. In addition to these data, this EN has been prepared using information available in the public domain, including journal articles, conference proceedings, scientific textbooks, government department reports, and industry and consulting reports.

The structure of this EN is, in summary, as follows:

- Section 2 provides background information on the production of CSG, including how a well is constructed, the physical processes relevant to CSG production, and the driving mechanisms of CSG-induced subsidence.
- Section 3 briefly discusses international and domestic examples of anthropogenic subsidence, with a focus on oil and gas production.
- Section 4 then presents information on sources and impacts of subsidence, with a focus on those most relevant to areas of CSG production in Australia.
- Section 5 presents subsidence monitoring techniques such as interferometric synthetic aperture radar (InSAR), along with examples of their use.
- Section 6 outlines approaches to subsidence assessment, including simple consolidation modelling and poromechanical analysis.
- Section 7 provides guidance on selection of relevant modelling parameters.
- Section 8 presents past analyses and a subsidence case study.
- Section 9 concludes the EN with a discussion of ongoing monitoring and assessment activity and future research requirements.

2. Mechanics of coal seam gas production

Coal seam gas (CSG), more commonly referred to as coalbed methane (CBM) outside of Australia, is natural gas extracted from coal seams. It is composed primarily of methane (CH4) and can be utilised for electricity generation, for industrial and residential heating, and as feedstock in manufacturing (e.g., fertiliser). It is the same as other *conventional* sources of gas and can be distributed similarly, either in gaseous form or after cooling to liquefied natural gas (LNG).

Commercial production of CSG commenced in Australia in the 1990s. To the end of 2019, approximately 8 trillion cubic feet (tcf) of CSG had been extracted, with a further 30 tcf of reserves and 24 tcf of resources (Geoscience Australia 2021) in place throughout Queensland and New South Wales. In 2014 the export of CSG as liquefied natural gas (LNG) commenced at Curtis Island in Queensland, resulting in a rapid increase in the number of wells drilled and the annual rate of production. In combination with gas production from conventional reservoirs, the CSG-LNG industry has positioned Australia as one of the two largest LNG exporters in the world.

2.1 What is coal seam gas?

The exploitation of *conventional* oil and gas reserves typically involves the extraction of liquid and/or gaseous hydrocarbons from porous, permeable formations remote from the original source rock. The classical example of this is an anticlinal trap, in which a sandstone reservoir holds hydrocarbons that have migrated from deeper source rocks due to buoyancy and been trapped by an impermeable caprock above. The production of CSG is classified as *unconventional* because the target hydrocarbons exist within and are extracted directly from the source coal seams. Additionally, the target formations may exhibit low permeability, requiring artificial stimulation (e.g., hydraulic fracturing) to promote economic rates of production. The (usually) lower permeability of unconventional reservoirs may also manifest in greater well densities and associated surface infrastructure than in conventional operations.

The methane in coal is generated via biogenic or thermogenic processes, or a combination of the two. Biogenic methane is a result of the breakdown of organic coal matter by methanogenic micro-organisms at moderate to low temperature (i.e., less than 56°C) and, therefore, depth. Conversely, thermogenic methane is generated at greater depth, where temperatures exceed 100°C, due to chemical degradation and thermal cracking of coal (Moore 2012). The elevated temperature at greater depth also means that methanogenic activity of microbes is improbable at those locations. Consequently, biogenic methane is more likely to be found in lower-rank coals, while thermogenic methane is more likely in mid- to high-rank coals subject to greater burial depth and temperature, as shown schematically in Figure 1(a). Assuming the methane does not escape, this also means that methane content increases for a given depth and coal grade (Aminian 2020), as seen in Figure 1(b). Noting that other hydrocarbons will exist, the proportion of methane in CSG relative to those gases is referred to as *gas quality*.

CSG manifests in three different states: free gas within coal pores and cleats, molecules adsorbed to coal surfaces, or adsorbed within the molecular structure of the coal (Moore 2012). The majority (between 90% and 98% of all gas), however, is adsorbed to the coal surface within macropores, mesopores and micropores, representing the greatest proportion of gas that is extracted during CSG production. Due to the hydrostatic pressure of pore water (or associated water), this adsorbed gas exists in a state of compression. The relationship between gas storage capacity and pressure is described by a sorption isotherm, represented by the data series in Figure 1(b) for coals of different maturity. In addition to the rank and pressure, these isotherms depend on the temperature, moisture content and mineral matter content of the coal.

Coal seams are typically interbedded between low-permeability geological units (e.g., siltstone) and are of varying thickness relative to overlying and underlying strata. Seams may exhibit thicknesses of multiple metres with good lateral continuity or, conversely, with thickness in the order of centimetres which pinch out (i.e., terminate) or bifurcate laterally, as shown schematically in Figure 2. In a macroscopic sense, coal seams usually possess cleats, which are discontinuities formed during coalification (i.e., desiccation), and may also possess natural fractures, which are formed by tectonic deformation. The cleats usually occur in two sets, called *face cleats* and *butt cleats*, that are perpendicular to one another and perpendicular to bedding. The face cleats form in one direction first and exhibit a high level of continuity. The butt cleats form in the other direction, are discontinuous and are frequently truncated by face cleats. The permeability of a coal seam is dominated by the cleat network (Laubach et al. 1998) and, in the Australian context, the natural fractures. The greater continuity of face cleats typically results in greater permeability than in butt cleats. However, both provide enhanced permeability with respect to that of the intact coal matrix.

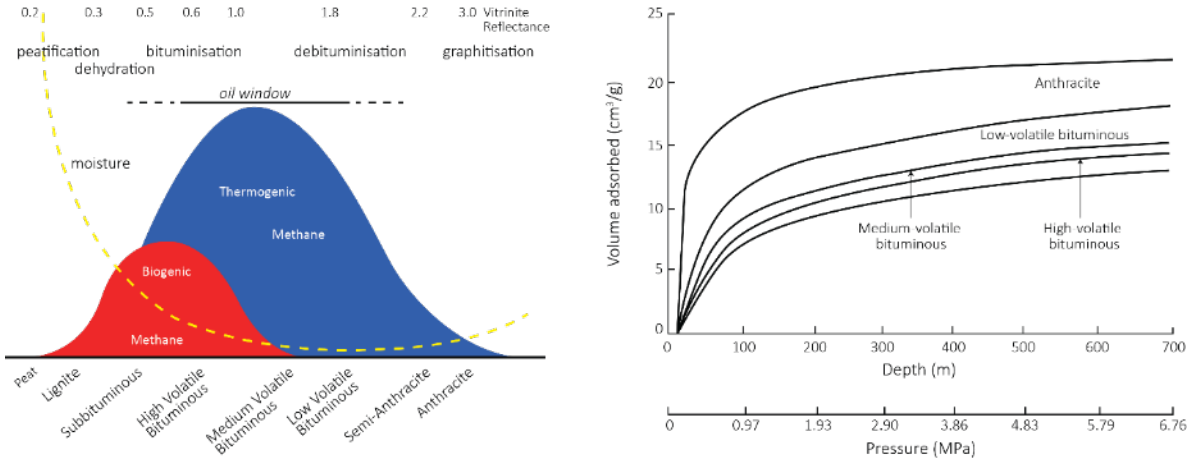

Figure 1. Relationship between coal rank/depth and gas type/content, showing (a) biogenic and thermogenic methane generation as a function of rank (reproduced from Moore 2012), and (b) gas content as a function of depth (reproduced from Aminian 2020)

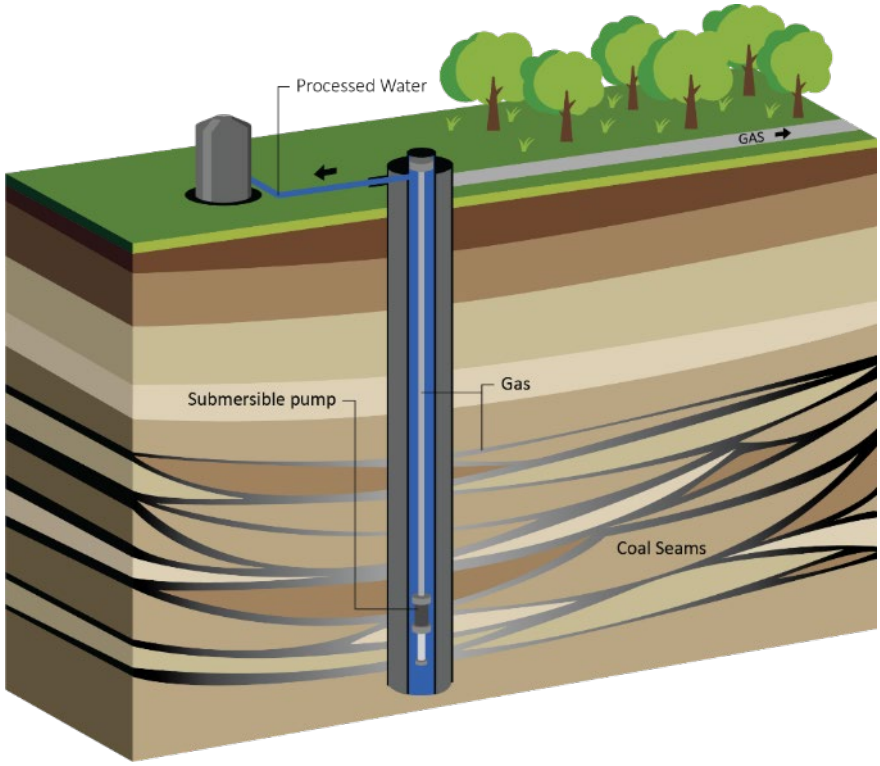

Figure 2. Schematic representation of CSG production, highlighting the existence of several adjacent seams that are initially saturated with water, as well as being potentially discontinuous and interleaved with other sedimentary layers

CSG production is typically undertaken in mid-rank coals (i.e., low- to high-volatile bituminous coals). This is because the desorption and diffusive transport of methane from high-rank coals such as anthracite is very slow (Levine 1993; Rice 1993) and the residual gas content is low. The liberation of adsorbed methane is driven by the reduction of pore pressure, which in practice is achieved by the reduction of pressure head by pumping associated water from the coal seam. This is central to the issues of compaction and subsidence and is discussed in more detail in Section 2.3.

More detailed discussion of the processes of deposition, coalification, and the genesis of methane, can be found in the comprehensive text edited by Thakur (2020) or the more concise review by Moore (2012).

2.2 Coal seam gas production in Australia

Onshore gas was first discovered and produced in Australia by accident during the drilling of a water bore outside Roma, Queensland, in 1900 (Roberts 1992). Numerous other instances of nuisance or unexpected gas discovery during the drilling of water wells and mineral exploration holes have been documented (Walker and Mallants 2014). However, it was not until the 1960s that conventional gas accumulations were commercially exploited.

Dedicated exploration for CSG as a target resource commenced in Australia in the 1970s. In the 1980s, methane was first extracted directly from Australian coal during the drainage of seams prior to underground longwall mining (Black and Aziz 2009). This was, and still is, necessary to reduce the risk of explosion during mining operations. Historically, the produced gas was typically flared off, but it is now captured and utilised on site. By 1990, approximately 30 CSG-specific wells had been drilled in the Bowen Basin. Approximately 160 wells had been drilled by 1995, mostly in the Bowen Basin. In 1996, commercial production commenced from the Baralaba Coal Measures at Dawson River, near Moura, to service the domestic market in south-east Queensland (Towler et al. 2016).

Commercial CSG production from lower-rank, sub-bituminous Walloon coal seams in the Surat Basin began in 2006 via the Tipton West, Kogan and Berwyndale fields located in the areas west of and between Dalby and Chinchilla. In 2007, CSG production exceeded conventional gas production in Queensland, and by 30 June 2008 certified reserves in the Surat Basin had surpassed those in the Bowen Basin. In 2011 the Surat Basin overtook the Bowen Basin as the chief producer of natural gas in general but of CSG in particular (Geological Survey of Queensland 2012). The construction of three distinct compression facilities at Curtis Island, near Gladstone in Queensland, facilitated the production of LNG from CSG and connection to global markets. In preparation for the first shipment of LNG in 2014, the rate of CSG well drilling increased in 2012. In 2022 the total CSG well count in Queensland was approximately 10,000, and this is projected to increase to approximately 22,000 by 2035 (OGIA 2021).

Contemporary CSG production in Australia is still dominated by plays in the Surat and Bowen basins in Queensland, whose locations are shown in Figure 3. In the Surat Basin, gas is primarily produced from thin, high-permeability coals in the Jurassic-age Walloon Coal Measures, while in the Bowen Basin production is sourced from several relatively thick Permian-age coal seams, of which the Baralaba Coal Measures and the Bandanna Formation are the most important (Towler et al. 2016). In New South Wales, exploration and approvals for the Narrabri gas project in the Gunnedah Basin (see Figure 4.) are, at the time of writing (2023), ongoing. Other past and proposed developments are located in the Sydney, Galilee, Clarence-Moreton, Gloucester, Otway, Gippsland and Cooper basins located across Queensland, New South Wales, Victoria and South Australia (Best et al. 2014).

The hydrogeological settings in CSG-producing basins typically comprise surficial alluvial aquifer systems (such as in sands or clays), underlain by consolidated sedimentary geological units (such as sandstone, siltstone and mudstone), with coal seams interbedded within the sedimentary units. The coal seams targeted for gas production are usually located at depths of 100 m or greater. Coal measures are the geological sedimentary units in which potentially multiple coal seams are interbedded within a sedimentary profile. As previously mentioned, the coal seam thickness can vary widely, along with their lateral continuity. For example, the Gloucester Coal Measures in the Gloucester Basin contain a number of relatively thick and continuous seams (as do the Baralaba Coal Measures of the Bowen Basin), while the Walloon Coal Measures of the Surat Basin comprise many discontinuous and relatively thin seams (Best et al. 2014). As indicated across Figure 3. and Figure 4., the Permo-Triassic age Bowen Basin forms the northern part of the Bowen-Gunnedah-Sydney Basin System of eastern Australia. The stratigraphic sequencing of the Bowen and Surat basins is shown schematically in Figure 5., highlighting the relative locations of the Moolayember Formation, the Baralaba Coal Measures, the Moranbah Coal Measures, the Burunga Formation, the Bandanna Formation, the Flat Top to Buffel formation, and the Walloon Coal Measures.

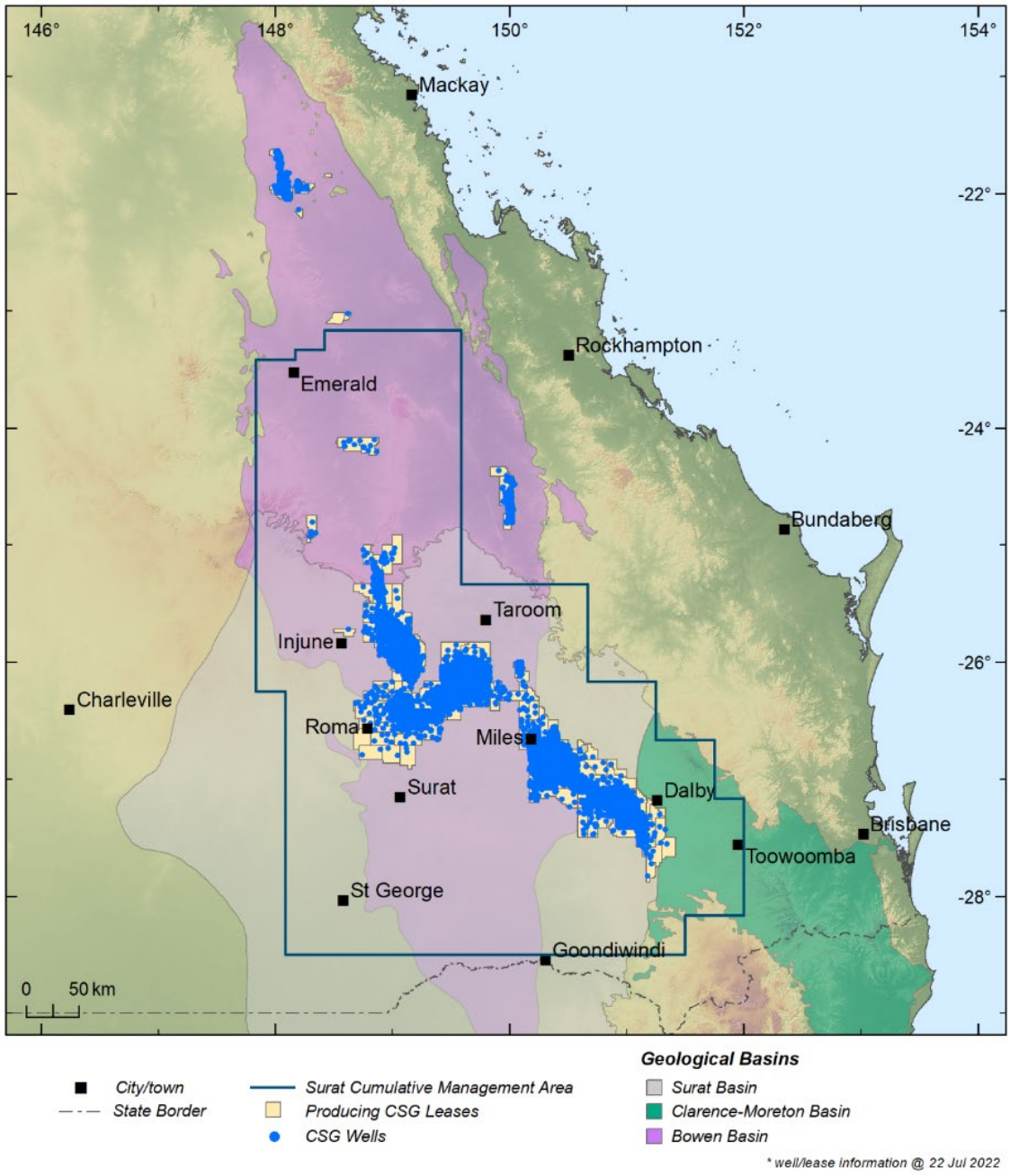

Figure 3. Map of the sedimentary basins, petroleum leases and wells relevant to the CSG industry in Queensland (outline of the Surat Cumulative Management Area included for reference)

The geological and petroleum-generating history of the Surat and Bowen basins is long and complex. These petroliferous basins contain multiple-source rock horizons, which include extensive coal deposits. Thermogenesis has generated both liquid and gaseous hydrocarbons that are stored in conventional and unconventional reservoirs. Extensive biogenic gas generation has also occurred (Al-Arouri et al. 1998; Golding et al. 2013; Hamilton et al. 2014), which continues today. Of Australia's 30 tcf of remaining proved and probable (2P) reserves (as at the end of 2019), 24 tcf is located in the Surat Basin and the balance is located in the Bowen Basin. Together, the Bowen and Surat basins hold 19 tcf of contingent resources (2C), with an additional 2.3 tcf in the Galilee Basin, 1.8 tcf in the Gunnedah Basin, and 0.6 tcf in the Clarence-Moreton Basin (Geoscience Australia 2021). Generally speaking, a resource is gas in place that cannot be commercially produced, while a reserve is gas in place that can be commercially produced.

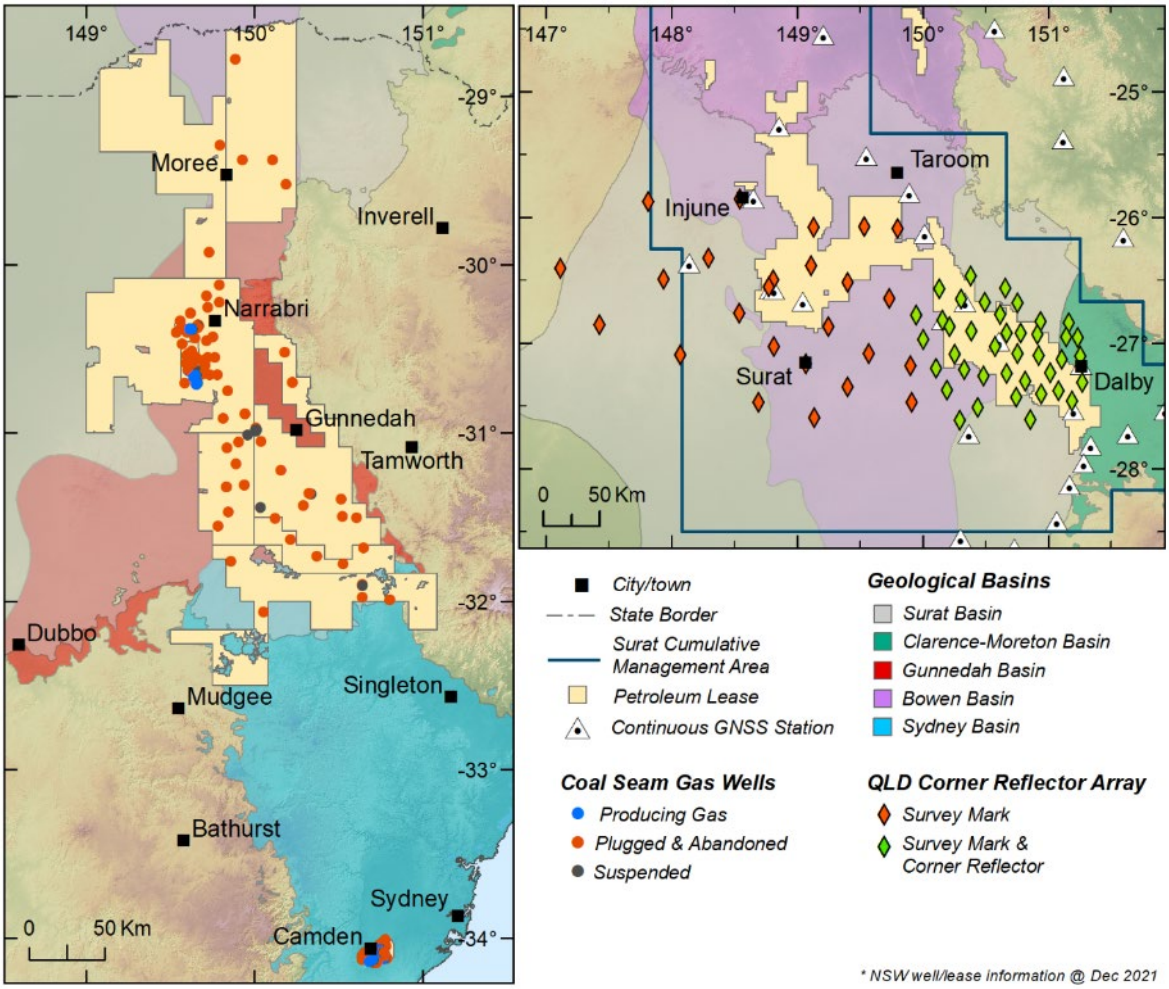

Figure 4. Map of (L) the sedimentary basins, petroleum leases and wells in New South Wales, and (R) the location of corner reflectors and permanent survey markers in southern Queensland (see Section 5.4)

The CSG activities of different operators in Queensland, as delineated by petroleum leases, are often located directly adjacent to one another. Although these activities are located in areas of low population density, they are commonly co-located with or near other economic activity such as intensive cropping (e.g., flood-irrigated arable farming), low-density grazing of livestock, high-density feedlots, or coal mining. Environmental, social and governance (ESG) challenges can arise when this combines with the large areas over which CSG production occurs, as compared to more conventional oil and gas production. One prominent example of the ESG challenge is the effect of coal seam dewatering on agricultural and domestic water wells completed in the coal measures, particularly in water-stressed areas. Another example of ESG challenges is the perceived possibility of localised changes in ground surface gradient caused by subsidence. If gradient change exceeds a threshold magnitude, this has the potential to alter the surface run-off characteristics of natural waterways, drainage networks, and irrigated paddocks. The last is of direct relevance to this document.

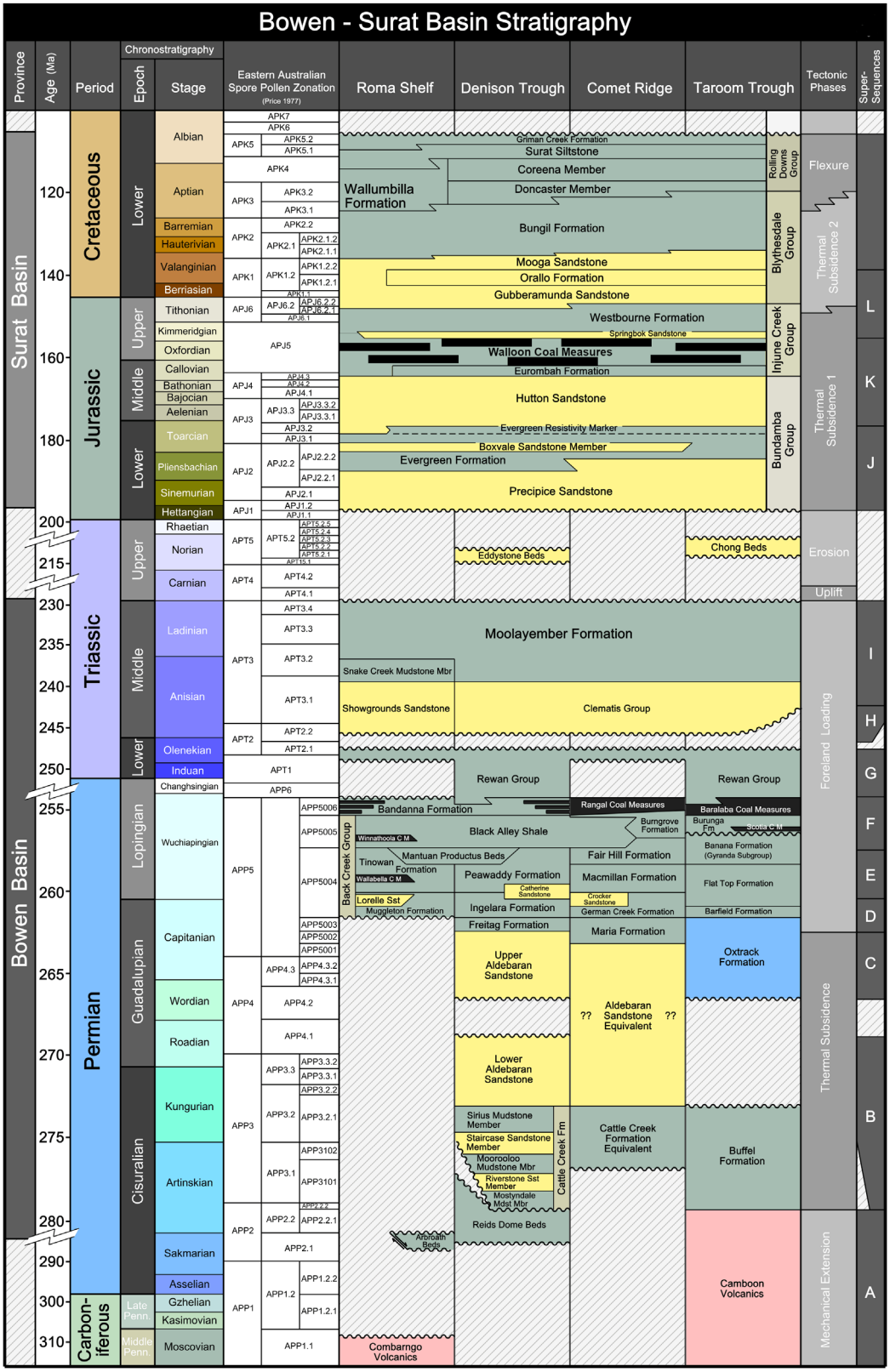

Figure 5. Stratigraphic diagram of the Bowen and Surat basins (original by Cook 2013, further modified by Santos and Origin Energy); formations of interest include the Walloon and Baralaba Coal Measures and the Bandanna Formation

2.3 Physical processes relevant to CSG production

As with conventional oil and gas production, the optimal choice of drilling, completion, stimulation and production techniques for CSG requires a comprehensive understanding of the subsurface, including geology, stratigraphy, geomechanics, and transport properties of the coal and adjacent rocks. However, the development and operation of a CSG field differs from that of conventional fields in a number of ways. Releasing adsorbed methane from the target coal requires pressure reductions which are induced by dewatering. Limits on the drainage area per well mean comparatively high well densities are required. CSG wells are typically shallower than shale or conventional wells, which reduces the engineering requirements of completion design, but the greater number of wells per unit area means field development must be optimised.

One challenge to CSG production is the degree of inherent heterogeneity of lithology, continuity, connectivity and stresses within and between coal seams, in addition to the variable interconnectivity between the coals and in the overlying and underlying aquifers and aquitards (Towler et al. 2016). Improved description of stratigraphy and structural geology in the CSG-producing basins in Queensland is an area of active and ongoing research (de Andrade Vieira Filh et al. 2021; Schultz et al. 2021; Sobczak et al. 2021).

2.3.1 Drilling and completion

Each CSG production tenement is composed of multiple wells, collectively known as a well *field*. The spacing of wells in a field is dictated by local conditions (e.g., permeability) and constraints. The average well density in Queensland is approximately 1.5 wells/km^2 (linear spacing of 800 m based on a square pattern). However, this varies in the Surat Basin from 1.2 to 1.7 wells/km^2 (900 to 750 m linear spacing), and in the Bowen Basin from 0.8 to 1.5 wells/km^2 (1,100 to 800 m linear spacing) (OGIA 2021). Deviations from these averages and their regular layout are common, however, after well locations have been negotiated with landholders.

A number of different CSG well trajectories have been installed or proposed in Queensland, including vertical, horizontal, multilateral, deviated, surface-to-inseam (SIS), and high-angle-sump-horizontal (HASH) (Lin et al. 2018). Verticals, which produce from a large number of distinct seams (see Figure 6.(a)), make up approximately 90% of wells drilled to date in the Bowen and Surat basins (OGIA 2021). Recently Arrow Energy has installed deviated wells in the Surat Basin as a means to reduce surface footprint while maintaining necessary contact with the reservoir (Rajora et al. 2019). A single *pad* can accommodate eight or more wells, which can in turn increase well head spacing to up to 2,400 m, reduce gathering network and land access requirements, and provide increased flexibility on pad location (e.g., paddock corners or boundaries). A larger number of well types are employed in the Bowen Basin, depending on coal permeability and depth. This includes vertical, horizontal, SIS, hydraulically fractured wells, and cavitation completions. According to Towler et al. (2016), historically the most common completion type in the higher-permeability fields of the Bowen Basin (e.g. Spring Gully, Fairview) was cavitation.

In addition to constraints related to land access, the trajectory of non-vertical wells is often a compromise between productivity and well stability. Drilling orthogonal to the dominant cleat or fracture set maximises effective permeability but can degrade wellbore stability, which is a function of effective stress magnitude and orientation, and the geomechanical properties of the reservoir. This is exacerbated when drilling in depleted reservoirs as part of, for example, an infill drilling campaign (Zare Reisabadi et al. 2020; Zhong et al. 2022).

A range of well completion strategies, which are designed to connect the coal seam(s) to the well but isolate them from the rest of the subsurface, have been deployed in Queensland. As shown in Figure 6.(a), a fully cemented casing is installed from the surface to the shallowest coal target to prevent migration of gas or brine to shallower aquifers or the surface. The integrity of the annular cement seal is pressure-tested after installation and can be inspected throughout the life of a well using, for example, a cement bond log (Jung and Frigaard 2022). Where a cavitation completion is employed, the target formations are drilled and then reamed to create a large cavity (i.e., increased surface area via a diameter of up to 3 m) and remove any formation damage that occurred during drilling. The well is

either left open or completed with an uncemented, slotted liner (Mastalerz and Drobniak 2020). It is also possible to case and cement the well throughout the reservoir and use perforations to make contact with the target coal seams. Similarly, wells that require hydraulic fracturing are cemented along their length and then perforated in stages, each of which serves as the initiation point for a hydraulic fracture in the target coal seam.

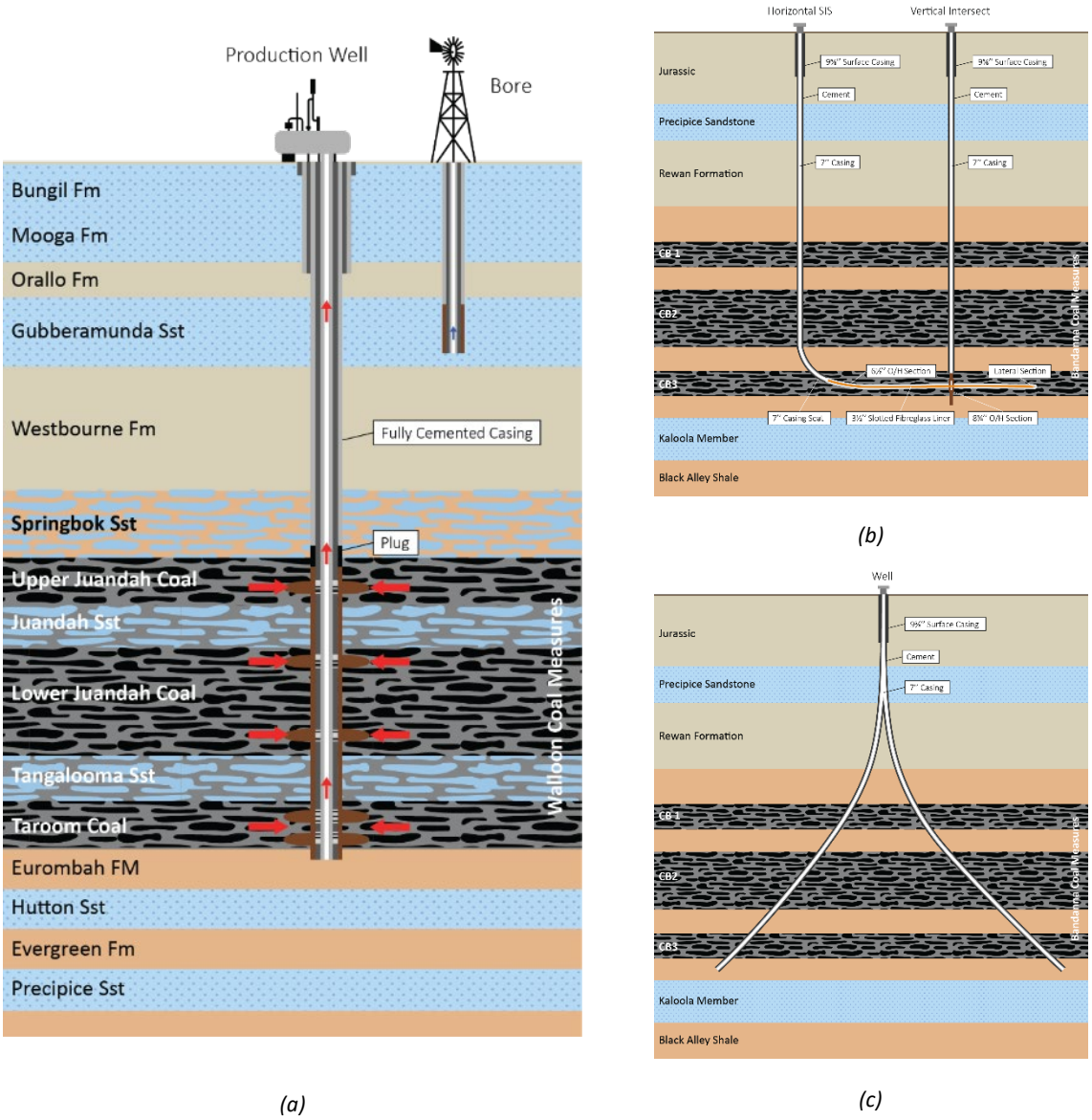

Figure 6. Schematic representation (not to scale) of CSG well trajectories: (a) a vertical completed to access multiple seams in the Walloon Coal Measures, (b) a horizontal well drilled to intercept a vertical in a surface-to-inseam (SIS) configuration, and (c) a deviated well

Note: (b) and (c) show interception of coals in the Bowen Basin.

2.3.2 Hydraulic fracturing

Hydraulic fracturing is a reservoir stimulation technique used to increase the contact area between the well and the target coal seam(s). It is used to attain economic rates of production in low-permeability formations. Hydraulic fracturing does not cause subsidence. When deployed, however, it increases the spatial extent and degree of

depressurisation that can be achieved from a well with naturally low deliverability, which in turn contributes to subsidence in a similar manner to that which occurs in higher-permeability, non-stimulated wells.

The widespread deployment of hydraulic fracturing was primarily responsible for the advent of the shale gas industry in the USA (MIT Energy Initiative 2011). Most CSG reservoirs exhibit sufficient permeability to negate the need for hydraulic fracturing, and thus only approximately 10% of Queensland CSG wells have been hydraulically fractured. This rate is anticipated to increase to up to 40% as operators target more challenging formations. However, in the 2020 financial year only 12% of Queensland CSG wells were hydraulically fractured (GasFields Commission Queensland 2021).

During hydraulic fracturing, a suspension of granular material, called proppant, is pumped into the reservoir, creating fractures that increase the volume of reservoir that is exposed to the well. This reduces the resistance to water and gas flow from the reservoir to the well and increases the rate of production. The role of the fluid is to induce stresses in the reservoir which are high enough to create a fracture and also to transport proppant. When the injected fluid is removed, the proppant remains in place to keep the fractures open. Additives are used to alter the rheology of the base fluid, which increases its ability to suspend and transport particles and changes the rate of fracture growth.

Hydraulic fracturing in CSG wells is commonly deployed in multiple stages on either vertical or horizontal wells, as shown schematically in Figure 7. Vertical wells can include in the order of five to 10 stages, each targeting different coal seams at different depths, while horizontal wells can include in the order of 20 stages (or more) with the intention of increasing the stimulated reservoir volume (SRV). Indicative fluid volumes pumped per well, both vertical and horizontal, are in the order of 2 ML (Johnson et al. 2021; Pandey et al. 2017). This is in contrast to shale gas wells in Texas, which pump between 10 and 20 ML (Nicot and Scanlon 2012).

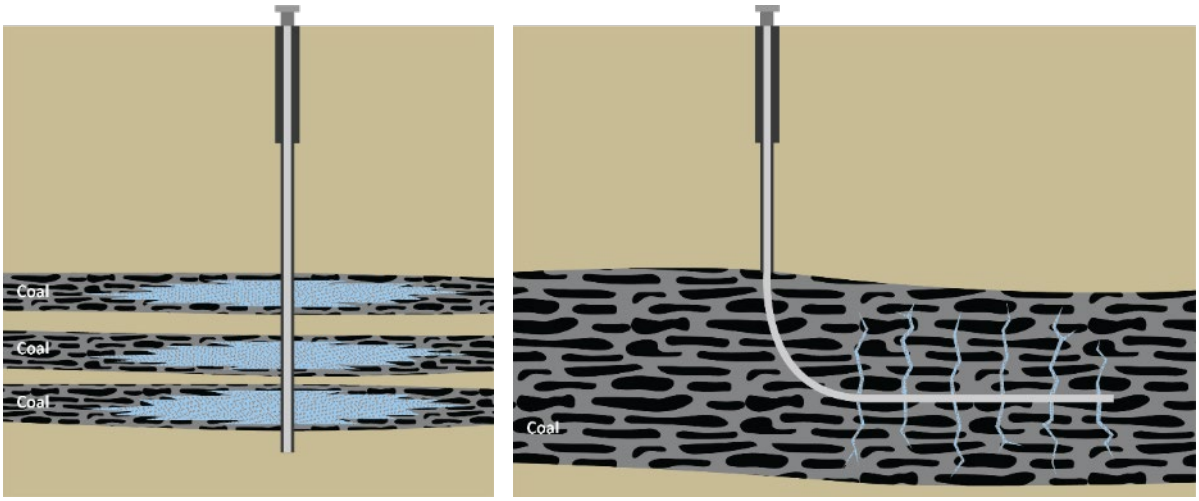

(a) *(b)*

Figure 7. Schematic diagrams of multistage hydraulic fracturing in (a) a vertical CSG well and (b) a horizontal CSG well

The direction of hydraulic fracture growth is governed by the subsurface stress regime, which comprises of the vertical, S_V, maximum horizontal, S_H, and minimum horizontal, S_h, principal stress components. In normal faulting, $S_V > S_H > S_h$, and strike-slip regimes, $S_H > S_V > S_h$, fractures grow vertically in the plane perpendicular to the minimum horizontal stress, S_h, direction. In the reverse faulting regime, $S_H > S_h > S_V$, which is common at shallow depths in Queensland, the minimum principal stress direction is vertical and so fractures tend to grow horizontally (Busetti and Flottmann 2018; Leonardi et al. 2019). This helps prevent propagation of fractures into aquifers above the fracturing stage. Horizontal fractures can also propagate when vertical fractures terminate at and then lubricate,

for example, the interface between coal and non-coal layers. Both types of horizontal fractures can result in small, temporary uplift of the ground surface, which can be measured using tiltmeter surveys of each of the well stages (Pandey et al. 2017).

2.3.3 Downhole pressure management

As shown in Figure 1(b), the volume of methane adsorbed to coal increases with pressure and so commercial CSG production typically requires a reduction of reservoir pressure to liberate gas. This is achieved by deploying a downhole pump to dewater the target coal formation(s). A progressing cavity pump (PCP) is installed on the tubing string close to, but not at, the bottom of the well, where it drives produced water up the central tubing of the well. This facilitates downhole separation of water from most of the gas, which flows to the surface via the annular gap between the well casing and the tubing. During this process, the groundwater level above the coal seam may remain largely unchanged, depending on the degree of hydraulic isolation, but the reduction in water pressure associated with groundwater abstraction from the seam promotes methane desorption (i.e., detachment from coal surfaces).

The rate of CSG-associated water extraction from Surat and Bowen basin wells in the Surat Cumulative Management Area (CMA) is summarised in Figure 8. This clearly shows the step-change in dewatering associated with the onset of CSG-LNG export. These data are collated and reported, along with future projections, by the Queensland Government's OGIA in its series of Underground Water Impact Reports (OGIA 2021). It has been observed that actual volumes of produced water are consistently lower than earlier industry predictions(Underschultz et al. 2018). Reasons for this include conservatism in research, regulation, and operation estimates; the use of basin-scale models that do not account for the effect of two-phase flow on near-wellbore saturation and permeability; decay of water extraction from wells with time; and installation of wells in infill locations where partial depressurisation (and potentially gas production) has already occurred (Underschultz et al. 2018).

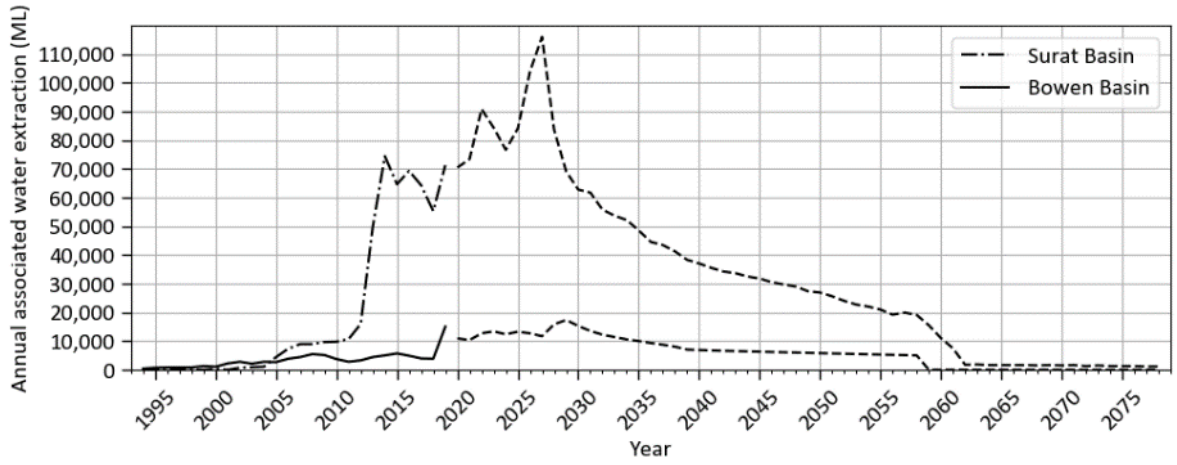

Figure 8. Annual rates of CSG-related water extraction from Surat Basin and Bowen Basin wells in the Surat CMA (reproduced from OGIA 2021); dashed lines represent future projections

The amount of water produced from an individual well is dependent on a number of factors, including the saturation and permeability of the coal, its internal connectivity and continuity, the nature of non-coal layers within the coal measures, and the regional state of water and gas depletion. Water rates are highest at the onset of production and then typically decay with time. The characteristics of methane desorption mean that the corresponding rate of gas production is initially low while initial depressurisation is occurring, and then increases to a peak a number of years after production commences (see Figure 9.(a)). Some Bowen Basin coals have been found to produce significantly less water than those of the Surat Basin (Towler et al. 2016), but this is possibly due to field (not basin) differences. Given the variability and uncertainty associated with the parameters that drive water production, and the spatial and temporal interaction of wells, it is almost impossible to precisely predict water production on an individual well basis.

The relationship between (pore) pressure and methane desorption from coals is not linear. This relationship is characterised using an adsorption isotherm test, which measures the maximum gas-holding capacity of a coal sample at any particular pressure at a stable temperature. These data can then be fitted to the Langmuir equation (Langmuir 1916),

$$V = \frac{V_L p}{p + P_L}, \quad (1)$$

where V is the maximum gas adsorption capacity at any particular pressure, p, and V_L and P_L are the Langmuir volume and pressure, respectively, which are both model parameters. Figure 9.(b) presents examples of adsorption isotherm curves for coals from the Bowen and Surat basins (Connell et al. 2016). These curves can be used to estimate the total gas content (and saturation) of a reservoir at a certain depth (and therefore pressure and stress (Liu et al. 2017)), as well as the degree of depressurisation required for economic gas production. It is worthwhile noting that at low pressures, more gas is desorbed per unit pressure change. In addition, the repeatability of adsorption tests is problematic, especially in the absence of a universal standard procedure, and it is generally accepted that their uncertainty ranges from 7% to 20% (Crosdale et al. 2008; Mavor et al. 2004). Given the relationship between desorption, coal shrinkage and compaction (see Section 2.4), these are important observations.

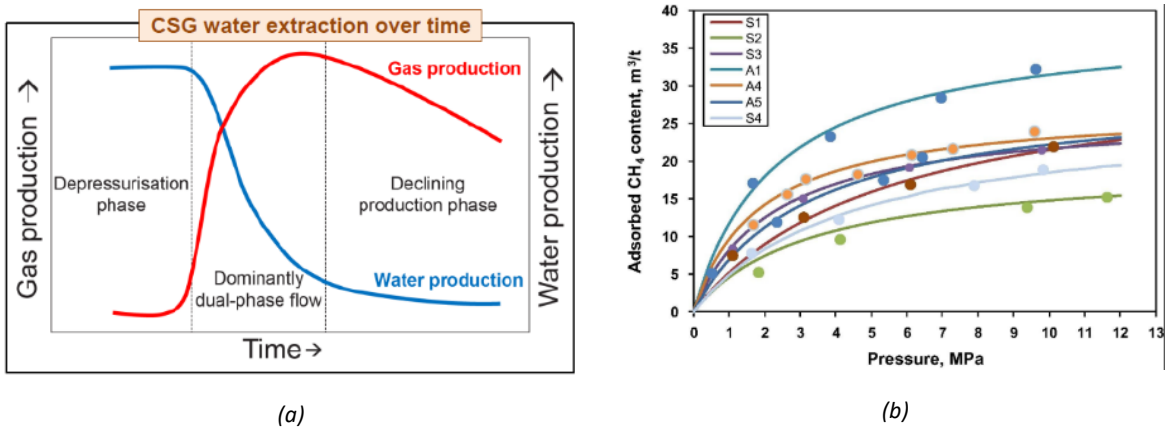

(a) *(b)*

Figure 9. Relationship between water production and gas desorption and extraction, showing (a) a schematic graph of the relationship between water and gas production rates, and (b) the Langmuir isotherm of select Queensland coals (reproduced from Connell et al.)

The abstraction of associated water is the primary driver of subsidence in areas where CSG is produced, as discussed in Section 2.4. The historical and significant extraction of water for agriculture and other non-CSG purposes therefore presents a challenge to identifying baselines for surface elevation and rate of movement and identifying the impact of CSG production in isolation.

As mentioned in Section 2.2, CSG operations are often located beneath or adjacent to agricultural activity, which can result in real or perceived impacts on groundwater resources (OGIA 2021). This is more acute in the Surat Basin, where intensive irrigated cropping occurs and the Walloon Coal Measures, which are the Queensland CSG industry's biggest producer, lie within the Great Artesian Basin (GAB). The GAB comprises a number of hydrogeological basins that cover an area of 1.7 million km^2. It is composed of a series of aquifers, which exhibit a high degree of spatial variability and vertical connectivity. In the GAB, aquifers are used to supply water to regional communities and agriculture, and its importance to regional communities is emphasised by their location in low-rainfall and drought-prone areas (Towler et al. 2016). Aquifers in the GAB supply water to many regional towns (more than 30 in Queensland), with tens of thousands of bores supplying water for farming, domestic and industrial use. They also provide irrigation water for major crops, such as cotton and grains, and horticulture. There is a long history of

declining aquifer pressures through over-extraction (Smerdon and Ransley 2012) with respect to the productive yield of the system, which has resulted in significant lowering of aquifer pressures.

2.4 Driving mechanisms of CSG-induced subsidence

In the context of gas production and the extraction of associated water from coal seams, the subsidence observed at the surface is driven by the depressurisation of the fluid-bearing formation(s) beneath. Reducing the pore pressure increases the effective stress, which causes poromechanical compaction of each depressurised layer. It also promotes desorption of methane, which results in *desorption-induced shrinkage*, which manifests as a reduction in the coal's bulk volume. These two phenomena are additive within a coal seam, resulting in a net change of height that can be summed over each depressurised layer. The fraction of this total compaction that propagates to the surface as subsidence is a function of the competence and thickness of the overlying and underlying strata. Similarly, groundwater abstraction for municipal or agricultural use can also contribute to the total subsidence observed at a location. Therefore, the ability to predict future or interpret historical subsidence requires an understanding of two-phase flow in the reservoir; the porosity, permeability and relative permeability of coal; changes in effective stress and poromechanical compaction of geological units; and coal shrinkage. These facets of the problem are described in this section, while their interdependencies are shown schematically in Figure 10. It is important to note, however, that they are all active areas of research.

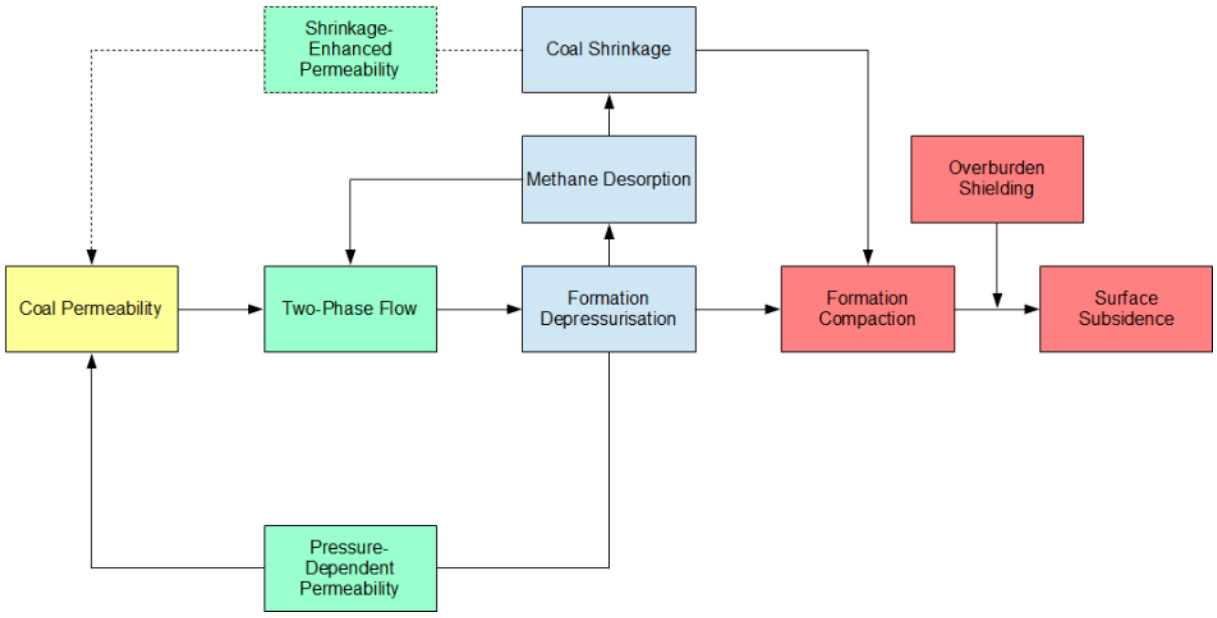

Figure 10. Schematic representation of the relationship between permeability, fluid flow, coal shrinkage, rock/coal compaction, and subsidence

Note: Both formation depressurisation and coal shrinkage (dashed lines highlight that this is a more recent concept, subject to ongoing research) provide feedback in the system via permeability change.

2.4.1 Two-phase flow in a coal seam

The production of gas and water from a CSG well is described by three distinct stages (McKee and Bumb 1987), as indicated in Figure 9.(a).

1. At the onset of production, associated water is pumped from the coal seam to reduce pressure. In this stage the flow is laminar and predominantly water in a saturated single-phase regime, even though some free and dissolved gas may exist within the cleats and macropores of the coal.

2. After sufficient depressurisation, gas begins to desorb from the coal surface and diffuse through the matrix to the cleats, where it begins to form bubbles. The wetting characteristics of the gas-water-coal system keep these isolated bubbles trapped in the cleats, where they partially impede the flow of water towards the well. Consequently, this stage is characterised by unsaturated single-phase flow of water, but not gas.

3. Methane desorption increases with further depressurisation, resulting in the coalescence of bubbles creating a continuous pathway for gas flow within the cleats towards the well. In this stage, both water and gas are transported, which is characterised by two-phase flow in the coal seam. As production continues, the volume fraction of water and gas in the two-phase flow regime changes as the water rate decays, peak gas production is reached, and then the gas rate decays.

These stages of flow are sequenced in both time and space around a well (McKee and Bumb 1987). Considering just the near-wellbore region, it transitions from saturated single-phase water flow to unsaturated single-phase water flow and then two-phase flow as time progresses. However, at any instant in time the degree of seam depressurisation decreases with distance from the well, meaning that when two-phase flow occurs near the well, unsaturated single-phase water flow occurs at some distance from the well, and saturated single-phase water flow occurs at greater distance from the well.

The saturated single-phase water flow in the seam is uncomplicated, in that it is laminar and can be modelled using Darcy's law. However, to accurately predict all regimes of gas and water flow in the seam, multiphase modelling with variable saturation is necessary. This is an important consideration, as the gas and water flow directly influence the spatial prediction of reservoir depletion, which is the key driver of subsidence. The evolution of mass and momentum balance for multiple, coexistent fluid phases in a reservoir can be modelled using a range of software packages (e.g., CMG-GEM, INTERSECT, MOD-FLOW). The Richards equation (Richards 1931) can also be used to approximate liquid flow in a variably saturated porous medium, in conjunction with the van Genuchten equation for saturation as a function of pressure (van Genuchten 1980). It is important to note that this approach does not capture the diffusion of gas through the coal matrix, or the transport of the gas phase. Rather, it is assumed that desorption occurs instantaneously, making gas immediately available within cleats and macropores. More information on modelling gas-liquid systems with Richards' equation can be found in the literature (Taigbenu 1999), including the basis for the approach taken by OGIA (Herckenrath et al. 2015).

2.4.2 Porosity and permeability of coal

As described in Section 2.1, coal is a naturally fractured medium that, in the context of a natural gas reservoir, is commonly described as a dual-porosity system (Clarkson and Bustin 1999). This system is composed of porous matrix blocks, with side lengths ranging from millimetres to centimetres, separated by face and butt cleats, which exhibit apertures ranging from micrometres to millimetres (Laubach et al. 1998). This is shown schematically in Figure 11. One of the properties that make coal such a unique material is its porosity, particularly the high specific surface area per unit volume. A single cubic centimetre of coal can contain pores with a total internal surface area of 3 m^2 (Mares et al. 2009; Radlinski et al. 2004). It has been reported (Yao et al. 2008) that the matrix pore network follows a fractal distribution, with individual pores classified by size as either micropores, mesopores or macropores (Şenel et al. 2001). A discussion of how these vary with coal rank can be found in Moore (2012). According to Gan et al. (1972), micropores have a diameter less than 2 nm, mesopores have a diameter between 2 and 50 nm, and macropores are larger than 50 nm. However, the usage of these terms is not universally consistent in the literature.

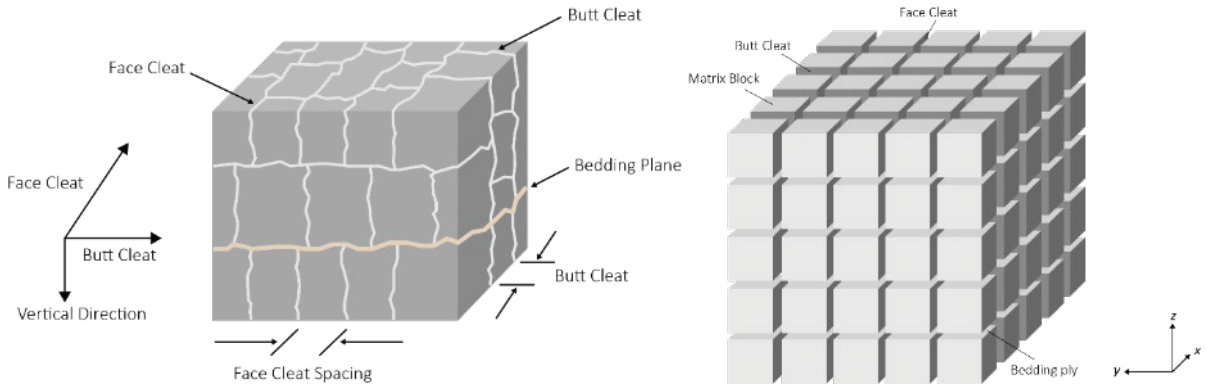

Figure 11. Schematic representation of cleats and matrix blocks in coal, showing (a) the relative orientation and termination of face and butt cleats with respect to bedding planes, resulting in anisotropic permeability, and (b) the simplification of the cleats and bedding planes as a cubic geometry (Robertson and Christiansen 2008) resulting in isotropic permeability

Typically the permeability of the pore network in the matrix will be orders of magnitudes lower than that of the cleat network in the same coal. However, in the micropores and smaller mesopores (as per the above size classification), the Knudsen number of methane (which in this context is a function of reservoir pressure and temperature) would suggest that a continuum description of transport is not valid and therefore phenomenological concepts such as permeability do not apply. Consequently, it is generally assumed that gas flow through cleats is laminar and can be described by Darcy's law, whereas gas transport in the coal matrix is controlled by a diffusive process that can be described (if it is to be included explicitly) by Fick's law. This diffusion links desorption of gas molecules from the coal to their subsequent viscous flow in cleats towards the well (Chen 2011; Masoudian et al. 2016; Webb 2006).

In the context of oil and gas production, coal seams are considered low-permeability reservoirs. The permeability of the cleat and natural fracture networks dominates flow behaviour (Laubach et al. 1998), as observed in the Walloon Coal Measures. In general, the properties of coal are anisotropic due to its depositional origin and the influence of the cleat network. This also applies to the *permeability tensor* because the horizontal permeability in the direction of face cleats, k_f, is typically 5 to 10 times higher than the horizontal permeability in the direction of butt cleats, k_b, (Best et al. 2014) and the vertical permeability perpendicular to the bedding plane, k_v, is typically lower than either horizontal permeability (Massarotto et al. 2003). Therefore, rigorous prediction of gas and water transport in coal seams requires incorporation of the three principal components of the permeability tensor, which is facilitated by most commercial reservoir simulators and some groundwater modelling packages.

It has been well documented that coal permeability decreases with increasing depth, most likely because the associated increase in geomechanical stress acts to close the cleats (Enever et al. 1999; OGIA 2016a; Somerton et al. 1975). For example, some coals can exhibit permeability in the order of hundreds of millidarcies (mD) at a depth of 100 m, which reduces to approximately 1 mD at a depth of 1,000 m. This relationship was demonstrated by Esterle et al. (2006) for coals from the central Bowen Basin and Hunter Valley, although it was noted that significant permeability variation (e.g. two orders of magnitude) can exist at any particular depth. In addition, Bustin (1997) found that vitrain banding in some Australian coal seams had a significant effect on permeability, which was sometimes greater than that of the effective stress.

The horizontal stress regime in a basin or sub-basin affects a number of facets of CSG production. In the context of fluid flow, the stress, σ^e, in a basin has been shown to affect permeability (Bell 2006; Sparks et al. 1995). The effective stress is defined as

$$\sigma^e = \sigma - \alpha p, \quad (2)$$

where σ is the total stress, p is the pore pressure, and α is the *Biot coefficient*. The horizontal components of the net effective stress are a measure of the mechanical load on the cleats, which acts to close them. Interpreted differently, the effective stress is the difference between the reservoir pore pressure and the cleat opening pressure measured in the borehole or well (Esterle et al. 2006). As the least principal stress (i.e., the minimum effective stress) in the basin increases, permeability can decrease from nearly 10 mD at 1 MPa to less than 1 mD at 8 MPa (Sparks et al. 1995).

As a consequence of this characteristic behaviour, a number of pressure-dependent permeability models have been defined for coal (see Pan and Connell (2012) for a review). These include the works of Palmer and Mansoori (1998), Shi and Durucan (2005), and Cui and Bustin (2005), all of which assume uniaxial strain conditions (i.e., constant total vertical stress and zero lateral strain). Using the matchstick model of the relationship between permeability and porosity (Seidle et al. 1992),

$$\frac{k}{k_0} = \left(\frac{\phi}{\phi_0}\right)^3, \quad (3)$$

the Cui-Bustin permeability model can be written as

$$\frac{k_s}{k_{s0}} = \exp\left\{\frac{3}{K_p}\left[\frac{1+\nu}{3(1-\nu)}\Delta\sigma^e - \frac{2E}{9(1-\nu)}\Delta\varepsilon^s\right]\right\}, \quad (4)$$

where K_p is the pore modulus; k_{s0} is the initial in situ intrinsic permeability of the coal seam; E and ν are the Young's modulus and Poisson's ratio of coal, respectively; $\Delta\sigma^e$ is the incremental change in the effective stress; and $\Delta\varepsilon^s$ is the change in desorption-induced volumetric strain (i.e., shrinkage). The change in effective stress, $\Delta\sigma^e$, is equal to the negative of change in pore pressure, $-\alpha\Delta p$, assuming a constant total stress given $\Delta\sigma^e = \Delta\sigma - \alpha\Delta p$. Note that the constant total vertical stress assumption has implications for the interpretation of saturation (i.e., water content) above the coal seam. The desorption-induced shrinkage, $\Delta\varepsilon^s$, is calculated as (Masoudian et al. 2019a)

$$\Delta\varepsilon^s = \varepsilon^s - \varepsilon_0^s = \frac{\varepsilon_L^s b_L p}{1+b_L p} - \frac{\varepsilon_L^s b_L p_0}{1+b_L p_0}, \quad (5)$$

where b_L is the Langmuir constant, ε_L^s is a constant representing the maximum volumetric swelling strain of coal, and p_0 is the pressure corresponding to a reference permeability (e.g., the critical desorption pressure P_{cd}).

The permeability–pressure relationship for the Palmer-Mansoori, Shi-Durucan and Cui-Bustin models is compared in Figure 12.(a). The difference between these models has in the past been (incorrectly) attributed to Palmer and Mansoori (1998) adopting a strain formulation, as opposed to the stress formulation adopted by Shi and Durucan (2004) and Cui and Bustin (2005) (Gu and Chalaturnyk 2006; Li et al. 2017; Palmer 2009). Zimmerman (2017) subsequently showed that the Palmer-Mansoori model is invalid when porosity is greater than zero or the Biot coefficient is less than one. Mathias et al. (2019) also analysed these three models by using them to derive associated expressions for the storage coefficient, the equation for which is well established for a reservoir under uniaxial strain. This found that only the Cui-Bustin model was able to reproduce the correct storage coefficient, and that issues with the Shi-Durucan model are due to inconsistencies in the theoretical derivations of both Seidle et al. (1992) and Shi and Durucan (2004). It was noted, however, that the Shi-Durucan model is often found (Shi et al. 2014; Zeng and Wang 2017) to better fit experimental data, but this was attributed to the availability of two fitting parameters, as opposed to one in the Cui-Bustin model (Mathias et al. 2019).

In the case where both water and gas flow through a cleat or pore, the *relative permeability* is the primary parameter used to describe the flow regime. This parameter is strongly influenced by the wetting characteristics of each fluid (i.e., the preference for a fluid to coat a solid material), which are in turn a function of the nature of fluids, local coal chemistry, minerals, surface morphology, and local pressure conditions (Zhang et al. 2015). However, the subsurface is a complex system and the wetting state varies spatially. The best way to quantify the influence of this variability is an area of active research (Armstrong et al. 2021). High-fidelity computational modelling of two-phase fracture flows

has recently been used (McClure et al. 2021) to study the influence of surface roughness, chemical heterogeneity, and dynamic events (e.g., Haines jumps). The quest to link these data to continuum-scale wettability indices continues (Sun et al. 2020a; Sun et al. 2020b).

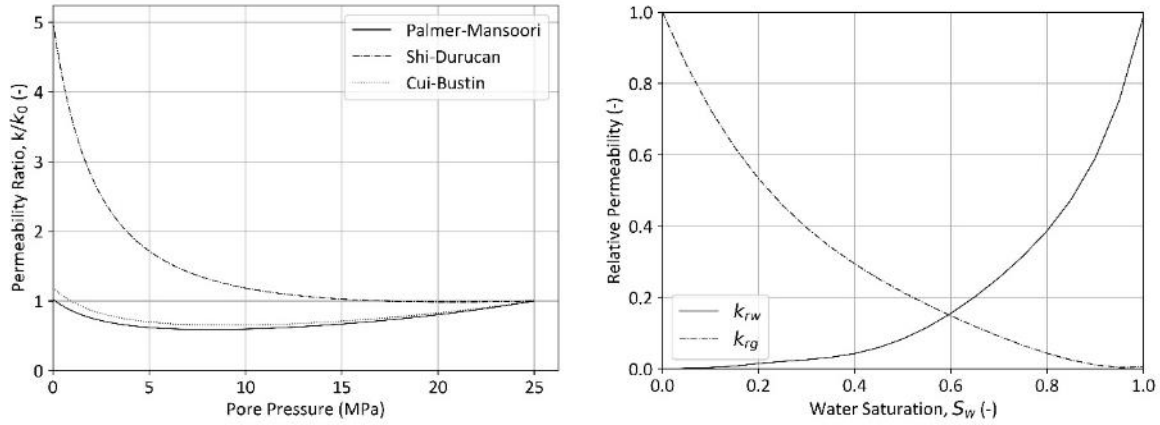

(a) *(b)*

Figure 12. Graphs of coal permeability, showing (a) a comparison of the stress-dependent permeability models of Palmer and Mansoori (1998), Shi and Durucan (2004) and Cui and Bustin (2005); and (b) the relative permeability curves of gas, k_{rg}, and water, k_{rw}, as a function of saturation (reproduced from Gash 1991)

Several methods exist to measure relative permeability in the laboratory, including unsteady-state, steady-state, capillary pressure, and numerical inversion methods. A survey of the contemporary literature reveals ongoing investigation of relative permeability related to coal rank and lithotype (Mahoney et al. 2015), dynamic behaviour (Shaw et al. 2019), history matching (Zhang et al. 2021), and more. The resulting data are used to inform curves like those shown in Figure 12.(b), which describe the relative permeability of each phase as a function of saturation. It is important to note that the precision of these experimental approaches depends on the interpretation of the measured data (Zhang et al. 2015). Further, it has been observed that upscaling laboratory data to real reservoir conditions is subject to a great level of uncertainty (Müller 2011), which propagates to predictions of gas and water production. Nevertheless, given the non-unique nature of gas-water relative permeability in coal and the complexity associated with measuring and upscaling it to that necessary for a field-scale simulator, it is common practice to choose a standard relative permeability curve and treat it as a model parameter subject to sensitivity analysis.

2.4.3 Poromechanical compaction

Poroelasticity defines the behaviour of a porous medium under internal and external forces. It relates the changes in internal pore pressures and external stresses to the deformation of the porous continuum and the solid frame. Reducing the pore pressure in a poroelastic subsurface material results in poromechanical compaction, which manifests as subsidence when propagated to the surface. Groundwater abstraction, oil and gas production, and the dewatering of shallow sediments can all cause compaction and subsidence but, depending on the degree of consolidation of the geological unit(s), these can differ by orders of magnitude per unit drop in pressure.

The withdrawal of water from a porous geological unit results in a commensurate decline in the water level or hydraulic head. The largest decline in the formation exists at the point of extraction and decreases with increasing distance from the well. As the pore pressure in the formation decreases, the effective stress increases proportionally. In unconsolidated sediments this can result in the rearrangement of grains, reduction of porosity, and ultimately

subsidence. In some areas where the formation is shallow and unconsolidated and groundwater extraction is extensive, this effect can become acute. For example, there are reports of up to 9 m of subsidence in Mexico City over regions of groundwater extraction from interbedded sand and clay layers (Ortiz-Zamora and Ortega-Guerrero 2010). However, subsidence of this magnitude is not typical for oil and gas extraction, particularly CSG, because the depressurised geological units are consolidated and less susceptible to grain-scale deformation. They also exist hundreds or thousands of metres below the surface and so, depending on the lateral extent of the depleted zone and the stiffness of the overlying geological units, the overburden may exhibit stress arching (Dusseault et al. 2007) or compaction-driven surface deformation (Dusseault and Rothenburg 2002; Geertsma 1973; Hettema et al. 2002). The magnitude of surface deformation depends on multiple factors, including:

1. rock mechanical properties of the geological unit and of the overburden and basement units
2. the lateral and vertical extent of the compression causing matrix compaction
3. the magnitude and orientation of the compaction with respect to vertical.

The magnitude of subsidence mainly depends on the depth and thickness over which depressurisation and compaction occurs, and the properties of geological units overlying the compacting geological units. Assuming that the mechanical behaviour of a rock or coal layer can be described by linear poroelasticity, the relationship between stress and strain can be modelled using Hooke's law. The normal strain in the three Cartesian directions can be written in terms of the effective stresses as

$$\varepsilon_{xx} = \frac{1}{E}\left[\Delta\sigma^e{}_{xx} - \nu\left(\Delta\sigma^e{}_{yy} + \Delta\sigma^e{}_{zz}\right)\right], \quad (6)$$

$$\varepsilon_{yy} = \frac{1}{E}\left[\Delta\sigma^e{}_{yy} - \nu\left(\Delta\sigma^e{}_{xx} + \Delta\sigma^e{}_{zz}\right)\right], \quad (7)$$

$$\varepsilon_{zz} = \frac{1}{E}\left[\Delta\sigma^e{}_{zz} - \nu\left(\Delta\sigma^e{}_{xx} + \Delta\sigma^e{}_{yy}\right)\right]. \quad (8)$$

assuming uniaxial strain conditions means that $\varepsilon_{xx} = \varepsilon_{yy} = 0$ and total vertical stress, σ_{zz}, is constant. After some manipulation (see Wu et al. (2019) for more details), an explicit equation for the strain in the vertical direction, ε_{zz}, can be derived and interpreted as the ratio of the change in height, Δh, and original height, H, of the target formation

$$\frac{\Delta h}{H} = \varepsilon_{zz} = -\frac{1}{E}\frac{(1+\nu)(1-2\nu)}{(1-\nu)}\Delta\sigma^e{}_{zz}. \quad (9)$$

Substituting for the effective vertical stress and extracting the layer compressibility (see Section 7.2),

$$C_m = \frac{(1+\nu)(1-2\nu)}{E(1-\nu)}, \quad (10)$$

results in

$$\Delta h = C_m H \alpha \Delta p_f. \quad (11)$$

The summation of Δh values for all depressurised layers gives an indication of the maximum subsidence expected at the surface due to poromechanical compaction.

The assumption of uniaxial strain is appropriate because the subsidence due to poromechanical compaction is primarily vertical. Formation heterogeneity, in terms of both geometry and permeability (i.e., propensity for depressurisation), can result in non-uniform compaction of a geological unit. At the surface, this can manifest as variation in subsidence as well as net horizontal movement. Extreme cases of differential surface movement, vertically or horizontally, could induce ground failures such as surface faults and earth fissures (Holzer 1984). However, neither presents a significant risk in the context of CSG production (see Section 4.2 for discussion).

In unconsolidated sediments, where grain rearrangement can occur, the rate of poromechanical compaction is greatly influenced by the lithology. Faster rates of compaction are observed in large-grained sand and gravel formations even

though the extent of total compaction is limited. Conversely, clays and fine siltstones, which are fine-grained lithological units, compact at a slow rate because of their low hydraulic conductivity. This means that their mechanical response to pressure change, either compaction or uplift, is time dependent and could take several years to equilibrate (Budhu et al. 2014).

It is important to note that aquifer pressure cycling has the potential to result in irreversible compaction, or inelasticity. If the pressure head is reduced below the pre-consolidation head, inelastic compaction of clay units will occur, which in turn results in pore collapse and an irreversible loss of water storage and permanent drainage. This can also be interpreted as the effective stress increasing to greater than the pre-consolidation stress, and is most significant in unconsolidated and loosely consolidated sediments. Budhu et al. (2014) demonstrated this by investigating ground movements from aquifer recharge and recovery in Arizona. This was undertaken using a coupled groundwater flow-soil deformation model. The subsidence and uplift related to groundwater withdrawal and recharge, respectively, clearly demonstrated hysteresis. In areas of CSG production where aquifers have a prolonged history of excessive depressurisation, this suggests that historical, irreversible subsidence may have already occurred.

2.4.4 Desorption-induced shrinkage

One of the key differences in geomechanical behaviour between coal seams and conventional reservoirs is that the adsorption and desorption of gas lead to swelling and shrinkage of the coal matrix, respectively (Larsen 2004; Saghafi et al. 2007). This behaviour manifests as volumetric strain that is analogous to the thermal expansion and contraction of materials, and distinct from elastic and poroelastic behaviour. Under the common assumption of uniaxial strain, desorption-induced shrinkage has an effect on the change in effective stress and permeability (via cleat aperture) caused by depletion (Masoudian 2016). While reservoir models consider the shrinkage phenomenon when investigating the variation of the fracture aperture and subsequently the fracture permeability (as discussed earlier in this section), many geomechanical models neglect or at best oversimplify its influence on the bulk volumetric response of the coal seam and consequently the displacement of the ground surface (Masoudian et al. 2016; Wu et al. 2018). Nevertheless, the total displacement at the ground surface is the sum of all compaction mechanisms occurring in multiple geological units. It is dependent on the magnitude and direction of compression (which are dictated by pressure changes from extraction of associated water and desorption of gas from coal seams), the depth and depth-interval over which compression occurs, and the geomechanical properties of the geological units throughout the entire depth profile. While the desorption-induced shrinkage of coal is well understood at the laboratory scale, including the stress-dependence of the processes at work (Liu et al. 2017), the degree to which this behaviour translates to the reservoir scale in CSG production is an ongoing area of research.

The rate of coal shrinkage or swelling with pressure change can be measured experimentally (see, for example, Dudley et al. 2019). This is usually undertaken using small coal samples (i.e., matrix blocks) to eliminate the effect of cleats that exhibit much greater compressibility than the matrix. The data are then fitted to the Langmuir equation to describe the volumetric shrinkage strain, ε^s, as a function of pressure, p,

$$\varepsilon^s = \frac{\varepsilon_L^s b_L P}{1+b_L P}, \quad (12)$$

where b_L is the Langmuir constant and ε_L^s is a constant representing the maximum volumetric swelling strain of coal at infinite pore pressure. As described in Masoudian et al. (2016b), the desorption-induced shrinkage can be incorporated as an additional term in the elastic stress-strain constitutive equations. By again invoking the uniaxial strain assumption, the net shrinkage in the vertical direction, Δh_s, can be defined as

$$\Delta h_s = \frac{1+\nu}{3(1-\nu)} \frac{\varepsilon_L^s b_L (P-P_{cd})}{(1+b_L P)(1+b_L P_{cd})} H \quad (13)$$

Similarly to that for poromechanical compaction defined Equation 11. Here P_{cd} is the critical desorption pressure.

It is pertinent here to consider the relationship between the adsorption isotherm (Equation 1) and the sorption strain (Equation 12) for a particular coal sample. Just as the former has been noted to vary considerably for different coal types and ranks, the same is true for the latter (although considerably less shrinkage data are publicly available). In addition, both equations have the same characteristic form, resulting in an increase in the rate of change of desorbed gas or shrinkage with respect to pressure as the pressure decreases. In the context of subsidence, this suggests that the desorption-induced shrinkage component of coal seam compaction may increase as the reservoir pressure approaches its end state. This has been reported internally by the industry (Rai and Hummel 2019); however, no evidence to support or refute this observation can currently be found in the literature.

Due to their depositional nature, coal seams contain bedding planes that are approximately horizontal and perpendicular to the face and butt cleats. Consequently, coal at the bulk scale is completely anisotropic (Saurabh and Harpalani 2019). This can be simplified for the purpose of flow modelling to assume that properties in the horizontal direction are uniform and the coal is thus transversely isotropic (Espinoza et al. 2015; Liu et al. 2016; Wang et al. 2014). Laboratory studies (Day et al. 2008; Pan and Connell 2011) have shown that this concept of transverse isotropy also applies to desorption-induced shrinkage. The work of Day et al. (2008) showed that when coals were injected with supercritical CO_2, the expansion was 70% greater in the direction perpendicular to the bedding plane than in the parallel plane for two coal samples from the Hunter Valley and Bowen Basin, and approximately 30% greater for a sample from the Illawarra. The Illawarra coal sample was higher rank, with a mean vitrinite reflectance of 1.29%, while the mean vitrinite reflectance was 0.89% and 0.95% for the Hunter Valley and Bowen Basin samples, respectively. These results indicate that lower-rank coal tends to show stronger anisotropic swelling. Pan and Connell (2011) investigated the effect of different gasses on a Hunter Valley coal sample and revealed that the swelling strain in the direction parallel to the bedding was approximately 47%, 52% and 60% of that in the direction perpendicular to the bedding for N_2, CH_4 and CO_2 adsorption, respectively. These results can be seen in Figure 13., where it can also be seen that swelling behaviour for different gases varies significantly but in a similar order to adsorption.

If the constants ε_L^s and b_L have been determined perpendicular to bedding (i.e., in the approximately vertical direction) they can be used directly in a uniaxial prediction of shrinkage (i.e., Equation 13). However, anisotropic shrinkage will have implications for the calculation of effective horizontal stresses and the permeability derived from them (e.g., Equation 4), or for more complicated models in which a fraction of the total volumetric shrinkage strain is apportioned to permeability change and the rest is assigned to bulk shrinkage (Wang et al. 2014).

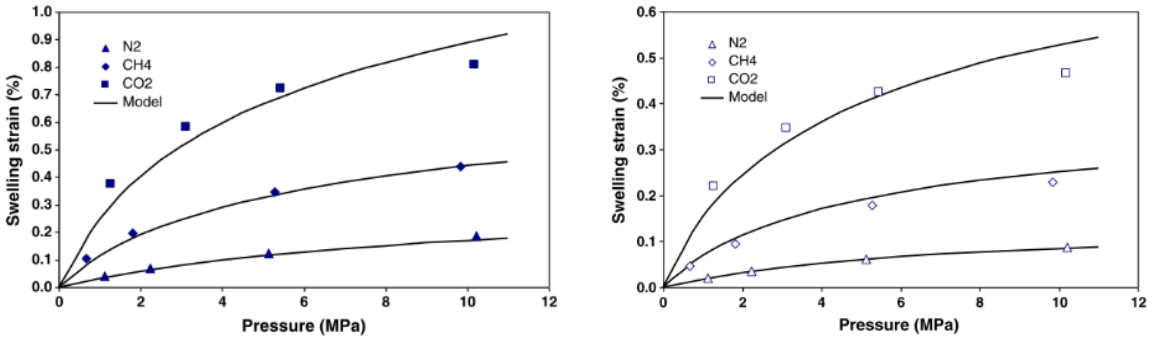

Figure 13. Volumetric swelling/shrinkage strain for a Hunter Valley coal sample when injected with N_2, CH_4 and $C0_2$, showing (a) the strain perpendicular to bedding, and (b) the strain parallel to bedding (Pan and Connell 2011)

2.5 Considerations for shale gas and underground coal gasification

A literature search did not uncover any published research on subsidence associated with shale gas production. It has not emerged as an issue of interest in the widespread shale gas industry in the USA. Shale is significantly less compressible than coal and does not contain adsorbed gas to the same extent as coal. It is therefore not prone to poromechanical compaction or desorption-induced shrinkage, which probably explains the dearth of papers on the topic.

Underground coal gasification (Bhutto et al. 2013) necessitates the creation of a substantial underground void as the coal combusts. In this way it is more closely linked with underground coal mining methods and is therefore out of the scope of this document.

2.6 Beneficial aquifer injection and associated uplift

The associated water produced from CSG operations can be treated and injected into the subsurface to replenish depleted aquifers and, consequently, raise the groundwater table or pressure (Hayes et al. 2020). This process is known as managed aquifer recharge (MAR). One local example of this is the Reedy Creek project managed by Origin Energy (upstream operator for the Australia Pacific LNG joint venture), in which produced water is pumped into the Precipice Sandstone aquifer in the Surat Basin. In general, injection pressures are subject to limits so as to minimise the risk of creating new underground fractures which can damage aquitards and result in the unwanted hydraulic connectivity of geological units. As a consequence of the poromechanical behaviour described in Section 2.4, MAR has been associated with observed uplift of the ground surface (Parker et al. 2021); however, no public documentation of this phenomenon related to Queensland CSG activities exists. The elevation of pore pressure in the proximity of faults can be associated with elevated risk of induced seismicity (Ellsworth et al. 2019; Zang et al. 2014). However, injection into high-permeability formations means that the pressure diffuses and does not localise around the injection site.

A number of cases of surface uplift have been reported worldwide. These vary significantly in terms of magnitude and timescale. One renowned example is the Wilmington oil field (see Section 3.2 for more information), which is composed of unconsolidated loose silty to sandy formations interbedded with shale layers (Mayuga and Allen 1969), and where hydrocarbon production had resulted in surface subsidence of as high as 9 m (Colazas and Olson 1983). In an attempt to reverse the subsidence, approximately 175,000 m^3/day of water was injected into the field in the 1960s (Mayuga and Allen 1969), which was later reduced to 90,000 m^3/day (Otott and Clarke 1996). Subsidence was stopped for most of the field, with the subsidence rate in the middle of the reservoir reduced from 71 cm/year in 1951 to zero by 1968. However, in some parts of the field, excessive injection resulted in uplift of 20 to 30 cm above the original ground elevation (Colazas and Olson 1983).

3. National and international context

Causes of subsidence include groundwater abstraction, conventional oil and gas production, drainage of shallow soils, underground mining, earthquakes, and natural compaction such as that caused by sinkholes, peat oxidation or thawing permafrost. Subsidence associated with CSG production simultaneously combines two of these processes, namely the depressurisation of geological units and the depletion of gas reservoirs. Mechanical sources of subsidence, such as the creation of a void during underground mining, are addressed in the companion to this document (Hebblewhite 2003).

3.1 Subsidence due to groundwater abstraction

The development of subsidence in response to groundwater abstraction has been documented extensively in the literature. Gambolati and Teatini (2015) summarised a number of locations worldwide where the removal of groundwater had resulted in or was continuing to (at the time of publication) cause subsidence. A selection of these case studies is listed in Table 1.

Table 1. Selected cases of subsidence caused by groundwater abstraction

Location	Maximum subsidence (m)	Recent subsidence rate (cm/year)	Depth of pumping (m)	Area of subsidence (km^2)	Principal references
San Joaquin Valley	10 (1930–)	30 (2007–2011)	60–600	13,500	Galloway et al. (1999) Borchers and Carpenter (2014)
Mexico City	13 (1960–)	30 (2007–2011)	0–350	250	Ortiz-Zamora and Ortega-Guerrero (2010) Chaussard et al. (2014)
Jakarta	4.1 (1974–2010)	26 (2007–2011)	40–240	660	Ng et al. (2012)
Tokyo	4.3 (1900–1975)	−0.3 (1991–2005)	0–400	3,400	Ling et al. (2009)
Ho Chi Minh	0.4 (1996–2005)	4 (2006–2010)	50–240	250	Erban et al. (2014)
Venice	0.12 (1952–1973)	0.1 (2008–2011)	70–350	150	Gambolati (1974) Teatini et al. (2012)

Data sourced from Gambolati and Teatini (2015)

In the San Joaquin Valley, USA, more than 13,000 km^2 of farmland exhibited subsidence of approximately 10 m over a period of 50 years. This remains one of the most prominent documented examples of surface elevation changes as a consequence of groundwater extraction. Numerous other examples can be found in more than 60 countries

worldwide, where groundwater use for irrigation, industry and water supply has resulted in subsidence and other surface impacts. In the Houston-Galveston region, Texas, approximately 1 m of subsidence was measured in the period 1975 to 2015 (Kasmarek 2012), including subsidence rates of 7.59 mm/year and 4.7 mm/year at Long Island and Galveston, respectively (Kolker et al. 2011). Between 2005 and 2009, 20 mm of subsidence occurred in the Tongchuan region, China, due to the extraction of groundwater (Wei et al. 2017). Surface movement rates varied from 2 mm/year uplift to 10 mm/year subsidence in Venice, Italy, between 1992 and 2002 (Tosi et al. 2009). Finally, an average annual decline of 0.3 m hydraulic head in the Mekong Delta, Vietnam, resulted in subsidence that averaged 1.6 cm/year (Erban et al. 2014).

In Australia, examples of subsidence as a consequence of groundwater extraction include the Lower Namoi Valley in New South Wales (NSW), the Latrobe Aquifer system in the Gippsland Basin, Victoria (see Section 3.3), and (potentially) the NSW Riverina. Ali et al. (2004) modelled the predicted subsidence in the Lower Namoi Valley, where groundwater extraction and crop irrigation have been occurring for approximately 60 years. A singular subsidence maximum of 0.5 m was found; however, subsidence in the range of 0.05 to 0.3 m was more widely spread. This is consistent with the work of Ross and Jeffrey (1991), which reported subsidence of 0.07 m to 0.21 m in the period from 1981 to 1990. This study also found that groundwater drawdown can cause residual compaction (40 m drawdown caused land subsidence of 0.16 m) for a long period of time after the groundwater levels have stabilised (i.e., there can be a temporal lag between depressurisation and subsidence). The work of Castellazzi et al. (2023) developed surface movement maps using Sentinel-1 InSAR data for the period 2015 to 2020 and used this to investigate correlation between subsidence and agricultural groundwater extraction. Although this study did not claim to definitively present a causal relationship between the depressurisation of aquifers and measured subsidence, it did demonstrate spatial and temporal correlation between downward surface movement, groundwater level fluctuations, and drops in critical head (defined as the historical minimum of head in an aquifer).

To summarise this brief discussion of examples, it can be seen that there are approximately two orders of magnitude difference between the subsidence observed in the San Joaquin Valley and Venice. However, in combination with rising sea levels, the comparatively small amount of subsidence in Venice comes with disproportionately large consequences (i.e., flooding of urban streets and buildings with tidal fluctuations). Therefore, it is important to note that the absolute magnitude of subsidence is not the sole driver of the impacts it generates (see Section 4.2 for further discussion of this point). It is also important to note that groundwater abstraction (e.g., for municipal or agricultural use) in areas of CSG production will also contribute to the subsidence at those locations, which complicates the assessment, measurement and attribution of the CSG-induced component.

3.2 Subsidence due to oil and gas production

Subsidence associated with conventional oil and gas production is driven by the same mechanism as in groundwater abstraction. The extraction of fluids from the reservoir reduces the pore pressure, which results in an increase in effective stress. This manifests as increased mechanical force on the porous skeleton of the reservoir, which causes compaction that propagates to the surface. The first documented case of subsidence caused by hydrocarbon production is generally assumed to be the Goose Creek oilfield on the Texas coast of the Gulf of Mexico (Pratt and Johnson 1926), where surface faulting and roadway subsidence were first noticed in 1918.

The brief review of compaction and subsidence associated with the petroleum industry by Nagel (2001) stated that hundreds, if not thousands, of academic and industrial documents have been published on the topic of oil- and gas-related subsidence, with many dedicated to the analysis of a specific field. A survey of the contemporary literature shows that this number has continued to grow, as the challenges (and opportunities) that arise from subsidence are explored. It is prudent to note that reservoir compaction drive has the potential to provide a significant portion of the total drive energy of some reservoirs, resulting in increased production and ultimate recovery (Nagel 2001).

A very small subset of subsidence cases related to oil and gas production from around the world is summarised in Table 2, including the Groningen natural gas field, which is located in the north-eastern part of the Netherlands. It is estimated that Groningen contained 97 tcf of technically recoverable natural gas, making it the largest natural gas field in Europe and one of the largest in the world. It can be seen in Table 2 that the maximum subsidence at Groningen is at least one order of magnitude smaller than that in the other fields listed. Nevertheless, subsidence in the order of tens of centimetres represented a serious challenge to the operation of the field as large parts of the Netherlands are below sea level and protected by dikes. From the 1980s, production-induced subsidence was also accompanied by an increased level of seismicity (van Elk et al. 2017).

To help monitor subsidence above Groningen and calibrate predictive models of future movement, 16 levelling campaigns were undertaken in the period from 1964 to 2018. These data were used to forecast accumulated subsidence at 2025, 2031 and 2050 for a number of different operational scenarios (TNO 2021) which decrease production to zero no later than 2030. Figure 14. compares subsidence predictions and measurements for the period 1972 to 2018, clearly showing a subsidence bowl with a maximum magnitude of approximately 35 cm in the centre. Good correspondence between the predictions and measurements can also be seen. Future predictions indicate that the maximum at the centre of the bowl will reach 42 cm by 2031 and then not change significantly by 2050. At the time of writing (2023), production from the Groningen field is scheduled to cease before reserves have been exhausted, because of the challenges presented by induced seismicity. Damage associated with subsidence is still possible due to differential movement of the phreatic groundwater level with respect to the surface.

Table 2. Selected cases of subsidence caused by conventional oil and gas production

Location	Maximum subsidence (m)	Reservoir thickness (m)	Reservoir depth (m)	Principal references
Ekofisk Field, North Sea	6.0 (1971–1998)	Up to 300	>3,000	Smith (1988) Sulak et al. (1991)
Bolivar Coastal Fields, Venezuela	5.0 (1929–1988)	Up to 180	>300	Escojido (1981) Finol and Sancevic (1995)
Wilmington Field, California	9.0 (1932–1968)	800–2,000	700–1,800	Mayuga (1970) Mayuga and Allen (1970)
Groningen Field, Netherlands	0.3 (1972–2018)	120–270	~3,000	Schoonbeek (1976) TNO (2021)
Po Delta, Italy	3.2 (1951–1973)	Up to 600	100–600	Cassiani and Zocatelli (1998)

Data sourced from Nagel (2001)

Outside of Australia, there exists little documented discussion of subsidence associated with CSG production. Grigg and Katzenstein (2013) reported on InSAR observations of subsidence above CSG operations in the Powder River Basin, Wyoming. The data indicated that in the periods from July 1997 to July 2000 and from August 2004 to July 2007, up to 4.7 cm and 8.3 cm of subsidence occurred, respectively. In this location, groundwater was reported to have been extracted at a rate of approximately 355 ML/day. In the east-central part of the study area, the largest subsidence values were found to be correlated with large clusters of CSG wells. In comparison to the typical CSG operation in the Bowen Basin, the target Powder River Basin seams are thick (between 7 m and 22 m, with an average of 11 m), shallow (depths ranged from 140 m to 460 m), and low-rank sub-bituminous. In contrast to these

observations, Best et al. (2014) reported on predictions made by Case et al. (2000) using a simple formula for subsidence and an aquifer storage coefficient of 1×10^{-4} for the coal seam. The results suggested a total subsidence of less than 13 mm in the Gillette area of the Powder River Basin. It was also estimated that only a part of this compaction would be seen at the surface. In addition, the compaction of overburden was not included in the assessment and therefore this would have contributed to the underprediction of total subsidence. More recently, Du et al. (2018) reported on the use of InSAR to monitor subsidence in the Liulin District, China, during 2003 to 2011. The observation of both low rates of subsidence and uplift across the region led to the conclusion that CSG production was not appreciably contributing to the signal (see Section 5.4 for more detail).

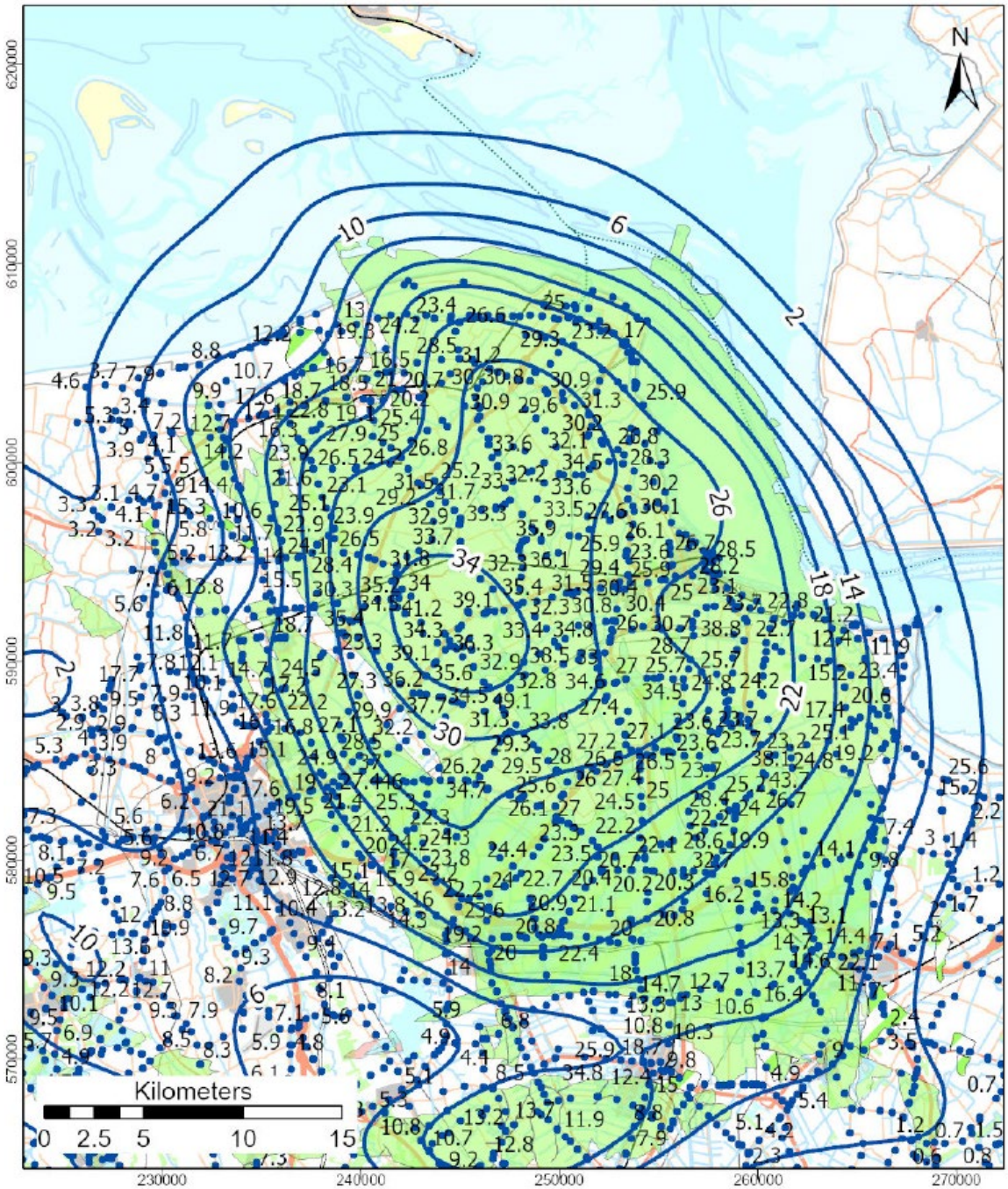

Figure 14. Predictions (solid blue contour lines) and measurements (labelled dots) of subsidence in centimetres above the Groningen gas field, Netherlands, in the period 1972 to 2018 (TNO 2021)

3.3 Subsidence in the Australian context

Over the past five years, an increasing amount of subsidence data related to CSG developments has become available in the academic and industrial literature. Work related to modelling and prediction is discussed in Section 8.1 of this document, while work related to monitoring is presented in Section 5.4. Beyond this, there are reports of land subsidence related to mining and the extraction of associated water. The subsidence occurring as a result of mining extraction is mainly related to the void being created due to the removal of coal, and to a lesser extent due to withdrawal of associated water. In most subsidence predictions of this kind, the subsidence as a result of water extraction is not considered.

3.3.1 The Gippsland Basin

The Gippsland Basin, located in south-east Victoria, comprises onshore and offshore components. Its onshore boundaries include the Eastern Highlands to the north and the Strzelecki Ranges to the west, while offshore the basin extends south-east into Bass Strait. The basin's sediments, which are composed of sands, clays, limestone, coal and some volcanics, are more than 1,000 m thick onshore and 3,000 m thick offshore. Its stratigraphy is well documented in the literature (Hocking 1980; Holdgate and Clarke 2000; Thompson and Walker 1982).

The Gippsland Basin contains vast brown coal resources, liquid and unconventional hydrocarbons, and significant groundwater resources. One of the main aquifer systems in the basin is the Latrobe Group. Coal has primarily been mined from the basin in the Latrobe Valley, requiring substantial dewatering to keep the mines dry, while conventional oil and gas production has occurred in Bass Strait. Groundwater from the Gippsland Basin is mainly used in support of agriculture and for municipal water supply. Since the 1960s the cumulative effects of these activities have led to a regional decline of water levels in the Latrobe Aquifer system (Holdgate et al. 2003). Hydrographs of the coastal area of the Gippsland Basin (Hatton et al. 2004) show water level declines ranging from 0.25 to 1.2 m/year over approximately 30 years. The potential impacts of the declining water levels were identified by Hatton et al. (2004) to be declining bore water levels, reduced availability of water to landowners, and risk of subsidence. Hatton et al. (2004) also noted that in the immediate vicinity of the Latrobe Valley mines, cumulative subsidence of up to 2.3 m has been measured. However, this includes contribution from the collapse of the underground mining void and so cannot be attributed solely to water extraction. In terms of subsidence, coastal areas of the Gippsland Basin are solely affected by water level decline.

Issues of groundwater decline in the Gippsland Basin motivated a study by Freij-Ayoub et al. (2007), who simulated the risk of coastal subsidence up to the year 2056 in parallel with a field study of high-resolution GPS measurements undertaken by the Victorian Department of Primary Industries (DPI). The DPI used surface movement data from 15 stations across the region over the period from June 2004 to November 2005. The computational geomechanical modelling conducted by Freij-Ayoub et al. (2007) used several different methods and assumptions, following the work of Acar Yalcin and El-Tahir El-Tahir (1986). One of these was to assume that the stiffness of geological units increases with confining pressure (i.e., depth) according to a power law with exponent 0.2 to 0.5. A second method (Helm 1976) suggested scaling the skeletal specific storage coefficient down as the effective vertical stress increases. Modelling results, which were calibrated using measured data, showed subsidence values from zero to 15 mm for the period from June 2004 to November 2005. The calibrated model was then used to forecast subsidence to 2056, resulting in a map of cumulative values showing magnitudes of up to 0.5 m along the Gippsland coastline by 2031 (see Figure 15.).

Following the work of Freij-Ayoub et al. (2007), Michael et al. (2013) further examined the distribution of Latrobe Aquifer drawdown and the potential for CO2 storage in the offshore regions. Further, Ng et al. (2015) used InSAR data to investigate surface movement over the Gippsland Basin between 2006 and 2011 and compared their findings with the predictions of Freij-Ayoub et al. (2007) to 2031. The work found that 98% of the InSAR surface movement data fell in the range of ±10 mm/year. Along the Gippsland coast, the InSAR data were in general agreement with

the high-resolution GPS data collected by the DPI and as of 2011 were less than pro rata cumulative subsidence predicted by Freij-Ayoub et al. (2007) out to 2031. However, Freij-Ayoub et al. (2007) mentioned that their modelling results indicated lower rates of subsidence in earlier years.

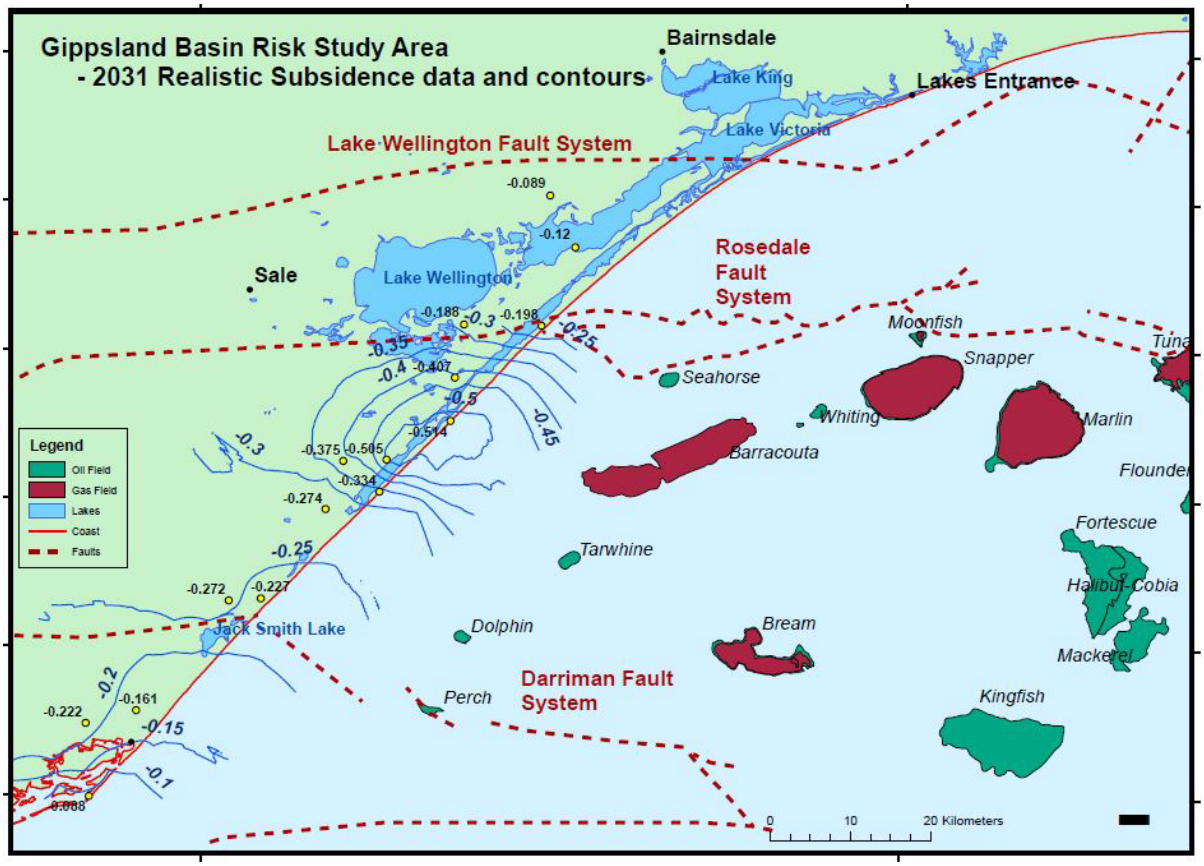

Figure 15. Contours of predicted cumulative subsidence (m) by 2031 due to declining water levels in the Latrobe Aquifer in the Gippsland Basin (reproduced from Freij-Ayoub et al. 2007)

4. Sources and impacts of subsidence

Subsidence associated with CSG production does not occur in isolation. Depending on the characteristics and usage of the land above a CSG field, other contributors to observed *surface movement* can include the shrinking and swelling of soils, depressurisation of shallow aquifers, and surface compaction and erosion. It is, therefore, important to be able to untangle the different components of net surface movement. This will facilitate better understanding of the distribution and significance of CSG-induced subsidence in the context of key geomechanical characteristics and processes of the shallow geological framework, more accurate forecasting of future subsidence caused by CSG production, and a sound technical basis on which the industry and regulators can respond to real or perceived impacts of CSG development.

The concepts of disentangling the simultaneous processes that drive subsidence and establishing a baseline for surface movement have received some attention in the literature (Fokker et al. 2019; Masoudian et al. 2019b), but these works are far from complete, especially in the context of CSG production. In its latest Underground Water Impact Report, OGIA assessed, observed and predicted CSG-induced subsidence in the context of a background trend of surface movement, rather than a reference level for surface elevation (OGIA 2021). This was intended to acknowledge the seasonal fluctuations in surface elevation that occur due to farming activities or the prevailing weather (i.e., rainfall), as well as the long-term trends that are seen in various locations throughout the Surat CMA but are not yet fully explained (Masoudian et al. 2019b).

In this chapter, a selection of natural and anthropogenic sources of subsidence (besides CSG production) and surface movement are discussed. Their relative magnitudes are contrasted with those related to CSG production and other activities such as groundwater abstraction, conventional oil and gas production, and underground mining. In closing, the potential impacts that could occur due to CSG-induced subsidence are discussed in the context of other more significant causes of subsidence. It should be noted that it is outside the scope of this EN to discuss, in detail, the potential impact of subsidence on agricultural practice and economics (e.g., drainage rates of irrigated cropping land, crop yield as a function of drainage) or surface- and groundwater-dependent ecosystems (GDEs) and associated ecosystems. At the time of writing (2023), complementary work on the potential for subsidence-induced impacts on farmland was being undertaken by the GasFields Commission Queensland (GasFields Commission Queensland 2023) and OGIA.

4.1 Natural and anthropogenic sources of surface movement

Recent and ongoing studies (see, for example, Leonardi et al. 2017) have attempted to quantify and then explain the drivers of surface movement that are unrelated to CSG production but still observed in large-scale InSAR (see Section 5.1 for a description of InSAR) surveys over the Surat CMA. Here, a summary of this work is presented, focusing on the most widespread and variable of these drivers, which is the shrinking and swelling of shallow soils due to change in moisture (which may be natural or anthropogenic). A brief discussion of erosion and sedimentation and the influence of agricultural activity, particularly grazing, is also included.

4.1.1 Compaction and swelling of soils

Soils may compact (i.e., shrink) or swell as a function of moisture change and material parameters, which can result in observable upward (i.e., uplift) or downward (i.e., subsidence) movement at the surface. The compaction of soil is a consequence of reduced pore volume and, when a soil is saturated, this volume change is equivalent to the amount of pore water expressed or removed. Conversely, the swelling of a saturated soil results from the absorption of additional water. The presence (or absence) of clays is a major contributing factor in the degree which these

phenomena occur. A summary of documented cases of subsidence and uplift related to soils and unconsolidated sediments is provided in Table 3, which has been reproduced from Leonardi et al. (2017). Where these examples are related to surface activities and anthropogenic activity they are defined as exogenic, and where they are related to natural earth movement they are defined as endogenic (Prokopovich 1986).

Table 3. Summary of subsidence and uplift processes related to soil and unconsolidated sediments

Location	Process	Endogenic or exogenic	Estimated subsidence or uplift (m)	Comments and references
Soils (up to a depth of approximately 10 m)	Swelling and shrinkage	Exogenic	Up to ± 0.16	Dependent on the clay type Tu and Vanapalli (2016) Crilly and Driscoll (2000) Briaud et al. (2003)
	Natural climate variation	Exogenic	0.06 maximum recorded	Fityus et al. (2004) McIntyre et al. (1982)
	Erosion and flooding near coastal areas	Exogenic	Approximately 0.001 to 0.015 per year	Erosion and flooding near coastal areas
	Earth tide and barometric loading	Endogenic	0.3 to 0.4 maximum	Phillips et al. (1999)
Alluvium (up to a depth of approximately 130 m) and colluvium	Earth tide and barometric loading	Endogenic	0.3 to 0.4 maximum	Phillips et al. (1999) Watson et al. (2006)
	Irrigation	Exogenic	Up to 0.04	Swelling clays in Namoi Valley Ross and Jeffrey (1991)
	Groundwater head fluctuation	Exogenic	0.04 to 0.075	Seasonally variable elastic compaction Fityus et al. (2004)
	Excessive groundwater pumping	Exogenic	0.08 in four years (Narrabri)	Inelastic compaction

Data sourced from Leonardi et al. (2017)

The degree to which clay-rich geological units will shrink or swell primarily depends on the mineralogical content of clays and the water retention properties of soils. Of the three main clay mineral groups, smectites have the greatest propensity for swelling with time, followed by illites and kaolinites (de Vallejo and Ferrer 2011). The (cyclic) phenomenon of soil shrinking and swelling can represent a significant natural hazard when it results in differential settlement of the ground surface (Nowamooz 2014). Changes in hydrogeological conditions, including natural groundwater response to rainfall recharge, response to groundwater abstraction, and also seasonal irrigation and

drainage, can result in cyclical fluctuations in volume in clayey material which then cause swelling or shrinking. The degree of tree and/or ground cover and the thickness of the vadose zone also influence this phenomenon.

Approximately 20% of the Australian land surface is covered by expansive clays (Fityus et al. 2004) and a number of studies have been undertaken to improve understanding of their behaviour. The active depth (seasonal water suction) is typically assumed to be between 1.5 m and 2 m when estimating the change in swelling and shrinking, which is in accordance with Australian Standard (AS) 2870 for the Newcastle area in New South Wales. At shallower depths, subsidence caused by water table changes is related to changes in soil saturation (i.e. drying) (McIntyre et al. 1982). It is important, therefore, to understand the relationship between soil suction, water retention, and volume change at these depths.

The magnitude of soil shrinkage can be irreversible if fissuring occurs, typically due to exceeding of the tensile strength (Pineda and Sheng 2013). During drying periods, soil cracks that develop can increase the hydraulic conductivity of soil by one to three orders of magnitude (Sadek et al. 2007; Yesiller et al. 2000). These cracks then provide high-conductivity flow paths that subject deeper layers to variations in water content (Auvray et al. 2014). Conversely, a rising water table will cause the expansion of swelling clays (e.g. Jahangir et al. 2012). Using a series of experiments, McIntyre et al. (1982) found that soil saturation occurs via two mechanisms. First, water enters the macropores of the soil and saturates the matrix, after which wetting is followed by filling of macropores. It was found that the extent of swelling and shrinking is dependent on the period in the wetting-drying cycle and, therefore, the soil suction, as well as whether the soil is in the initial state of saturation or has been rewetted before.

At a site near Newcastle, New South Wales, the extent of surface movement as a result of soil moisture change has previously been measured between 47 mm and 75 mm (Fityus et al. 2004). Crilly and Driscoll (2000), having focused on a site in Kent, England, found that surface movement varied between 60 mm and 160 mm for 35% water saturation and 100 kPa to 200 kPa soil suction. This study also found that the driver of movement occurred in the top 8 m of soil but was not limited to this depth. At a study site in Arlington, Texas, Briaud et al. (2003) found that the active zone extended to an approximate depth of 3 m and the heave on the surface was 37 mm.

The mechanism that drives compaction of shallow soils is analogous to that in deeper aquifers and reservoirs. The withdrawal of groundwater from storage lowers the hydraulic head, resulting in an increase in effective stress. Put another way, the mechanical load that was previously supported by the pore pressure is transferred to the soil skeleton. This can lead to irreversible compaction of the geological unit(s) if too much water is withdrawn and the mechanical loading on the soil skeleton is excessive (Alley et al. 2002). In addition to vertical compaction and subsidence, lateral shrinkage of geological units can occur where the water table is lowered (Pineda and Sheng 2013). Consequently, Doornhof et al. (2006) introduced side-burden as material which is not compacted during the fluid extraction but serves as support by providing an arching effect.

Owing to their relatively high porosity and permeability, water moves rapidly in and out of sand formations. Clay layers, however, require longer to depressurise and so drainage will occur in clays until the excess pore pressure equals that in adjacent sand layers. Although the processes that occur in clay and sand formations are similar, the orientation of clay particles changes becoming perpendicular to the applied vertical load during a reduction in hydraulic head (Kasmarek 2004). This change in grain orientation reduces porosity and manifests in compaction. The research of Gabrysch (1975) indicated that 90% of clay compaction is permanent and, therefore, changes in pore pressure will have little effect on surface movement. However, this work also concluded that if a significant number of clay layers are present, subsidence can occur due to the summation of subsurface compaction. In general, the process will take longer in silt and clay layers, which exhibit high compressibility and low hydraulic conductivity, and will continue until it reaches equilibrium. The time required to reach equilibrium is a function of the pore pressure change, vertical hydraulic conductivity, thickness of material, and specific storage.

Assuming no change in overburden load (i.e., constant total vertical stress), the compaction, Δb, for confined sediments is proportional to change in head, ΔH_f (Kasmarek 2004),

$$\Delta b = -S_s B_0 \Delta H_f, \quad (14)$$

where S_s is the skeletal component of elastic or inelastic specific storage and B_0 is the thickness of the layer. This equation gives no consideration to delayed drainage and thus assumes instantaneous equilibration of heads (Erban et al. 2014). Ideally this behaviour would be reversible under small strains. However, the behaviour of soil following repeated loading and unloading due to dewatering is not perfectly elastic (Galloway et al. 1998). The response of unconsolidated, higher-permeability sediments to change in head is different to that in clayey aquitards. The change in head in the former system will not change the geostatic pressure. As a result, the increase in effective stress will be equal to the decrease in fluid pressure and the compaction will be instantaneous. A proportion of the compaction will recover when the head recovers, but not entirely (Poland 1984).

4.1.2 Topography changes due to erosion, sedimentation and active tectonics

Weathering, erosion, sedimentation and dissolution are slow processes which occur over geological timescales (e.g., 1 cm to 2 cm per million years). Although erosion rates have increased during the recent Cenozoic era, the process is slow in comparison to the average human lifespan. For this reason, it is unlikely that any of these processes will make significant contributions to observed surface movement in areas of CSG production.

Active tectonics relates to the ongoing geological processes and movements of Earth's crust that result in the formation of earthquakes, faulting and deformation. A review of these processes concluded that they can be observed in the form of uplift, depressions, escarpments, upwarping, and earthquake records (Leonardi et al. 2017). The influence of active tectonics can also be seen in subtle changes in sedimentation behaviour. This is pertinent because both local and regional changes in topography (i.e., surface gradient) can affect the style and pattern of surface water flows, as well as discharge volumes, in alluvial systems.

The literature documents evidence of subsidence associated with the deposition of sediment in river systems, whereby the weight of deposited material results in grain rearrangement and compaction in deeper sediments. The Mississippi River delta is one example (Allen 1984). As reported by Ingebritsen and Galloway (2014), the compaction of unconsolidated river sediments can result in subsidence rates of 1 mm to 10 mm per year. Rising sea levels and more frequent climate extremes mean that river deltas are increasingly exposed to risks associated with subsidence (Knutson et al. 2010).

4.1.3 Movement of soil and sediments due to barometric (un)loading

The cyclic nature of earth tides and barometric pressure fluctuations means that they can exert loading and unloading effects both at the surface and on subsurface hydraulic heads (e.g., a fluctuation of 20 hPa in barometric pressure results in groundwater level changes of 20 cm). The barometric efficiency of an aquifer can be estimated as the ratio of the responses of hydraulic head to the atmospheric pressure change. The loading efficiency, which is defined as the reciprocal of barometric efficiency, can then be used to estimate the compressibility of a formation and the aquifer's specific storage.

A method that quantifies the earth tide component, thereby facilitating the analysis of aquifer properties, was developed by Acworth et al. (2016). This extended earlier research (Gonthier 2007; Merritt 2004) by improving the quantification and removal of earth tide impacts. The primary applications of this technique lie in the assessment of subsidence and groundwater resource evaluation, both of which result from groundwater extraction (Acworth et al. 2016). David et al. (2017) applied these techniques to estimate compressibility and storage changes in overburden rock during subsidence associated with longwall coal mining. Recent works by McMillan et al. (2019) and Rau et al.

(2022) have significantly improved in situ estimation of barometric and earth tide and the application of this method to both natural and induced groundwater level variations.

4.1.4 Other contributions to the background trend

To investigate the existence of a background trend of net surface movement in the Surat CMA, Masoudian et al. (2019b) analysed InSAR observations (see Section 5.1 for a discussion of InSAR) over regions featuring no active CSG wells (referred to here as non-producing regions) for the period July 2012 to November 2016. The first step in this process was to inspect the surface elevation change over the entire dataset to identify a number of regions of interest for further interrogation. This resulted in the selection of four focus areas, within which a maximum apparent subsidence of 50 mm (approximately 10 mm/year) was observed.

The spatial distribution of net surface movement and the temporal distribution of rainfall for two of these focus areas are reproduced in Figure 16. One focus area (FA1) covers more than 450 km^2 along the Dawson River, south-west of Taroom. Land use information for FA1 indicates that it is primarily classified as grazing native vegetation, with some cropping. The other focus area (FA4) is approximately one order of magnitude smaller than the others studied by Masoudian et al. (2019b). It is located near the Yuleba State Forest, between Roma and Miles, and covers almost 27.5 km^2. The land use classification for FA4 is primarily grazing native vegetation, with some production native forests and some cropping.

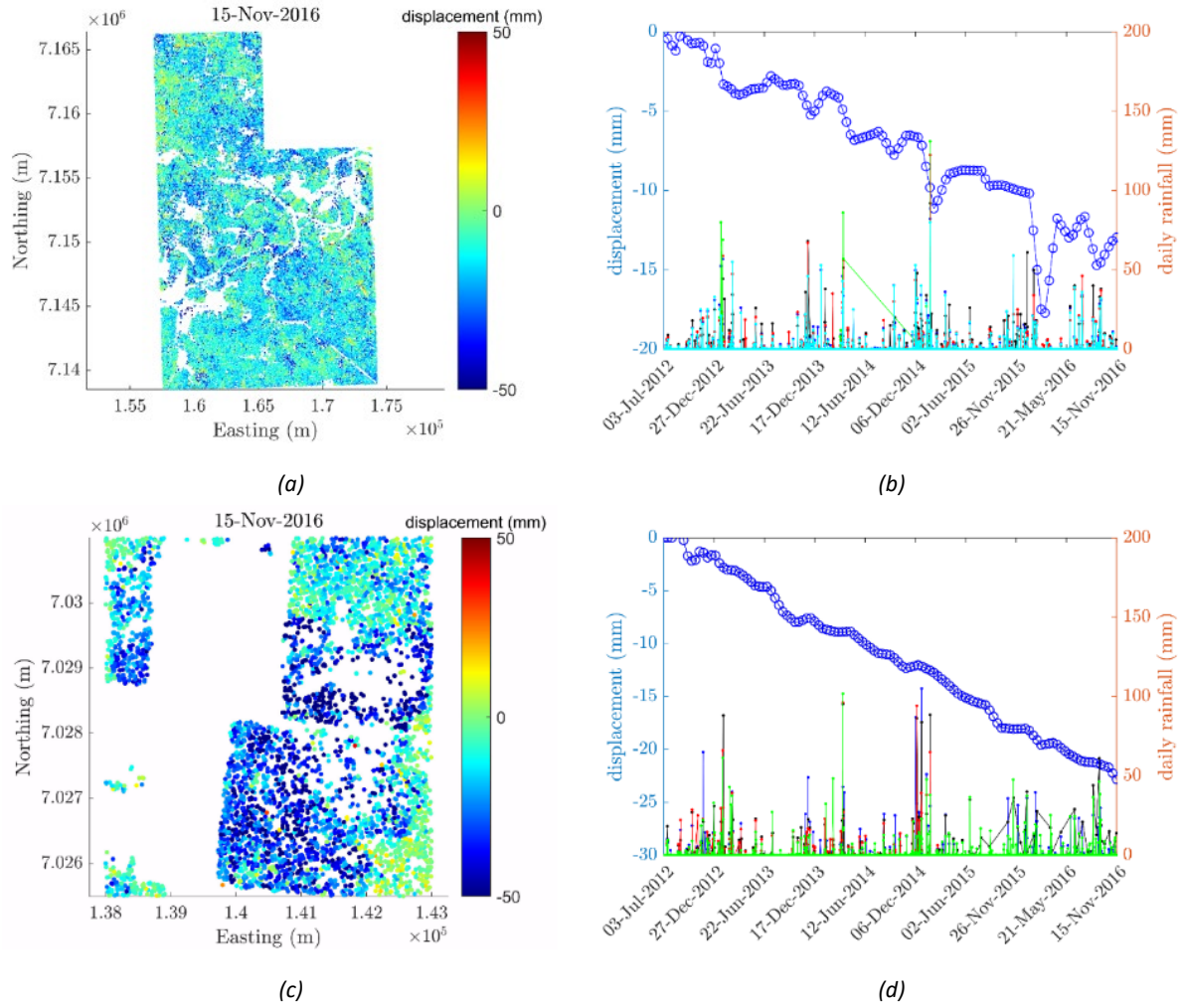

Figure 16. Observations of net surface movement and rainfall from July 2012 to November 2016 for two non-CSG producing regions (FA1 and FA4) in the Surat CMA, showing (a) InSAR measurements of net surface movement in FA1, (b) the average movement of FA1 and rainfall data from four gauges, (c) InSAR measurements of net surface movement for FA4, and (d) the average movement of FA4 and rainfall data from four nearby gauges (reproduced from Masoudian et al. 2019b)

While all of the four focus areas exhibited apparent downward surface movement (i.e., subsidence) over the period of observation, this was most pronounced in FA1 and FA4. In FA1 the apparent subsidence was widespread, with localised maxima of approximately 50 mm (see Figure 16.(a)). The average movement for the area showed a consistent downward trend, with temporal fluctuations that appear to correlate with periods of high rainfall (see Figure 16.(b)). The local, temporal minima coincide with heavy rainfall events during the wet season. It can be seen that following these events the ground surface moves upwards (uplift), reaching the largest uplift almost immediately after the peak of rainfall. Thereafter the ground surface returns to a downward (subsidence) trajectory during the dry season. This (and other cases discussed in Masoudian et al. (2019b)) suggests that the fluctuations observed in the mean surface displacement are due to the effect of rainfall infiltration into shallow soil layers near the surface. Further data interrogation in FA1 found that the soil composition is susceptible to consolidation and the swelling and shrinkage that can be induced by rainfall infiltration. However, this apparent correlation cannot fully explain the overall trend of downward movement of the ground surface. It can be argued that the effect of rainfall infiltration may be associated with some hysteresis so that the downward movement of the ground surface does not fully

recover during the wet season. Alternatively, the background trend may be due to a longer-term period of soil and alluvia drying due to below-average rainfall.

The surface movement data in FA4 (see Figure 16.(c)) showed a well-defined region of approximately 50 mm movement, which appears to align with paddocks. The absence of InSAR data in the middle of FA4 is most likely due to low coherence and poor data quality as a consequence of seasonal plant growth or erosion. Looking at the average movement for the area (see Figure 16.(d)), it can be seen that it does not fluctuate with rainfall to the same degree as FA1. This suggests that the (unattributed) cause of net surface movement associated with agricultural activity is a bigger contributor than seasonal infiltration and drying in this location.

Another interesting observation made during this study is highlighted in Figure 17., which plots the net surface movement observed in a diamond-shaped region at Savannah, south of Roma, which is remote from CSG production. This shows downwards surface movement of approximately 50 mm. However, interrogation of the satellite image of this area suggests that it is delineated by the line of a fence used for holding livestock which have (probably) contributed to compaction and or erosion. Although the magnitude of movement is similar to that observed in FA1 and FA4, the underlying cause is significantly different. As no CSG production occurs in this location, the inference made from the data is that the surface elevation change is a consequence of compaction and erosion caused by livestock.

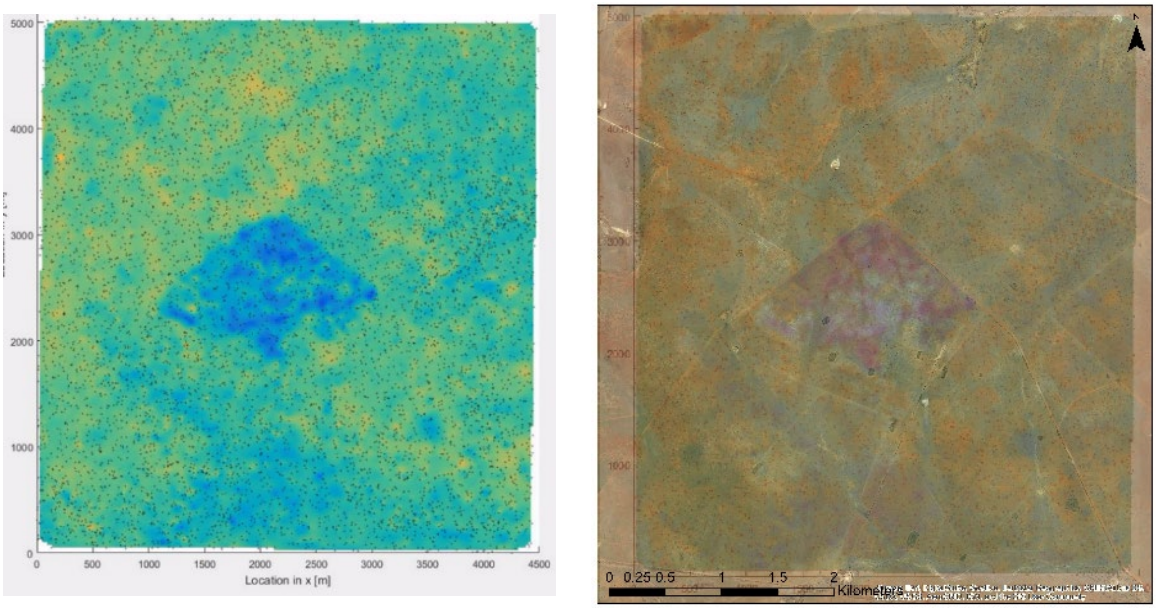

(a) *(b)*

Figure 17. Observed net surface movement in an area measuring 4.5 × 5 km at Savannah, south of Roma, showing (a) surface movement away from the satellite (i.e., downward) of approximately 50 mm in the period July 2012 to November 2016, and (b) a satellite image of the same location highlighting a fenced paddock (reproduced from Masoudian et al. 2019b)

4.2 Potential impacts of CSG-induced subsidence

Some of the subsidence magnitudes associated with aquifer depletion worldwide (e.g., San Joaquin Valley) are extreme. However, when considering the potential impacts of subsidence associated with CSG production, it is important to consider their magnitude in the context of other drivers, both natural and anthropogenic, particularly those likely in Australia. Figure 18. helps with this comparison by highlighting the characteristic subsidence profile

and typical magnitudes associated with CSG production, bord and pillar coal mining, longwall coal mining, and multi-seam coal mining. In terms of absolute magnitude (and also gradient), it is clear that underground coal mining is the most significant source of historical and potential future subsidence. By way of further comparison, local CSG-induced subsidence data are similar to those observed from CSG production in the Powder River Basin and of the same order of magnitude as surface elevation fluctuations caused by seasonal variation of clayey soils. The magnitude of subsidence expected from CSG production is not large and may be similar to other natural phenomena that could be expected to occur in the same area (e.g., localised erosion, the shrinking and swelling of soils and alluvia).

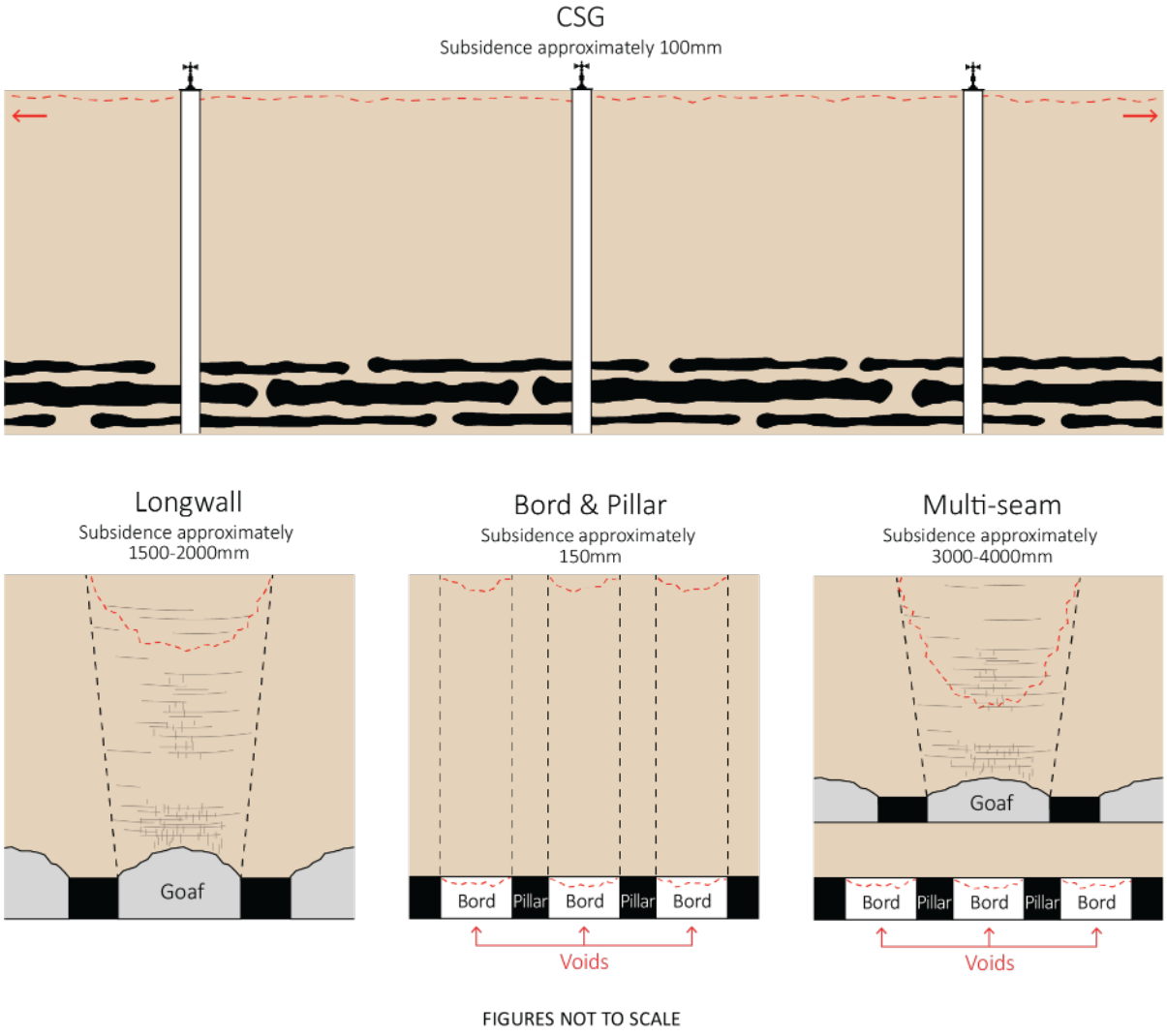

Figure 18. Comparison of the subsidence profile and magnitude associated with CSG production, longwall coal mining, bord and pillar coal mining, and multi-seam longwall mining in Australia

To assist with the management of potential impacts of CSG-induced subsidence, the GasFields Commission Queensland (GFCQ) commissioned two interrelated bodies of work in 2022. The first is a review of the regulatory framework related to CSG-induced subsidence; the second is an investigation of the potential for and consequences of CSG-induced subsidence at the scale of a co-located property, such as a farm. The review (GasFields Commission Queensland 2022) found that, although landholders are protected by existing compensation liability for CSG-induced subsidence impacts, there existed scope for enhancement and clarification of the regulatory framework. This resulted in the tabling of eight recommendations to the Queensland Government, which were designed to 'enhance existing protections and provide clarity to landholders and the gas industry' (GasFields Commission Queensland 2022).

Subsequent to the review, research on the potential for CSG-induced subsidence impacts and consequences at the farm scale is being conducted by the GFCQ (GasFields Commission Queensland 2023) in partnership with OGIA. At the time of preparing this document (2023), this work had reported that farm drainage is the key issue, CSG-induced subsidence must be considered in the context of other variations, each farm is unique and carries different susceptibility to subsidence impacts, further predictive modelling at the farm scale is critical, and it is expected that rectification work may be required on some farmland because of CSG-induced subsidence.

4.2.1 Impacts on built infrastructure

A review of the literature reveals no peer-reviewed research or verified accounts of adverse impacts caused by CSG-induced subsidence. Best et al. (2014) summarised a range of potential impacts based on the experience associated with coal mining and groundwater abstraction for irrigation or mining. In the intervening years, it has become apparent that many of the listed impacts are not relevant to CSG production in Australia because of increased understanding of the maximum subsidence magnitudes to be expected. In addition, CSG-induced subsidence will not result in the surface curvature that can be seen at the edge of a subsidence trough above a longwall coal mine. Therefore, the likelihood of impacts on built infrastructure due to differential settlement, such as large gradient change or surface fissures, is extremely low.

Some Queensland CSG production is co-located with intensive, irrigated cropping on vertosols that contain a high percentage of expansive clay minerals. Depending on the site classification of clay type and reactivity (Standards Australia 2011), the range of vertical soil movement (i.e., shrinking and swelling) can be up to 75 mm. Indeed, some Class E sites in south-east Queensland have been known to move up to and in excess of 150 mm (Queensland Building and Construction Commission 2022). The variation in soil moisture underneath and adjacent to building foundations can, consequently, induce differential movement which damages structures, as shown in Figure 19. Australian construction standards (Standards Australia 2011) prescribe the maximum design differential footing deflection for different types of construction. The maximum differential deflection gradient ranges from 1:300 for clad frame to 1:2,000 for full masonry construction, while the maximum differential deflections for these categories are 40 mm and 10 mm, respectively. These design gradients are several orders of magnitude greater than that expected and observed from CSG-induced subsidence (see discussion related to water resources and infrastructure below). In this context, the risk of additional impact on structures from CSG-induced subsidence is deemed low.

Induced curvature in buried pipelines can create tensile and compressive stresses due to bending. Bracegirdle et al. (1996) presented empirical data outlining the gradient limits beyond which damage would occur. For relatively rigid pipes, more than 200 mm in diameter, the induced slope limitation was listed as less than 1:140. For relatively flexible pipes, less than 200 mm in diameter, the induced slope limitation ranged between 1:140 and 1:40. Exceeding the more conservative of these limits (i.e., 1:140) would require 100 mm of subsidence to develop over a distance of 14 m, which is not expected to result from CSG production and thus is not a significant risk.

Subsidence has the potential to damage the casing of water bores and gas wells. Ross and Jeffrey (1991) reported on the increased failure rate of production bores in the Namoi Valley, which was attributed to the subsidence caused by groundwater removal. The greatest proportion of CSG-induced subsidence stems from compaction in the coals (Masoudian et al. 2019a). Many groundwater bores are completed in formations above the coals, which reduces the likelihood of damage to these bores. The potential for damage (e.g., casing shear and distortion, screen collapse) to deeper bores and gas wells remains.

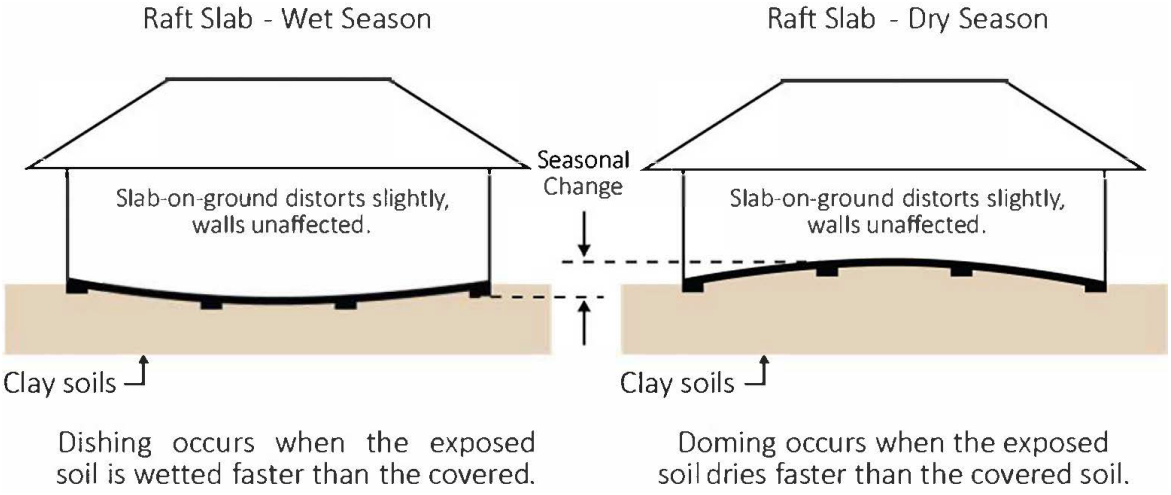

Figure 19. Mechanisms of foundation deformation due to gradients of soil moisture surrounding a structure (reproduced from Queensland Building and Construction Commission 2022)

Vertical settlement, horizontal strain and compaction, tilt and ground curvature can cause damage to roads, which may manifest as compression humps, tension cracks, and a distortion of the road surface (Best et al. 2014). The potential for this to be caused by CSG-induced subsidence is dependent on the change in surface gradient. The limits on allowable change in grade of road pavements are typically 0.3% in 40 years for concrete pavements and 0.5% in 20 years for flexible pavements (Wong and Summerell 2012), which are significantly greater than the predictions and measurements published by OGIA (2021). Therefore, the risk of impacts on roads associated with CSG production are considered small, and the same conclusion can be drawn for rail infrastructure. It should be noted that the ARC Training Centre for Advanced Technologies in Rail Track Infrastructure at the University of Wollongong, in collaboration with the University of Queensland, commenced research in 2022 investigating the effect of moisture and cyclic loading on the deformation of railway embankments and expansive soil subgrades. In 2021, this project established long-term field monitoring at the West Moreton System in Chinchilla for the collection of data on local weather conditions, surface settlement, and soil moisture and suction profiles with depth at two railway transects.

4.2.2 Impacts on water infrastructure and environment

Subsidence due to groundwater withdrawal can result in impacts on hydrological systems such as aquifers, lakes, streams, springs, and other surface water resources. This can manifest as a change in the drainage pattern of streams and channels, ponding of water in subsidence troughs (if they form), deepening or widening of pools in streams, or alteration of riparian ecosystems and geomorphological stability. Subsidence can also increase the impact of, or exposure to, riverine flooding or delayed drainage. Coastal impacts such as storm surge or the impact of tides are no risk to CSG-producing regions in Australia.

The potential connectivity of groundwater with surface waters and the possibility of impacts on subterranean, aquatic and terrestrial GDEs is challenging to predict and quantify. Nonetheless, these are important for evaluating the potential environmental repercussions of CSG production and induced subsidence that may affect groundwater and its dependent ecosystems. For example, CSG subsidence may have a subtle effect on surface drainage that could potentially change terrestrial GDEs. Although subsidence can affect different types of GDEs in different ways, detailed consideration of the ecological consequences of subsidence on groundwater-dependent species, biodiversity and ecosystem function is beyond the scope of this EN.

Where CSG operations are co-located with intensive agriculture, one potential impact relates to changes in terraformed surface gradients which are used to control the flood irrigation of crops such as cotton and grain (see Figure 20.). This approach to broadacre irrigation requires paddocks to have a planar, but furrowed, surface of

constant gradient in the order of 0.1% (i.e., 1:1,000, or 1 m fall per 1,000 m) but no less than 0.06%. Paddock slopes of less than 0.06% are considered too flat to drain effectively and will become waterlogged during periods of above-average rainfall (Purcell 2012). Flood irrigation is most effective in paddocks with uniform gradient as this helps maintain even wetting of the soil profile, and so farmers will periodically deploy techniques such as *laser levelling* to remediate gradient changes that occur over time (e.g., the formation of *gilgai*, or small water holes).

At the time of writing (2023), no scientifically verified accounts or technical reports of significant changes to surface gradient as a consequence of CSG-induced subsidence had been documented. However, it is instructive to consider the potential for this to occur based on the current understanding of likely subsidence magnitudes, noting that the thickness of compressible formations (e.g., coal seams) changes over large distances and the depressurisation of those formations is diffusive. Put another way, the two key drivers of CSG-induced subsidence vary in space over distances in the order of hundreds of metres, and thus the same could be expected of the associated compaction. Recent predictions and observations of maximum CSG-induced subsidence in the Surat CMA (OGIA 2021) are approximately 100 mm to 150 mm. If this magnitude of movement were to develop over a distance of 1 km, it would result in a gradient change of 0.01% to 0.015%, which could result in marginal to poor drainage of a paddock that was initially close to the threshold of 0.06%. However, according to OGIA (2021) the change in ground slope from CSG-induced subsidence in most areas is predicted to be less than 0.001% (i.e. 10 mm over 1 km), with some areas up to 0.004% (i.e. 40 mm over 1 km). During parametric uncertainty quantification, it was found that in a localised area north of Cecil Plains there exists 80% probability of the maximum change in slope exceeding 0.005% (OGIA 2021), which is still significantly less than that required to alter drainage patterns.

Figure 20. Flood irrigation of a furrowed cotton paddock near St George, in the south-west corner of the Surat CMA (modified from Wikimedia Commons, File:StGeorgeCottonIrrig.jpg)

As a part of the Draft Water Monitoring and Management Plan for the Surat Gas Project, Arrow Energy commenced the use of airborne LiDAR survey to measure baseline gradient changes within its tenements (Arrow Energy unpublished 2022). Among other objectives, the intent of this work was to describe the representative slope on dryland or irrigated cultivation within the company's tenure, the accuracy with which the surface and slope on cultivated land can be measured, and the variation in ground surface elevation that can be observed with soil moisture changes. According to the analysis of slopes, most of the cropping paddocks of the Darling Downs and within Arrow's tenements have slopes ranging from 0.12% to 0.5%, which are two orders of magnitude greater than any changes predicted by OGIA (2021). Using strip cropping as an indicator of swelling and shrinking, it was found that up to 200 mm surface elevation difference can result from soil moisture changes. As this longitudinal study continues, more quantitative

information on natural and anthropogenic sources of surface movement in locations of intensive agriculture will become available.

No documented cases of adverse impacts on agricultural dams caused by CSG-induced subsidence, or other sources of surface movement, could be found in the academic literature or Queensland Land Court records. Given that the magnitudes of elevation and slope change caused by CSG-induced subsidence are small, the future risk to agricultural dams is considered to be low.

5. Subsidence monitoring techniques

The large spatial extent of CSG production regions makes accurate monitoring of any widespread surface movement challenging. While in-situ monitoring techniques can produce high-accuracy measurements, the spatial extent is limited to the immediate installation location. This makes the widespread use of these techniques inadequate and cost-prohibitive for large-scale monitoring. They can, however, be used to complement large-scale monitoring methods. Outlined in this chapter is a summary of the main techniques that can be used to monitor surface movement in regions of CSG production.

5.1 Interferometric synthetic aperture radar

A well-established surface movement monitoring technique is interferometric synthetic aperture radar (InSAR). It has been successfully used for over 25 years to detect and monitor surface movement for a range of applications, including sub-surface infrastructure development (e.g. transport tunnels), underground mining activities (e.g. longwall mining), groundwater extraction, aquifer recharge and discharge, magma chamber inflation and deflation, and the interseismic, coseismic and postseismic stages of the seismic cycle (Ferretti 2014; Hanssen 2001; Moreira et al. 2013). For example, InSAR was used in combination with global navigation satellite systems (GNSS; see Section 5.2) and levelling measurements by Fuhrmann et al. (2015) to calculate the velocity of movement of the Upper Rhone Graben in central Europe, while Fakhri and Kalliola (2015) used InSAR techniques to monitor surface movement in central Greece. While InSAR provides large spatial coverage, it has lower accuracy compared to in situ measurements.

InSAR uses two synthetic aperture radar (SAR) images taken at different times over the same area to identify any topographic height changes. Each image observes the same ground point from slightly different geometry, which enables relative differences in distances (i.e., phase) between the images to be obtained via trigonometry. If the Earth's surface has moved between image acquisitions, a *phase shift* occurs, as shown schematically in Figure 21. This shift is represented in an interferogram as a series of colour cycles or interference fringes, where one fringe represents a phase change of 2π radians. The colour order determines if there has been a shift towards or away from the SAR sensor. The interferometric results provide estimates of topographic heights and surface movement, with height measurements comparable to optical remote sensing methods.

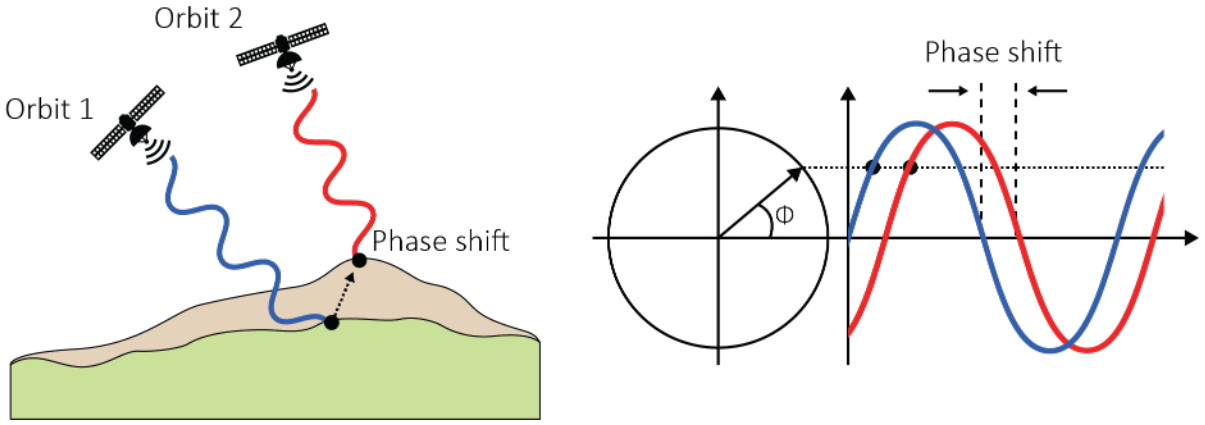

Figure 21. Schematic representation of the phase shift between SAR images where the Earth's surface has moved between image acquisitions

Differential InSAR (D-InSAR) takes InSAR a step further, by isolating surface movement signals through the removal of the topographic signal component (Hanssen 2001). For monitoring slow (i.e., over a number of years) surface movement changes, such as those that may be associated with CSG production, a time-series dataset using multiple interferograms is required.

5.1.1 Synthetic aperture radar systems

SAR systems transmit pulses of microwave energy to the Earth's surface and record the amount backscattered. The pulses' two-way travel time is then used to resolve a surface object's range and physical characteristics. The ability of microwave energy to penetrate rain (unless wavelength is less than 4 cm) and clouds provides SAR systems with an all-weather, day and night capability (Hanssen 2001; Jensen 2000; Ulaby and Long 2014).

SAR systems are side-looking, and most SAR satellite systems are right-looking systems: they transmit energy pulses from the system's right side relative to the flight direction (line of sight (LOS)). All systems have the same geometric components (see Figure 22.(a)); however, the parameters for components such as altitude, incidence angle and swath width can vary between systems. The resulting SAR imagery appears with slant range geometry, which looks different to the imaged ground surface. However, the imagery can be corrected to ground range geometry.

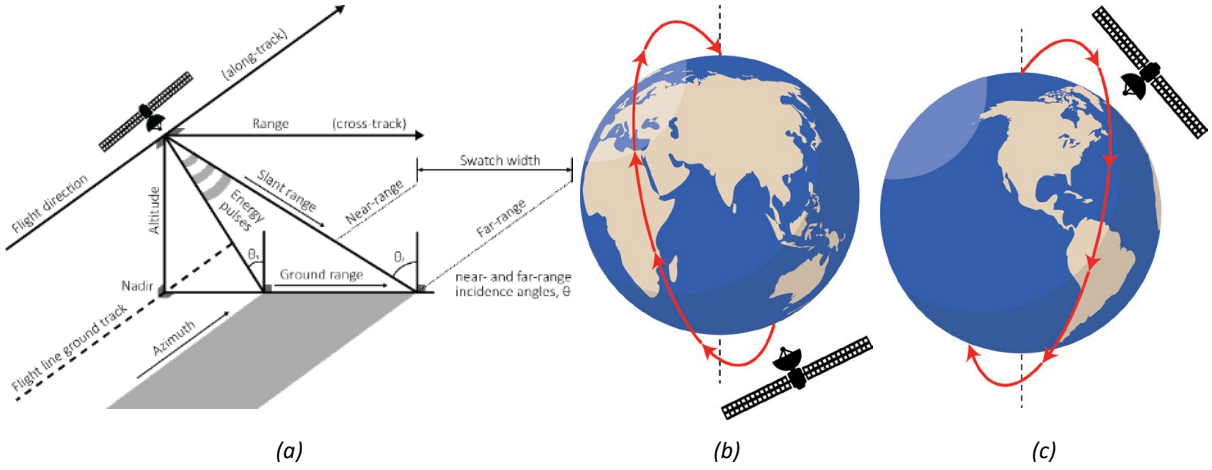

Figure 22. Aspects of a right-looking SAR satellite's trajectory, showing (a) the azimuth direction (parallel to the flight direction), emitted energy pulses perpendicular to the azimuth (range direction), the nadir (the point on the ground directly below the satellite's position), and the incidence angle (angle between the energy pulse and the nadir line) including near- and far-range angles as these constrain the swath width (modified from Jensen 2000); and the general polar sun-synchronous orbit orientation for SAR systems, showing (b) south to north (ascending) tracks and (c) north to south (descending) tracks

Each pixel in a single look complex (SLC) SAR image contains a complex number, with real in-phase (I) and imaginary quadrature-phase (Q) components. These components may also be described as amplitude and phase information. The amplitude details the ground surface's backscatter properties, and the phase represents the two-way travel distance. Phase differences between two SLC SAR images are exploited in the D-InSAR technique.

Due to the oblique or slant range geometry, geometric distortions are inherent in SAR imagery and need to be considered when working with such imagery. Topographic distortions occur in nearly all imagery, unless the ground surface is truly flat. The distortions include foreshortening, layover, shadowing and speckle (Jensen 2000; Ulaby and Long 2014; Woodhouse 2006).

SAR satellite systems use a polar sun-synchronous orbit which allows the same ground spot to be revisited at the same local time, thus enabling the same region to be imaged through time along a pre-defined pass or track. As the systems orbit, they can image the same region in ascending (south to north) and descending (north to south) tracks (Figure 22.(b) and (c)). Imagery acquired along each track can then be sliced into products or frames for further processing.

5.1.2 Coherence

For interferometry to be effective, the phase signals need to be coherent. This means that while the amplitude and phase components differ between two SAR images, the waves for each image have identical frequency signatures (see Section 3.4 of Ferretti (2014) for a detailed description). Coherence loss, or decorrelation, can be caused by either geometric or temporal factors. Geometric decorrelation occurs when the perpendicular baseline between images is too large, there are very steep topographic slopes, and/or the surface deformation gradient is too great for surface changes to be detectable. Temporal decorrelation results from changes in surface properties with time, such as weathering and vegetation changes (Ferretti 2014; Hanssen 2001; Woodhouse 2006). The effects of decorrelation can be reduced through selection of interferometric image pairs with small perpendicular and temporal baselines. Coherence information can also be used to identify surface changes, such as soil moisture and the extent and complexity of ruptured fault traces.

5.1.3 D-InSAR time-series processing workflow

To create a D-InSAR time-series dataset, there must be regular, repeat SAR imagery acquisitions over the study area. It is important to note that not all SAR imagery is suitable for interferometry. Some SAR satellite systems automatically take repeat acquisitions (e.g., ALOS1/2, Sentinel-1), while other satellite systems need to be tasked with taking imagery over specific areas (e.g., RADARSAT-1/2, TerraSAR-X). For the Surat CMA, full or partial coverage of suitable SAR imagery since 2007 is available.

Interferogram generation

A range of software packages are available for the generation of differential interferograms (e.g., SNAP, GAMMA, GMTSAR, ICSE). While each program has its own processing workflow, they all incorporate the necessary steps required to produce interferograms. Each initial interferogram contains different signal components that can be represented as (Pepe and Calò 2017)

$$\Delta\emptyset_{int} = \Delta\emptyset_{def} + \Delta\emptyset_{orb} + \Delta\emptyset_{topo} + \Delta\emptyset_{atm} + \Delta\emptyset_{scat} + \Delta\emptyset_{noise} \quad (15)$$

To isolate the deformation signal, $\Delta\emptyset_{def}$, the initial interferogram (Figure 23.(a)) is refined by estimating and removing other phase signal contributions. The expected phase for a *curved earth*, the orbit geometry, $\Delta\emptyset_{orb}$, is calculated (Figure 23.(b)) and removed to *flatten* the interferogram. A digital elevation model (DEM) is used to calculate the expected phase signal from topography, $\Delta\emptyset_{topo}$, (Figure 23.(c)) and is removed from the flattened interferogram. The flattened interferogram is then filtered to further reduce any residual noise, $\Delta\emptyset_{noise}$, and scattering, $\Delta\emptyset_{scat}$, effects. The resulting filtered interferogram should contain the isolated deformation signal and potentially atmospheric signals if the deformation signal is small. Atmospheric effects, $\Delta\emptyset_{atm}$, are not mitigated during interferogram generation but are considered during time-series generation.

The filtered interferogram is *wrapped* and displays deformation signals as a series of fringes or 2π cycles (Figure 23.(d)). To obtain the continuous phase signal, the fringes can be *unwrapped* to show the net relative surface movement between the two SAR image acquisitions in radians (Figure 23.(e)). The final step is to geocode the interferogram by converting from radar to geographic coordinates. There is an option to convert the radian values to linear displacements at this stage as well.

Time-series generation

In order to detect slow movements, such as interseismic deformation or groundwater extraction, a stack of interferograms (i.e., more than 20) covering a long time period is required to generate a time series of cumulative surface movement. Time-series techniques can be based on the use of persistent scatterers (PS), distributed scatterers (DS) or a combination of both (Xue et al. 2020). As the name suggests, persistent scatterer interferometry (PSI) relies on PS, while small baseline subset (SBAS) uses DS. Regardless of the time-series technique used, phase signals from atmospheric effects need to be considered, as these can mask signals related to slow surface movement. This is achieved by either estimating atmospheric signals through spatio-temporal filtering or calculating signals from external weather model data using, for example, PyAPS (Jolivet et al. 2011). A more detailed overview of time-series techniques can be found in the literature (Crosetto et al. 2016; Osmanoğlu et al. 2016; Xue et al. 2020).

SBAS was developed by Berardino et al. (2002). It utilises DS targets in interferograms separated by small baselines to minimise spatial decorrelation. DSs tend to be found in rural and mountainous terrain and are characterised by having several small and random scatterers that can be used to create a stable scatterer. This technique requires multi-looking to improve signal responses and therefore reduces image resolution (Osmanoğlu et al. 2016; Xue et al. 2020).

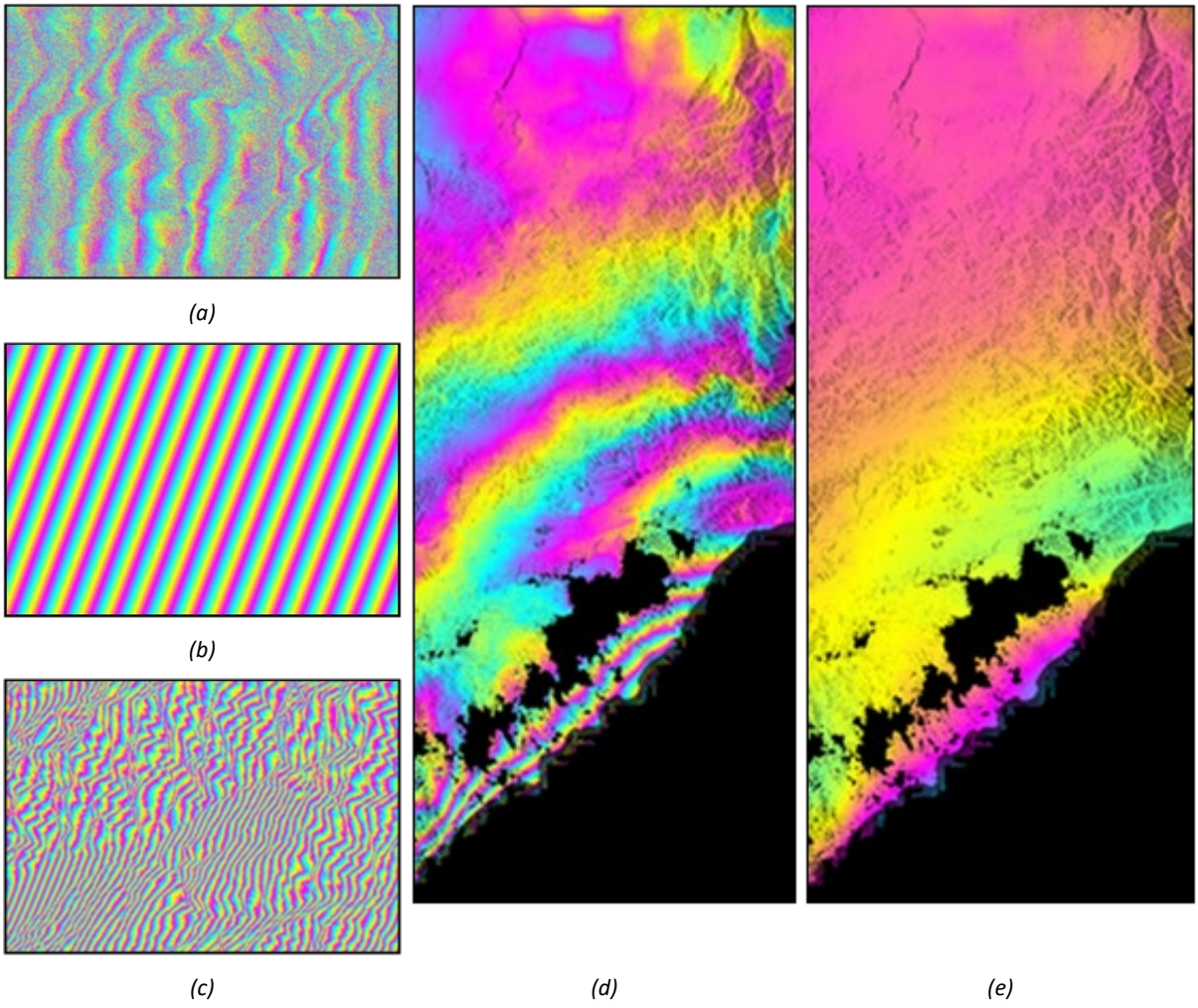

Figure 23. Steps in the D-InSAR processing workflow, showing (a) the initial interferogram, (b) orbital signal correction, (c) topographic signal correction, (d) wrapped differential interferogram, and (e) unwrapped differential interferogram (reproduced from Lawrie 2012)

PSI was first introduced by Ferretti et al. (2001) with the development of permanent scatterer SAR interferometry (PSInSAR®). PSI uses PS targets, which have a strong, stable response over long time periods. PSs are commonly found in urban areas, where buildings and other infrastructure provide ideal target responses. In contrast, they are often not present in rural and mountainous terrain because of the changing nature of the landscape. These scatterers also have dimensions smaller than the image resolution cell, which makes them unaffected by baseline decorrelation, unlike SBAS (Osmanoğlu et al. 2016; Xue et al. 2020). To overcome the limitations of PSI in non-urban areas, an advanced PSI technique, SqueeSAR®, was developed to integrate PSInSAR® into the SBAS technique (Ferretti et al. 2011). Other techniques that use PSI include interferometric point target analysis (IPTA) (Werner et al. 2003) and the Stanford method for persistent scatterers (StaMPS) (Hooper et al. 2004).

The time-series results represent the relative surface movement measurements in the LOS. To obtain absolute surface movement measurements, the use of in situ monitoring measurements is required in combination with, for example, corner reflectors. The geometry, orientation and size of these reflectors are linked to the microwave wavelength properties used by the SAR sensor. If they match, the reflectors will appear as a distinct pattern in the SAR imagery. This enables the reflector's precise ground location to be tied to a pixel location in the imagery, and the rate of change of absolute elevation to be calculated (Garthwaite et al. 2015).

Resolving three-dimensional movement

D-InSAR measurements are one-dimensional along the LOS, so measured movement is either towards or away from the satellite. To resolve movement in three dimensions (i.e., north, east, and up), different viewing geometries are required. One limitation is that D-InSAR derived from SAR satellite systems is insensitive to north–south movements. This is due to the near-polar orbits and small variation in incidence angles in the north–south direction. By using SAR imagery from ascending and descending tracks (see Figure 22.(b) and (c)), different viewing geometries are available, making it possible to resolve both horizontal (east–west) and vertical (up–down) movements (Hu et al. 2014; Ozawa and Ueda 2011; Wright et al. 2004).

Some D-InSAR processing workflows mathematically convert LOS measurements to vertical while disregarding the horizontal component. This often occurs when only one viewing geometry is available (i.e., ascending or descending). While this approach makes it easier to explain movement results to end users, it is likely to lead to errors. Pure vertical movement is unlikely to occur across a whole study area and there will be some horizontal component present in, for example, a subsidence bowl. If only one viewing geometry is available, it is preferable to leave the results in LOS and not approximate the vertical component of movement.

5.1.4 Limitations of InSAR techniques

Surface movement, topography changes, flat-earth differences in range, noise, and atmospheric effects all contribute to the total interferometric phase calculated from SAR data (see Equation 15). Air temperature, pressure, and water vapour (i.e., the weather) all contribute to the atmospheric phase effects, while vegetation and surface water induce dispersion in the reflected SAR signal (Tomás et al. 2014). It is, therefore, important to be cognisant of the precision and accuracy that is inherent in InSAR measurements of surface movement.

The maximum surface movement detectable by InSAR is governed by the wavelength, λ, of the radar. The maximum difference in phase for two neighbouring pixels can be 2π. This corresponds to one fringe which is equal to $\lambda/2$ (Mastro et al. 2020; Zhou et al. 2009). A number of precision estimates for both velocity (i.e., displacement rate) and total displacement can be found in the literature. For example, Tomás et al. (2014) calculated precisions of $\pm$1 mm/year and $\pm$5 mm for displacement rate and total displacement, respectively, using InSAR data from Spain. The work of Finnegan et al. (2008) estimated the uncertainty of relative displacement measurements to be approximately 5.4 mm by comparing GPS measurements with InSAR data from RADARSAT-1. This result was similar to the uncertainty estimate of 5.6 mm presented by Casu et al. (2006) using data from the Los Angeles area. In this work, it was also noted that uncertainty can increase at a rate of approximately 0.05 mm/km as observations get further from a reference pixel (e.g., a high-quality estimate from a reflector location). Finally, the work of Reeves et al. (2014), which is discussed further in Section 6.5, estimated the uncertainty of surface movement estimates from InSAR to be approximately 10 mm.

The most significant limitation on the utility of D-InSAR is temporal and geometric decorrelation. Depending on the satellite and wavelength used, decorrelation may not be a major issue. Recent satellites, such as Sentinel-1, have regular revisit times and small perpendicular baselines, so decorrelation is more likely due to major surface changes between acquisitions. Longer wavelengths (L-band) are more tolerant of larger temporal baselines, compared to shorter ones (e.g., C-band). Topographic characteristics can impact geometric decorrelation through the presence of geometric distortions (e.g., layover, foreshortening), but different viewing geometries can reduce the impact of these distortions. Vegetation density and growth can also affect geometric decorrelation, and the use of longer wavelengths in affected regions can mitigate the impact. This is particularly relevant over areas of intensive, irrigated cropping.

There are other limitations or considerations that should be understood when using D-InSAR. The insensitivity to north–south movement from satellite-derived SAR imagery can limit some study areas, such as faults oriented in the same direction. This can be overcome by using airborne SAR systems, as the flight path can be customised.

Understanding that the relative surface movement in the LOS is being recorded is important, along with the fact that D-InSAR cannot be used for real-time monitoring as the revisit time is fixed for satellites.

5.2 Differential global navigation satellite systems

Precise location information for a ground point can be derived from global navigation satellite systems (GNSS). GNSS is the generic term used for satellite positioning systems which consist of satellite constellations that transmit positioning and timing data to ground receivers. There are several constellations currently deployed, including Galileo (European Union), GLONASS (Russia), BeiDou (China), and GPS (USA). Data from a minimum of four satellites are required to obtain precise three-dimensional locations; however, signals can suffer from errors or delays during transmission to the Earth's surface. These errors can be mitigated via differential GNSS (DGNSS), by using data from one or more GNSS receiver stations whose precise locations are known (Hofmann-Wellenhof et al. 2008; Kaplan 2017).

DGNSS has the ability to measure locations with centimetre precision and be used to identify changes in location through time. In a partnership between Australia and New Zealand, the Southern Positioning Augmentation Network (SouthPAN) is working towards improving positioning accuracy from 5 m to 10 m down to 3 cm to 5 cm where mobile internet exists, and to 10 cm elsewhere. This will particularly benefit regional and remote areas, providing improved access to precise positioning services (Geoscience Australia 2022b).

Data can be collected by campaign measurements or from continuously operating reference stations (CORS). Campaign data collection requires temporary installation of a GNSS receiver for a specified period of time. To obtain a time series of any 3D location movement, repeat campaigns are required. There are 25 CORS currently operating in the Surat CMA (Geoscience Australia 2022c). However, the spacing of these sites is likely to be too large to detect local or regional scale surface movement (Garthwaite et al. 2015).

In 2014 a regional network of 65 permanent survey marks and 40 co-located corner reflectors was installed across the northern Surat Basin. The aim of this network was to use InSAR and GNSS observations to understand how resource extraction impacts the ground surface, with annual campaign GNSS surveys proposed (Garthwaite et al. 2015). To date, three campaigns have been conducted: in 2015, 2016 and 2019. In 2020 a report on the status of the 40 corner reflectors' positions was produced to refine the locations and associated uncertainties for satellite calibration and validation activities (Fuhrmann et al. 2020). A 2022 report showed that statistically significant downward movement was measured at 18 of the sites between the 2015 and 2016 or the 2015 and 2019 measurement periods, or both. At SB36, near Miles, 125 mm of downward movement was measured between 2015 and 2019, while at SB49, near Wandoan, 218 mm of downward movement was measured in the same period. However, neither of these data points compared well with InSAR measurements of surface movement, which were significantly lower, for the same period (Geoscience Australia 2022a). Possible explanations for this discrepancy include measurement uncertainty, the swelling and shrinkage of soils due to moisture changes, spatial averaging, human activity at the surface, movement of the GPS infrastructure, penetration of the satellite radar, and the limited number of GPS data points.

5.3 Light detection and ranging

LiDAR is a remote sensing technique that is used for a range of applications, including atmospheric studies, surface characteristics and heights, infrastructure monitoring, and navigation. LiDAR systems transmit electromagnetic energy in the optical and infrared ranges to detect objects, calculate distances between objects and the sensor, and determine physical properties of phenomena. The output produced is a highly accurate point cloud with 3D geometric information, with vertical accuracy less than 10 cm (Benedek et al. 2021; Diaz et al. 2017; McManamon 2019).

LiDAR systems are mainly airborne mounted, with unmanned aerial vehicles (UAVs) or fixed-wing aircraft used for data acquisition. These systems rely on a local GNSS data network to tie observations to ground control points (McManamon 2019). For monitoring gradual changes in ground movement, repeat acquisitions are required at regular intervals. While LiDAR is an active remote sensing system, like SAR, its use of shorter wavelengths may cause dependencies on day/night operations and weather conditions (Diaz et al. 2017; McManamon 2019).

In terms of ground surface elevation, the airborne LiDAR surveys commissioned by Arrow Energy are precise to 5 cm (Arrow Energy unpublished 2022). However, the relative accuracy between points in any single observation is much better than this. In practice this means that, although LiDAR survey is not well suited to monitoring changes in absolute surface elevation, it performs very well for monitoring changes in gradient.

5.4 Application of InSAR to the monitoring of CSG fields

The application of InSAR to the monitoring of subsidence above CSG fields has been documented in a limited number of cases. Grigg and Katzenstein (2013) reported on the use of InSAR to measure subsidence above CSG operations in the Powder River Basin (see Section 3.2 for further discussion). More recently, Du et al. (2018) reported on the use of InSAR to monitor subsidence in the Liulin District, China, during 2003 to 2011. The results of the study suggest that the surface was largely stable over the observation period. The findings are questionable, however, due to peculiarities in the workflow. The SAR data used are prone to large errors due (in part) to poor constraint of the satellites' orbital tubes. The interferogram network used does not attempt to mitigate this factor and even suggests that different acquisitions have identical baselines, which is extremely unlikely given the orbital tube constraints. The wrapped interferograms clearly contain a strong topographic signal. This shows the workflow is inadequate in mitigating this signal and it will impact the final surface movement signal calculations. Beyond these examples, the most widespread and advanced application of InSAR to monitor CSG-induced subsidence now occurs in Australia. Two examples of this are discussed in the remainder of this section.

5.4.1 The Camden Environmental Monitoring Project

A recent study commissioned by Geoscience Australia (Garthwaite and Fuhrmann 2020) used InSAR and GPS to identify subsidence over the Camden Gas Project (CGP), which is located approximately 65 km south-west of Sydney. A total of 144 producing gas wells have been drilled in the CGP since it was commissioned in 2001. However, these are being progressively decommissioned and all production is scheduled to end in 2023 (AGL 2022).

As a part of the Camden Environmental Monitoring Project (CEMP), a new geodetic monitoring network was installed to facilitate direct comparison between the InSAR and GPS measurements. The locations of the 20 new geodetic monitoring sites, CA01 to CA20, are shown relative to the location of the CGP wells in Figure 24. Of these sites, 16 were used to acquire campaign measurements, while the other four were measured continuously. Each measurement campaign involved collecting 24 hours of GPS observations concurrently across all geodetic monitoring sites in the network, at approximately monthly intervals. These data were supplemented with data from three pre-existing, continuously operating reference stations from the CORSnet-NSW network (NSW Department of Customer Services Spatial Services 2020).

InSAR data from three satellite missions were used in the analysis. These included Envisat, a C-band (56 mm wavelength) radar operational between 2006 and 2012; ALOS, an L-band (236 mm wavelength) radar operational between 2006 and 2011; and RADARSAT-2, a C-band radar operational since 2007. Data from RADARSAT-2 were acquired during the period July 2015 to July 2019 for both ascending and descending tracks (see Figure 25.(a)). Each track makes an acquisition every 24 days, with an offset of 12 days between them. The GAMMA interferometry software (Wegmüller and Werner 1997) was used to generate a network of interferograms for every viewing geometry of each satellite. StaMPS (see Section 5.1) was then used to conduct independent time-series analysis of every interferogram network and derive LOS displacement and velocity datasets. Finally, the LOS displacement and

velocity data from ascending and descending tracks were used to calculate vertical and horizontal surface displacement and velocity data for each satellite (Fuhrmann and Garthwaite 2019).

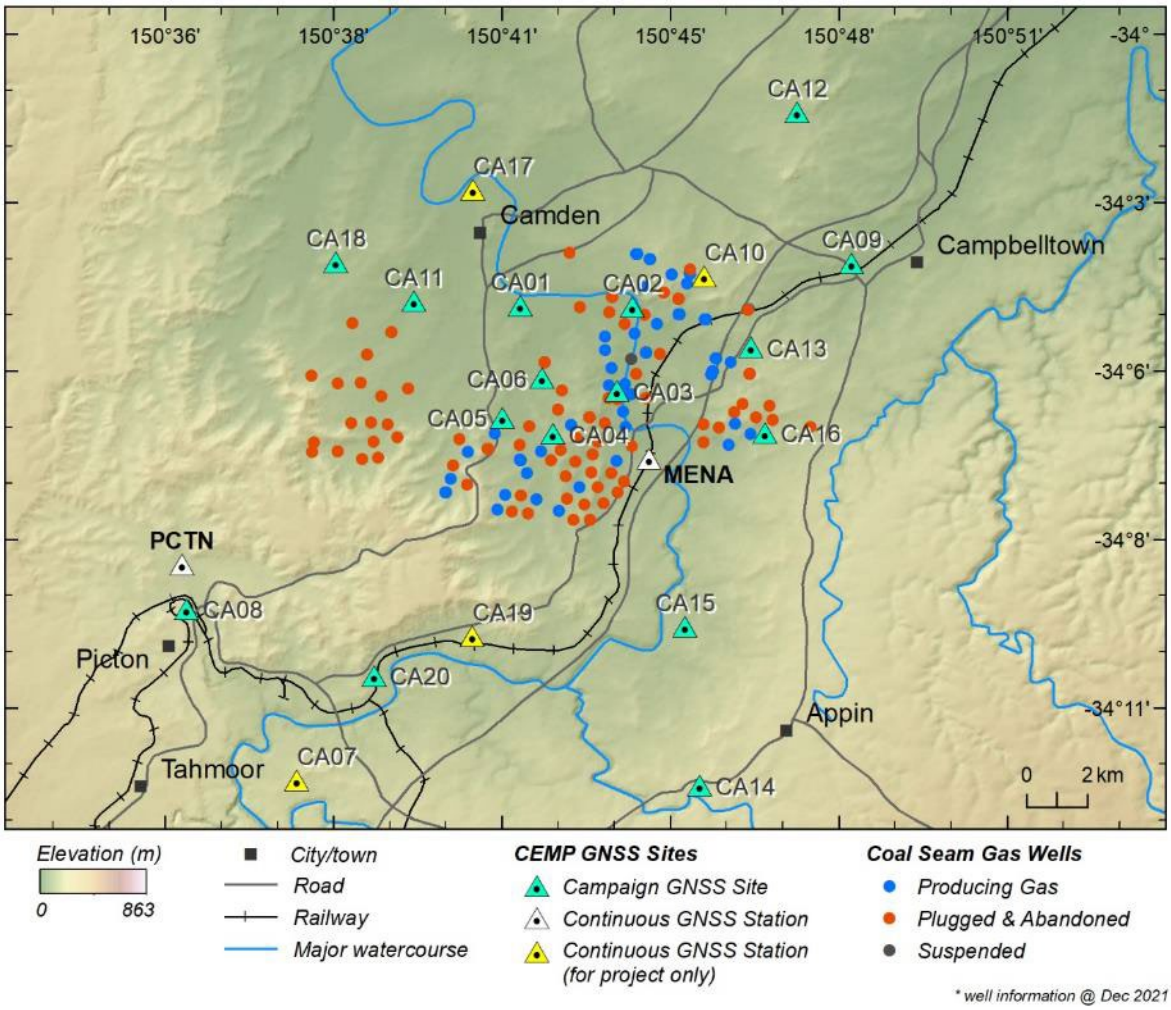

Figure 24. Location of geodetic monitoring sites installed as part of the Camden Environmental Monitoring Project (Garthwaite and Fuhrmann 2020); and location of the CSG wells, both producing and plugged and abandoned, of the Camden Gas Project

The CEMP made some significant findings, which are briefly summarised here. The comparison of RADARSAT-2 and GPS data for the period July 2016 to June 2019 showed that the LOS displacements observed in ascending and descending InSAR tracks are relatively consistent and within 5 mm of the GPS displacements (which had to be converted from the up–down, east–west coordinate system to LOS). This provided confidence in the InSAR technique as a large-scale subsidence monitoring system. In general, no significant subsidence was observed over the CGP. However, Envisat and RADARSAT-2 produced almost no useful data in that area because of the inability of the shorter wavelength (56 mm) to penetrate vegetation on the surface. Low coherence and poor data quality is also a challenge to InSAR observations at locations of intensive cropping in the Surat CMA. More broadly, the Envisat data in the period 2006 to 2010 showed 96.8% of velocity measurements to range between ±3 mm/year. The RADARSAT-2 data in the period 2015 to 2019 showed 96.7% of velocities also being within the range of ±3 mm/year, while the ALOS data showed that 78.0% of velocity values were within the uncertainty range of ±4.2 mm/year. These small fluctuations were attributed to seasonal changes in soil moisture and associated shrinking and swelling. No correlation between subsidence and the location of CSG wells could be found. The most noticeable subsidence observed in this study was found to be located above underground coal mines in the Southern Coalfields, including 800 mm at the Tahmoor mine and 600 mm at the Appin longwall mine, as shown in Figure 25.(b).

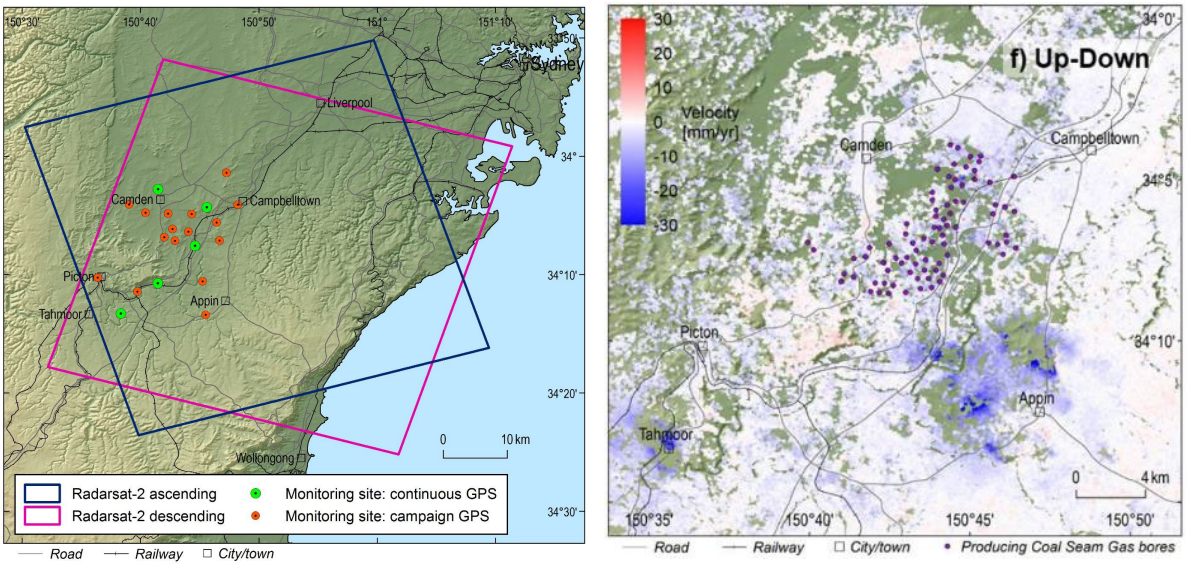

(a) *(b)*

Figure 25. Aspects of the Camden Environmental Monitoring Project, showing (a) the overlap of the ascending and descending tracks of RADARSAT-2, and (b) the up–down velocity data from ALOS in the period 2008 to 2010 (reproduced from Garthwaite and Fuhrmann 2020)

5.4.2 The Underground Water Impact Report

Following legislative changes in 2016, OGIA is now required to report in its Underground Water Impact Report (UWIR) on subsidence that has occurred or is likely to occur. In the latest UWIR (OGIA 2021), this was done by presenting an analysis of InSAR data along with predictive modelling of compaction and subsidence. To support the InSAR analysis, OGIA acquired surface movement data that had been purchased by the major Queensland CSG producers (Santos, Origin Energy, Shell QGC, Arrow Energy) from a commercial provider. These data included ALOS observations at an interval of 46 days for the period 2006 to 2011, RADARSAT-2 observations at an interval of 24 days for the period 2012 to 2017, and Sentinel-1 observations at an interval of 12 days since 2015 (six-day interval from 2017 onwards). As had been identified by Masoudian et al. (2019b), background trends of surface movement are observed at locations remote from CSG production. In some locations, the trend suggests consistent downward movement (i.e., subsidence) with seasonal fluctuations due to rainfall. Such background trends will also exist above CSG fields, so OGIA aimed to report on CSG-induced subsidence in the context of the surface movement baseline. This approach is necessary to try to understand impacts associated with CSG production.

Interrogation of the InSAR data showed maximum downward surface movement of approximately 100 mm in the CSG fields in the east of the Surat CMA, which correlates well with the onset of CSG production in the area. Less surface movement was observed at the edge of these CSG fields. No significant surface movement was observed outside these fields. These trends are summarised in Figure 26. Figure 26(c) indicates that the rate of subsidence might be reducing with time (OGIA 2021).

Inspection of surface movement in non-producing regions, both within and outside the Condamine Alluvium, indicated velocities of up to 25 mm/year and localised displacement fluctuations of 25 mm over a separation distance of 100 m. This is broadly consistent with the findings of Masoudian et al. (2019b) and was similarly attributed to variations in soil type in combination with changes in moisture content. Some regions of uplift were also observed in the eastern part of the Condamine Alluvium, which appeared to correlate with rainfall pattern.

Poor coherence resulting in a lack of data coverage was also identified in cultivated regions. Nevertheless, it was inferred from the available data that surface movement on farms is highly variable, both spatially and temporally, and therefore it is not appropriate to use changes in surface elevation as a metric of the influence of CSG production.

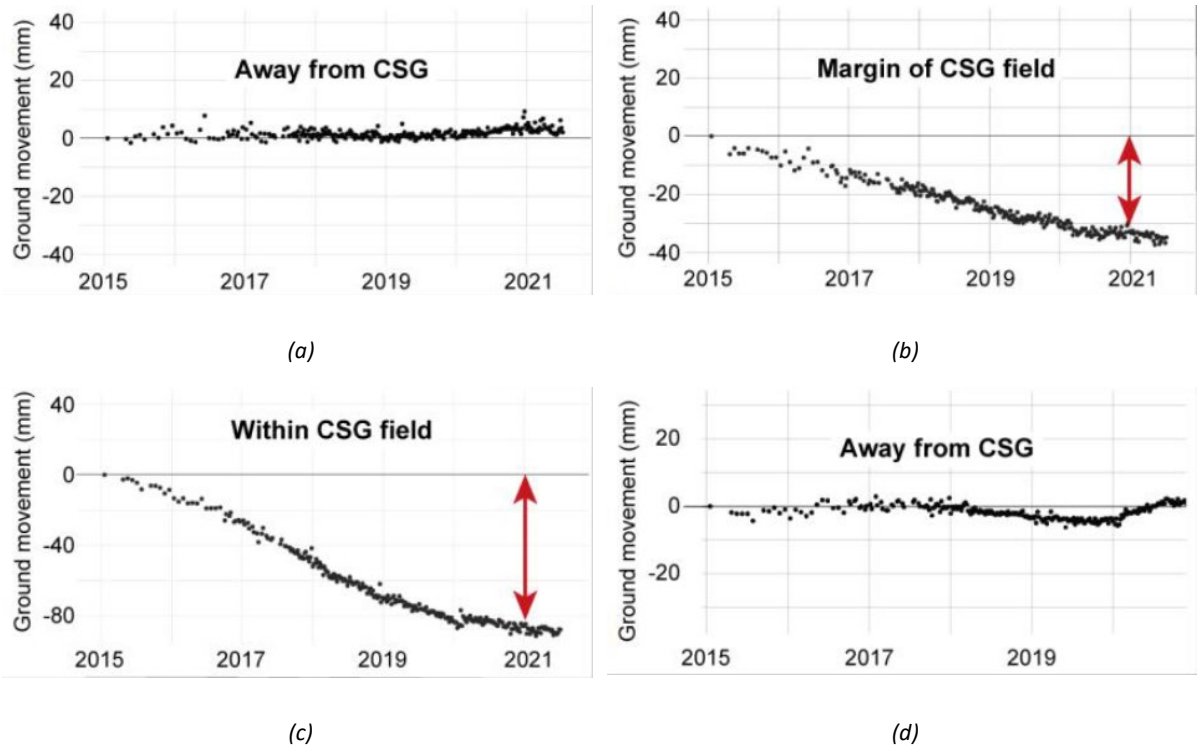

Figure 26. InSAR measurements of surface movement at four locations, moving from west to east in the Surat CMA: (a) approximately 15 km from CSG production on the western side, (b) at the boundary of CSG production on the western side, (c) within the CSG producing field, and (d) approximately 10 km from CSG production on the eastern side (reproduced from OGIA 2021)

Note: Plots have been generated using an average of all surface movement data over respective squares of 250 m × 250 m.

5.5 Subsidence monitoring strategies

Subsidence monitoring can be used to meet a number of objectives. These include quantification of the baseline trend of surface movement in areas where CSG is not (and will not be) produced, and in petroleum leases prior to CSG development; estimation of the surface movement that is attributable to CSG-induced subsidence after production commences; and validation of predictive tools for calculating CSG-induced subsidence. Further, surface movement data can be used to calibrate predictive models in a process called history matching. However, this must be approached with caution because the surface movement signal from InSAR, for example, will aggregate the contribution from a number of additional processes (e.g., shrinking and swelling of soils) which might not be captured in the model being calibrated.

An example of current best-practice subsidence monitoring is documented in Arrow Energy's unpublished 2022 Draft Water Monitoring and Management Plan (Arrow Energy unpublished 2022). This comprises of large-scale InSAR monitoring of changes in ground surface elevation (i.e., surface movement), annual LiDAR surveys to monitor ground surface slope and any change in slope since the last survey, and geodetic measurement using a combination of GNSS reference stations and survey markers as quality assurance on the InSAR and LiDAR data. The GNSS and survey locations were deliberately chosen to be adjacent to permanent scatterers, where the quality of InSAR is likely to be

greatest, and to capture a variety of land resource areas (i.e., combination of geology, topography, soil, vegetation and land use) as well as spatial distribution across areas of CSG production.

This approach is recommended for the assessment of new developments, whereby InSAR is used for field-scale monitoring of elevation change, LiDAR is deployed only in locations that might be sensitive to small changes in slope or where InSAR coherence is poor or anticipated to degrade, and fixed monitoring stations are used as a control on the two remote sensing techniques. To assist the determination of the surface movement baseline, both inside and outside a proposed CSG development, it is recommended that InSAR and LiDAR (where deemed necessary) data acquisition commence prior to production to establish temporal trends. The interpretation and analysis of surface movement data should be supported by the ongoing monitoring of groundwater pressures.

The accessibility of InSAR data continues to increase, including, for example, surface movement reporting by OGIA and Geoscience Australia. If necessary, commercial operators routinely provide processed InSAR data as a service. Further, surface movement mapping can be completed independently using the free and open data acquired by the European Space Agency's Sentinel satellites. Similarly, a number of companies can provide aerial LiDAR surveys.

6. Approaches to subsidence assessment

Subsidence is the manifestation of subsurface compaction driven by fluid extraction and the resultant interaction of the remaining fluid and porous solid. Consequently, predictions of subsidence (or uplift) require an approach that considers both of these coupled processes (i.e., fluid dynamics and solid mechanics). By extension, the quality of subsidence predictions is heavily dependent on the quality of predictions of water (and in the context of CSG production, gas) flow in the subsurface.

Compaction and subsidence magnitudes are dependent on the mechanical and transport properties of the depressurised geological units and the mechanical properties of any overburden. Tectonic strains can also contribute to the subsurface stress state. Predictions of subsidence (or uplift) are complicated by the fact that the region of interest is usually large (in the order of hundreds of metres to kilometres in each direction) but contains much smaller features which influence behaviour (e.g., thin geological units with low hydraulic conductivity). In addition, the transport and mechanical properties used in subsidence predictions vary spatially (see Section 6.4) and are often sparsely quantified, both of which introduce uncertainty. Consequently, subsidence predictions are typically restricted to small scales with moderate to high model complexity and fidelity or large scales with low model complexity and fidelity. The two broad classes of techniques used in subsidence predictions, namely analytical solutions and numerical methods, are discussed in this chapter.

The magnitude of any subsidence induced by CSG production will be a function of the cumulative compaction of each depressurised geological unit. In the Surat CMA, the compaction of a number of coal seams (of varying thickness) and interbedded sedimentary units will propagate through overlying geological units with some degree of attenuation. These units include mudstones, siltstones and sandstones, as well as surficial alluvial aquifer systems composed of both clays and sands, or clays, whose thickness generally increases the closer they are to drainage channels (i.e. rivers) (Best et al. 2014).

As a consequence of its geological history, the Bowen Basin typically contains geological units with lower permeability than those in the Surat Basin. It could, therefore, be assumed that poroelastic compaction would be greater in the Surat Basin. The volume of water produced from CSG operations in the Bowen Basin is lower than that from operations in the Surat Basin, which also indicates that CSG-induced subsidence in the Bowen Basin would be lower. The typically greater volumes of water produced in the Surat Basin are a consequence of higher permeability, which means it can take considerably longer (i.e., up to months) to reach the target reservoir pressure. This could result in greater production-induced compaction. In the regions co-located with or adjacent to Australian CSG production, sandstones and claystones are the non-coal geological units most susceptible to compaction (Best et al. 2014) and so their contribution to total subsidence cannot be ignored. This is also relevant to locations where groundwater is pumped for water supply.

6.1 Analytical and closed-form solutions

Analytical, semi-analytical and closed-form solutions leverage a number of simplifications to solve problems related to compaction and subsidence. They can use as their basis Terzaghi's principles of consolidation, an elastic half-space (Booker and Carter 1986; Booker and Carter 1987), or the concept of a nucleus of strain (Fokker 2002; Fokker and Orlic 2006; Geertsma 1973). To generate solutions using these approaches, it is necessary to make assumptions about the stratigraphy and the mechanical properties of each geological unit therein. In practice, this means homogenising the subsurface into a limited number of continuous geological units, whose properties are isotropic and elastic. Nevertheless, the use of multiple-strain nuclei and superposition facilitates the generation of solutions where multiple wells are present.

For more than 50 years, analytical solutions have been a staple of subsidence predictions. For example, Gambolati and Freeze (1973) and Gambolati (1974) used a three-dimensional, finite element model of the flow with a one-dimensional compaction model to simulate subsidence caused by groundwater withdrawal in Venice, Italy. A similar approach was taken by Calderhead et al. (2011) to simulate subsidence in the Toluca Valley, Mexico; however, InSAR and borehole extensometer data were used to validate the model. Numerous other examples can be found in the literature (Epstein 1987; Hanson 1988; Helm 1984; Helm 1978; Liu and Helm 2008a; Liu and Helm 2008b; Pope and Burbey 2003; Pope and Burbey 2004), where simplified compaction models have been combined with groundwater levels and borehole extensometer data to predict future subsidence.

Models of one-dimensional consolidation ignore horizontal displacement and therefore assume compaction only occurs in the vertical direction. This uniaxial strain assumption, which is discussed in Section 2.4 and central to the definition of Equation 9, is necessary to ensure that analytical solutions remain tractable. However, this assumption is not always appropriate. Wolff (1970) highlighted the importance of considering horizontal strains while Burbey (2001b) also demonstrated that vertical compaction can be overestimated when horizontal deformation is ignored.

In the context of CSG production, Best et al. (2014) applied one-dimensional consolidation to a homogenised coal-bearing formation to predict subsidence. Simplification of the stratigraphy meant that each geological unit was assigned uniform, averaged hydraulic and geomechanical properties. Above the coal-bearing formation, it was assumed that the geological rock units remained saturated, which precluded any significant change to the water table. Four different formulations of the model, each with an increasing amount of model complexity, were tested:

1. Uniform geology model: This employed one-dimensional consolidation theory and assumed that the groundwater was at steady state and the consolidation and hydraulic properties were uniform. Total subsidence of 97 mm was predicted.

2. Variable permeability model: This again employed one-dimensional consolidation theory and assumed that the groundwater was at steady state and the consolidation properties were uniform. However, the hydraulic properties (i.e., permeability) were allowed to vary. A reduction in the total subsidence to 86 mm was predicted.

3. Variable ground model: This again employed one-dimensional consolidation theory and assumed that the groundwater was at steady state. However, both the hydraulic and consolidation properties were allowed to vary. A further reduction in the total subsidence to 72 mm was predicted.

4. Transient groundwater flow model: This coupled one-dimensional consolidation theory to a two-dimensional transient analysis of groundwater head, which was performed using ECLIPSE and SEEP/W. This significantly reduced the total subsidence predictions, with an estimated maximum of 38 mm in the vicinity of the well after two years of production.

The results show that the one-dimensional variants of the consolidation model give similar estimates of subsidence. By solving for the pore pressure field, the transient model generated a significantly lower prediction of subsidence, which is likely to be more realistic (in the context of contemporary InSAR observations). This approach also facilitated the investigation of a two-dimensional well configuration and the models interaction.

The application of analytical compaction modelling to CSG-induced subsidence was also demonstrated by Brown et al. (2014). This study employed the analytical solution of Geertsma (1973) to predict subsidence in the region of Surat Basin operations. The predictions were compared with those from a coupled three-dimensional numerical model that had previously been applied in the Iona gas field by Tenthorey et al. (2013). In terms of both subsidence and uplift, reasonable correspondence was found between the predictions of the analytical and numerical models.

More recently, Wu et al. (2018) compared predictions of CSG-induced subsidence made using two analytical solutions and one numerical solution. The analytical solutions were based on a disc-shaped reservoir with the nucleus of strain concept (Geertsma 1973), and uniaxial compaction (including desorption-induced shrinkage). The

numerical solution was based on a finite element solution for linear elastic solid mechanics and two-phase Darcy flow solved using COMSOL. Subsidence predictions from the nucleus of strain model were unable to incorporate the permeability of layers above the coal seam and were also found to be heavily dependent on the assumed depth. The uniaxial compaction solution, by definition, could not incorporate lateral variations in pressure distribution that drive subsidence. Ultimately it was shown that CSG-induced subsidence is difficult to predict using analytical methods due to the complex response of pore pressure within the typically discontinuous geological profile.

To summarise the discussion in this section, the combination of one-dimensional consolidation theory with one- or three-dimensional models of flow is considered by hydrogeologists to be the standard approach for predicting subsidence (Hsieh 1996). Indeed, one-dimensional consolidation has underpinned the majority of estimates of CSG-induced subsidence to date (see Section 8.1). However, this approach is not without its shortcomings. While many (e.g. Gambolati et al. (2000) and Burbey (2001b)) have been able to demonstrate that both one-dimensional consolidation theory and three-dimensional poroelasticity (solved numerically) theory result in similar predictions of pressure and volumetric deformation, the subsidence displacement fields do not always match well. This is most evident in the presence of subsurface heterogeneity where horizontal displacements are significant and, in some cases, adjacent to the location of pumping (Burbey 2001a, 2001b, 2002). Therefore, the complex and heterogeneous nature of CSG reservoirs means that the application of analytical models to predict subsidence must be performed with an understanding of the associated limitations.

6.2 Numerical modelling in two and three dimensions

Numerical modelling of compaction and subsidence is based on the solution of the Biot (1941) equations, typically using a computer. Such models can be formulated in one, two (including axisymmetric, which is useful in the study of a single well) and three dimensions. The coupled interaction of the fluid flow and mechanical deformation can be captured, noting that each can influence the other (e.g., pore pressure affects effective stress, or the stress acting on the solid matrix; and mechanical deformation affects permeability). It is, however, more common to assume one-way coupling such that the pressure field within an aquifer or reservoir is calculated and then imposed on the structural field to calculate compaction and subsidence. Software packages such as MODFLOW, FEFLOW and SEEP/W are commonly used for single-phase modelling of groundwater flow. The simultaneous transport of water and gas is an important aspect of CSG reservoirs, so multiphase reservoir simulators such as INTERSECT or GEM can be employed to more accurately capture the pressure field. For full 3D geomechanical simulation of compaction and subsidence, commercially available finite element method (FEM) or finite difference (FD) modelling packages such as VISAGE, Elfen, PLAXIS, ABAQUS, SLOPE/W and FLAC can be employed. Assuming they are applied in a manner consistent with their formulation, any combination of these software packages could be employed to analyse CSG-induced subsidence. This is, however, not an exhaustive list of the available packages.

The application of numerical models to predict compaction and subsidence has expanded with the increasing capabilities of digital computers. This reliance on significant computational resources is a consequence of the scale of the problem. Subsidence occurs over large areas and depths, yet much smaller features can be important (e.g., geological units in the order of 1 m thick). Examples of the application of FEM to predict subsidence abound in the literature (Sandhu 1979). Lewis and Schrefler (1978) performed coupled poroelastic modelling to predict subsidence in Venice, Italy. Safai and Pinder (1979), Safai and Pinder (1980), Bear and Corapcioglu (1981), Hsieh (1996) and Burbey and Helm (1999) all documented the application of a similar approach to analysis. More recently, Hernandez-Marin and Burbey (2010), Hernandez-Marin and Burbey (2012), and Yeh and O'Sullivan (2007) demonstrated the application of ABAQUS and ANSYS, which are both commercial FEM packages, in surface movement predictions. ABAQUS was also successfully employed to predict the uplift measured by tiltmeters during an aquifer recharge test in Upper Palatine, Germany (Jahr et al. 2008; Teatini et al. 2011).

As discussed in Section 2.4, the assumption of linear elasticity may not hold when cyclic fluid extraction and injection is applied to an aquifer (e.g., unconsolidated strata subject to grain realignment). Where poromechanical compaction is not fully recovered by a reversal of pore pressure decline, elastoplastic constitutive material models might be considered. This was demonstrated by Budhu et al. (2014) in the simulation of uplift caused by the ingress of water into an aquifer from injection ponds. The model utilised the elastoplastic, modified Cam-Clay model (Roscoe and Burland 1968), with the results validated using InSAR measurements of surface movement. Huang et al. (2015) performed a similar study of artificial recharge in the Yangtze Delta, China, which concluded that the use of a Cam-Clay model generated results that were more reliable than those from an elastic model. Given that the depressurised geological units in Australian CSG operations are consolidated and not prone to grain realignment, the use of advanced constitutive models is not likely to be necessary in the numerical modelling of compaction and subsidence.

It was noted by Best et al. (2014) that the gradients induced by surface movement could be increased by the presence of subsurface faults. This has the potential to create a discontinuity in the pressure field and associated compaction that propagates to the surface as subsidence. This was also recognised by OGIA in the most recent UWIR (OGIA 2021) (see Section 8.1). Three-dimensional numerical modelling has the potential to capture the influence of faults on subsidence, as demonstrated by Ferguson et al. (2016). In this study, compaction, subsidence and fault reactivation due to oil production from a field off the coast of Brazil were predicted using the finite element-discrete element (FEM-DEM) code Elfen. The model domain, which had transverse extents of 25 km, is shown in Figure 27. In the figure it can be seen how the network of major faults was explicitly included in the geometry. The analysis predicted a maximum fault slip of 0.8 m and maximum subsidence at the sea floor of 1.9 m; however, it is important to note that movements of this magnitude are not possible in the context of CSG production (see Section 2.4).

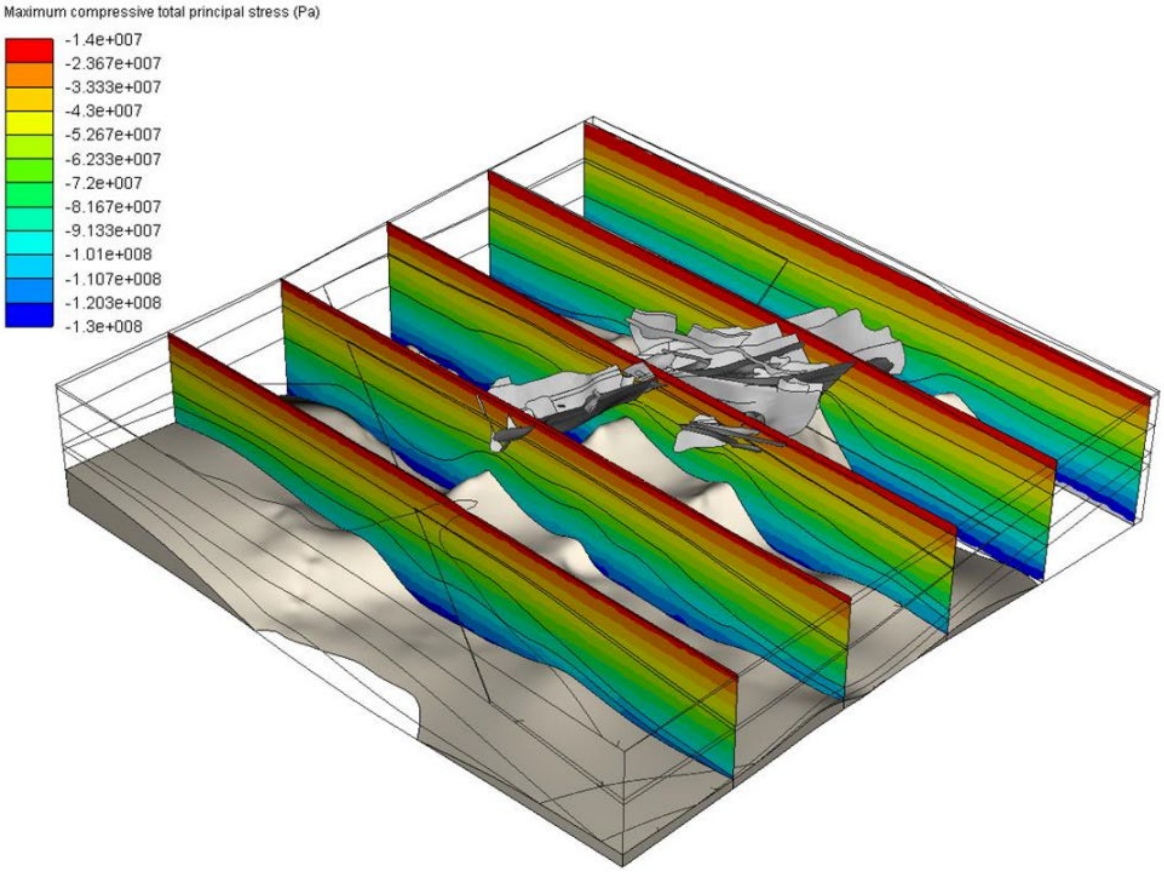

Figure 27. Application of FEM-DEM to the analysis of compaction, subsidence and fault reactivation in a faulted reservoir, showing the distribution of the pre-production stress within the field (reproduced from Ferguson et al. 2016)

Three-dimensional numerical modelling of subsidence offers a number of advantages over the analytical approaches discussed in Section 6.1. These include the two-way coupling of geomechanics and porous media flow, the capturing of subsurface heterogeneity (including faults) in the model domain, and the availability of advanced constitutive and transport models. The pore pressure can be chosen to be modelled as static or transient. In the former, data from hydrographs or the outputs of a fluid flow simulation are imposed directly on the geomechanical model. In the latter, the model is formulated to simultaneously solve for the evolution of pore pressure and mechanical stress; or a dedicated flow simulator such as ECLIPSE, MODFLOW, FEFLOW or SEEP/W is coupled to the dedicated geomechanics solver. The three-dimensional nature of the predicted stress and displacement field means that numerical modelling is also able to capture the influence of overburden on the propagation of compaction to the surface. Competent geological units above the depressurised zones have the potential to attenuate subsurface compaction. This behaviour will be captured by a geomechanical model, along with any induced horizontal movement and subsidence variation as a function of distance from the well(s). This is not possible with a one-dimensional consolidation model. However, the additional fidelity offered by numerical methods comes at a significant cost. Solution times can be in the order of hours or days and high-performance computing (HPC) infrastructure may be required. This limits the applicability of numerical methods in sensitivity analysis or inverse modelling, where multiple runs are required. Limitations in HPC memory also constrain the size of the domain that can be simulated. Further, the additional model complexity requires additional parameters, which may not be available, and highlights issues related to the subsurface heterogeneity of coals (see Section 6.4).

6.3 Advanced numerical modelling: internal and external shrinkage

As described in Section 2.4, coal is usually simplified as an assemblage of matrix blocks separated by orthogonal cleat sets and bedding plies. Models based on the resultant matchstick geometry have subsequently been developed to describe the change in effective stress and permeability that occurs with pressure change and processes such as sorption-induced shrinking or swelling. Such models assume that the matrix blocks are completely isolated by the cleats between them, which is not physically possible. In recognition of this, Wang et al. (2014) argued that the matrix blocks must be connected by bridges that traverse the cleats, as shown in Figure 28. During gas adsorption under confined geomechanical conditions, the coal bridge and the local matrix block around the cleat would swell. Because of the larger area of the matrix block, its swelling force is greater than that of the matrix bridge and as a result the coal bridge and the cleat are compressed by the internal swelling of the matrix block. As gas continues to diffuse into the matrix, the swelling front advances into the blocks and causes external swelling. The internal swelling effect leads to reduced cleat aperture and, consequently, reduced permeability of the coal seam. The external swelling, however, leads to the expansion of bulk coal (cleat-matrix system), as shown in Figure 28.

Masoudian et al. (2019a) applied the concept of internal and external shrinkage to a two-dimensional model of subsidence around a single CSG well. The internal shrinkage contributed to changes in cleat geometry and permeability, while the external shrinkage contributed to bulk volumetric changes of the coal seam at the field scale. Therefore, only a fraction of the Langmuir shrinkage, ε^s, was apportioned to the internal shrinkage (and subsequent permeability update),

$$\varepsilon_{in}^s = F_{in}\varepsilon^s, \quad (16)$$

with the balance apportioned to the external shrinkage and bulk deformation of the coal seam,

$$\varepsilon_{ex}^s = (1 - F_{in})\varepsilon^s \quad (17)$$

The distribution of internal and external shrinkage is thus governed by the model parameter, F_{in}, which may be a function of coal structure, cleat aperture (porosity), and confining stress (Wang et al. 2014; Zang et al. 2015). The internal and external shrinkage terms were then employed in the calculation of permeability and stress, respectively.

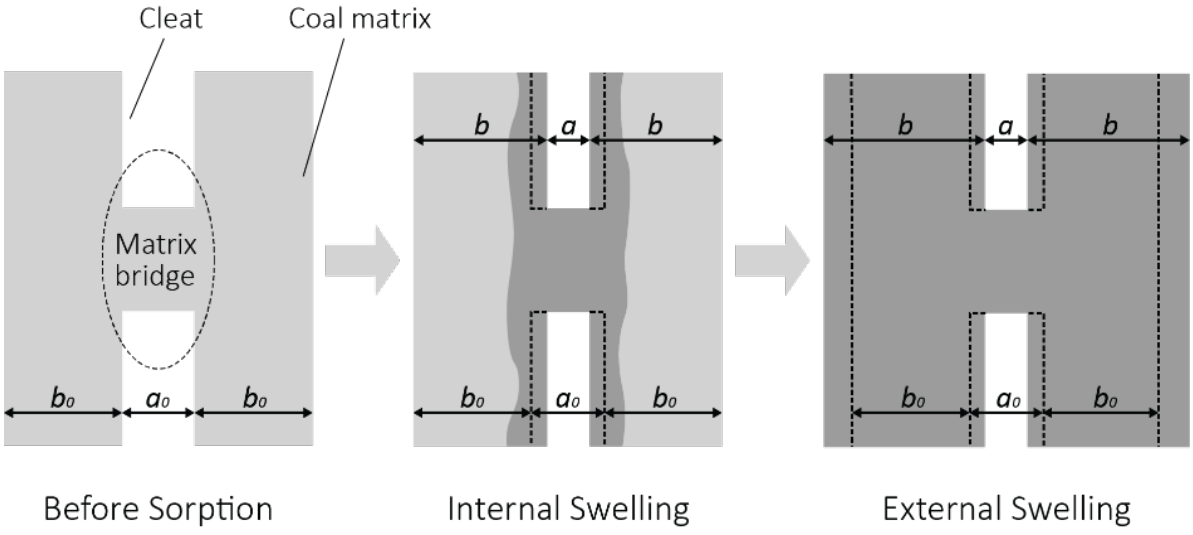

Figure 28. Schematic diagrams highlighting the concepts of internal and external swelling and shrinking, showing (a) the conceptual model of a matrix bridge, (b) internal swelling resulting in cleat width narrowing from a_0 to a, and (c) external swelling resulting in volumetric expansion of the matrix width from b_0 to b (reproduced from Wang et al. 2014)

The model developed by Masoudian et al. (2019a) was applied to a case study inspired by the simplified stratigraphy presented by Best et al. (2014), except three thinner coal-bearing formations were used in place of a single one. The results clearly showed the competing effects of internal shrinkage and higher permeability versus external shrinkage and greater compaction. Increased permeability led to more uniform pressure depletion within the coal-bearing formations and, therefore, a more uniform subsidence profile at the surface. Increased volumetric shrinkage, and thus less permeability enhancement, led to a more pronounced subsidence bowl around the well. For F_{in} values of 0.9, 0.5 and 0.2, the maximum subsidence predicted was 90 mm, 112 mm, and 105 mm, respectively, as shown in Figure 29.(a). This showed that the relationship between F_{in} and subsidence is not monotonic, and that there is a combination of permeability enhancement (and thus reservoir depletion) and volumetric shrinkage that results in maximum subsidence. The results also confirmed what is widely understood: that most of the subsidence signature comes from compaction of the coal layers, as shown in Figure 29.(b).

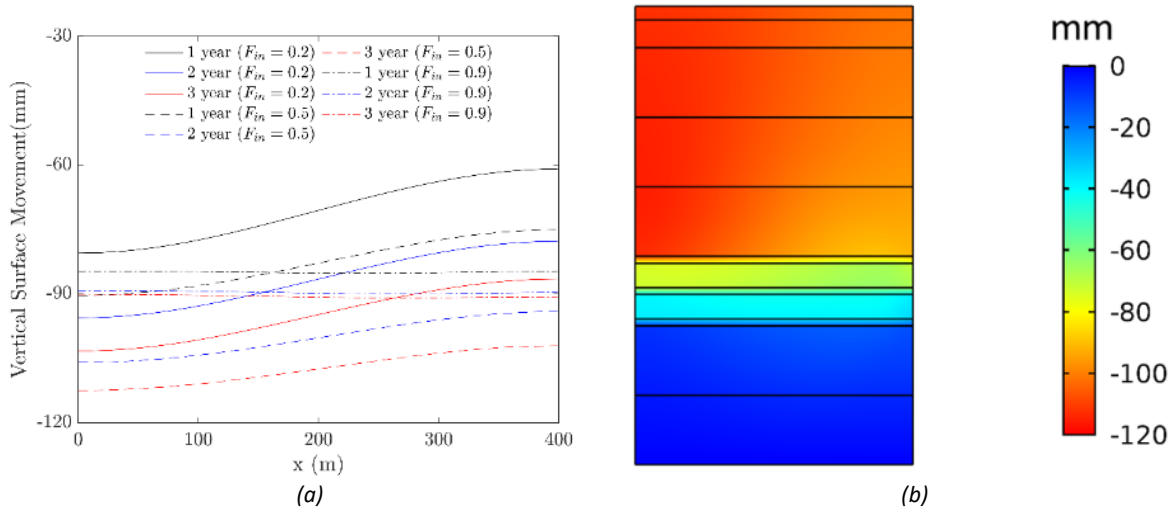

Figure 29. Selected results from modelling of subsidence with internal and external shrinkage incorporated, showing (a) distribution of subsidence around the well at different depressurisation times and values of F_{in}, and (b) compaction distribution throughout the subsurface (reproduced from Masoudian et al. 2019a)

6.4 Advanced numerical modelling: stochastic stratigraphy

One of the most significant challenges associated with modelling the subsurface flow and geomechanics that drive compaction and subsidence lies in determining the input parameters for the associated governing equations (e.g., the distribution of coal and non-coal materials, the distribution of relative permeability for two-phase Darcy flow). The challenge relates not only to a choice of each parameter value but also to how those values are distributed within the model. Key parameters that this applies to include porosity, permeability, compressibility, relative permeability, capillary pressure, Young's modulus, Poisson's ratio, Langmuir volume, Langmuir pressure, and gas content.

In reality, the subsurface is often extremely heterogeneous, but this heterogeneity can be difficult to capture in the models used to predict the pressure changes used in calculations of subsidence. As an example of this, one can consider the Walloon Coal Measures (i.e., the target of CSG production in the Surat Basin). It has been noted (e.g. by Cardwell (2018)) that the coal measures vary significantly between wells at relatively short (e.g., 50 m) spacing, with entire coal packages appearing or disappearing over this distance. This clearly presents a challenge when trying to create models based on data gathered at a more typical CSG well spacing of 750 m.

One approach to modelling these coal measures is to create relatively simple layered models, where coal packages are represented by coal and non-coal (i.e., interburden) layers (Masoudian et al. 2019a; OGIA 2021; Wu et al. 2018). While this is likely to result in models that are straightforward to create and run, the issues with parameterising these upscaled models would still need addressing. This is a particular issue in the Walloon Coal Measures, where the coal and interburden have significantly different properties, making upscaling challenging (Cardwell 2018).

An alternative to layered models would be to use geostatistical modelling such as kriging, Gaussian simulation, or simulated annealing to represent extreme subsurface heterogeneity. To illustrate how heterogeneity influences depressurisation and compaction within coals, two models covering an area of 750 m × 750 m were created based on a section, approximately 80 m thick, of a real CSG well. Using wireline logs from the well, coal intervals were identified. In one of the models, each of these coal intervals was represented by a homogeneous coal layer, with interburden layers between them, resulting in 20 layers in total. The other model was structurally identical to the layered model, but with heterogeneous layers that could contain both coal and interburden (but which would match

the coal present in the wireline log). Both models were parameterised with typical properties from the Walloon Coal Measures, where the coal has significantly higher permeability than the interburden. In the layered model each layer was homogeneous and was assigned a single permeability value, while the heterogeneous model had permeabilities that varied across individual layers, as shown in Figure 30. The spatial distribution of coal and permeability within the layers of the heterogeneous model was populated using copula geostatistics (Hoerning and Rodger 2021).

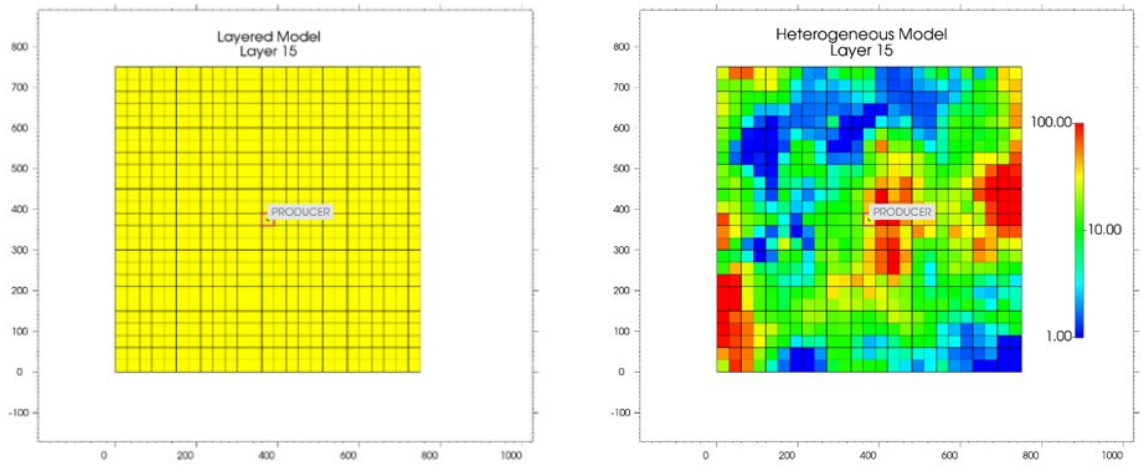

Figure 30. Permeabilities in layer 15 of the (a) layered and (b) heterogeneous models (note that the value at the well location (i.e., in the centre of each model domain) is identical)

These models were used to simulate one year of production from a well in the centre of the model domain, using CMG's GEM compositional simulator, including using GEM's geomechanical model to predict compaction of the modelled layers. The depletion in the various layers after one year is shown in Figure 31.(a) and (b), and the compaction calculated after one year of production is shown in Figure 31.(c) and (d). Compaction in the layered model is predicted to be almost perfectly radial (i.e., decreasing with distance from the well) and is distributed much more evenly across the model domain. The heterogeneous model shows more variation in compaction due to the discontinuous nature of the coal within the model (which could be considered a more realistic representation of the Walloon Coal Measures). The execution of a large number of subsurface realisations, based on the statistics derived from well logs, could thus be used to generate a stochastic distribution of compaction and subsidence probability around a well, rather than a single deterministic value. Note that the compaction calculations shown in Figure 31.(c) and (d) do not include the mechanical contribution of any overburden, which would attenuate the localised compaction seen around the well as it propagated to the surface as subsidence.

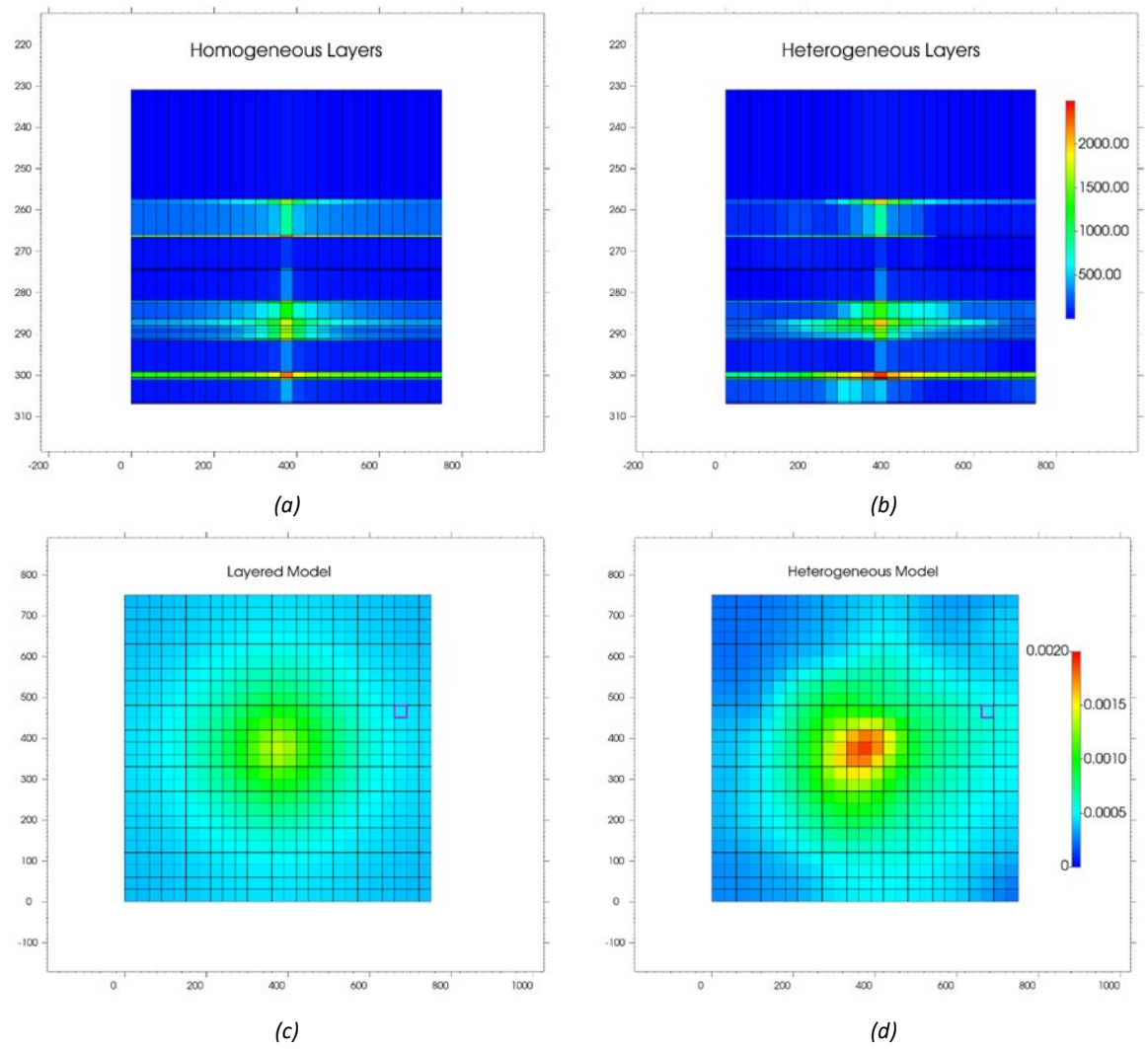

Figure 31. Comparison of subsurface pressure distribution for (a) the layered model, and (b) the heterogeneous model; and layer compaction (not surface subsidence) for (c) the layered model, and (d) the heterogeneous model

6.5 Integration of InSAR data

Surface movement observations, such as those acquired using InSAR, can be incorporated with predictions of compaction and subsidence to perform inverse modelling, or model calibration. If effective, the integration of field data can reduce the uncertainty associated with transport and geomechanical properties. For example, Fokker (2002) used inverse modelling with measurements of surface subsidence to estimate the change of mass in a reservoir. This work demonstrated that well-characterised subsurface material properties are necessary to derive benefit from the inverse modelling approach utilised.

Muntendam-Bos et al. (2008) used subsidence measurements to develop a time-dependent inversion scheme for resolving reservoir pressure changes with time. A significant advantage of this approach was that it was able to capture the temporal lag between a change in reservoir pressure and subsidence. This work used the same analytic, linear forward model presented in Fokker (2002) that was based on the nucleus of strain concept (Geertsma 1973) and subsequently applied and improved by others. An analytical model of the reservoir geomechanics is less computationally demanding than a high-fidelity numerical model (e.g., finite element analysis), which is advantageous

during inverse modelling (which could involve a large number of repeated computations). The inverse modelling approach was validated using a synthetic case study based on a gas field in the northern Netherlands and then applied to demonstrate that the time-dependent inversion outperformed the static scheme presented in earlier works.

InSAR data is spatially dense but the temporal density is dependent on the visit frequency of the host satellite. Reeves et al. (2014) explored the use of InSAR data to generate greater temporal resolution of hydraulic head measurements in a confined aquifer system in the San Luis Valley, USA. The aim of this was to overcome the fact that hydraulic head measurements were approximately one year apart (i.e., quite infrequent), and more frequent head measurements would aid the calibration of groundwater models. One of the major assumptions in this study was that all of the surface movement observed in the InSAR data was attributed to compaction of the confined aquifer system. This means that other natural or anthropogenic sources of surface movement were ignored, and the subsurface compaction propagated to the surface without any overburden shielding. While the hydraulic heads predicted in this work showed reasonable correspondence with the intermittent measured values, it was suggested that atmospheric phase effects (as discussed in Section 5.1) could have degraded results.

An increasing number of studies using InSAR data assimilation have appeared in the literature. Chen et al. (2016) used surface movement and well data to estimate the pressure head in an aquifer over a broad region where vegetation caused significant decorrelation of the InSAR measurements. This is relevant to the situation in the Surat Basin, where intensive cropping affects the coherence of InSAR data above CSG fields. The application of data assimilation in reservoir and aquifer management has continued to evolve such that the state-of-the-art application is able to account for and reduce the uncertainties associated with flow and geomechanical modelling in a stochastic framework (Gazzola et al. 2021). Further, Candela et al. (2022) showed that it was possible to discriminate which rock compaction model driving subsidence was activated at depth. Similar model calibration using InSAR data is now undertaken by OGIA in its series of UWIRs (OGIA 2021).

7. Selection of modelling parameters

This chapter provides guidance on the selection of modelling parameters used in the calculation of compaction and subsidence. Irrespective of whether an analytical or a numerical approach is taken, this requires material properties related to linear poroelasticity (Young's modulus, E; Poisson's ratio, ν; and Biot coefficient, α) and desorption-induced shrinkage (Langmuir constant, b_L; and maximum volumetric swelling strain, ε_L^s). Analytical solutions based on the concept of uniaxial strain commonly make use of the coefficient of compressibility, C_m; however, this can be calculated directly from the Young's modulus and Poisson's ratio.

Calculation of the effective stress change that drives compaction requires an understanding of the in situ stress state, including pore pressure, prior to the onset of production. This is typically performed by integrating well density logs to calculate the total vertical stress and applying poroelastic theory (and an understanding of prevailing tectonic strains) to calculate the total horizontal stress, both as a function of depth. The identification of borehole breakouts and tensile fractures in well image logs can be used to identify the orientation of maximum and minimum horizontal stresses. This basic workflow has been well documented in the oil and gas industry (Zoback 2007), and therefore is not discussed here.

The change in subsurface pressure distribution, which drives changes in effective stress, is best calculated via a computational reservoir or groundwater simulation (e.g. the work that underpins OGIA 2021). In this context, comprehensive modelling of flow and geomechanics requires data or estimates for porosity, permeability, relative permeability, capillary pressure, Langmuir volume, Langmuir pressure, and gas content, in addition to poroelastic properties and the distribution and thickness of coals and other geological units. Guidance on reservoir simulation and the estimation of these parameters is beyond the scope of this document. However, a brief discussion of hydraulic conductivity is included in Section 7.3 to highlight the variability that exists in the geological units in the Surat CMA.

The calculation of the total compaction of coals and surface subsidence requires summation of contributions from all depressurised geological units, as well as the behaviour of any additional overburden. Each will exhibit different material properties, and variations within each unit will exist both laterally and with depth. Exhaustive laboratory testing of all coal and rock layers is not feasible and, even if it were, would be challenged by differences in scale. For example, triaxial testing of competent rocks such as sandstone and shale is unable to capture the influence of natural fractures that are spaced metres apart and would act to reduce the stiffness and strength measured. A similar challenge exists with coal and cleats. In addition, it is difficult to extract a core sample from the subsurface, where it exists under pressure, without fundamentally altering it (e.g., desorption of gas, opening of cleats) prior to testing. Many heavily cleated coals (i.e., the ones likely to exhibit the highest compressibility) cannot be subjected to standardised laboratory testing because core samples disintegrate once they are brought to the surface and destressed. To summarise, there exists wide natural variability in the parameters that contribute to subsidence prediction and there are varying degrees of uncertainty as to what those parameters are at any one location.

A common approach to managing the uncertainty associated with model parameters is to conduct an uncertainty analysis, in which a model is run for a number of different combinations of parameters, each of which is varied within an expected range (i.e., sensitivity analysis). In the context of subsurface pressure prediction, this can be accompanied by model calibration, or *history matching*, whereby parameters are adjusted so as to match field observations (e.g., monitored groundwater levels). This type of field-scale calibration is more difficult to achieve with poroelastic parameters.

7.1 Elastic properties: Young's modulus and Poisson's ratio

Young's modulus, E, is one of the coefficients that link stress and strain in a solid under the assumption of linear elasticity. It is, therefore, also referred to as the elastic modulus. The Young's modulus of many metals is typically isotropic and scale-independent. In sedimentary rocks, however, the Young's modulus may be anisotropic, meaning that the value of E is different across two or more directions. Where natural fractures or other defects are present, the bulk Young's modulus of the rock mass is typically lower than that of small, homogeneous samples (which are more likely to be used in laboratory testing). The presence of fractures and defects also means that the bulk Young's modulus increases with applied stress, as these fractures and defects close under incrementally increasing load.

Poisson's ratio, ν, is another of the coefficients that link stress to strain in a linear elastic solid. It quantifies the deformation of a material perpendicular to the direction of loading. For example, in Figure 32.(a) the column is subjected to vertical uniaxial stress, with no lateral constraint, and the Poisson effect causes it to widen as it shortens. Under uniaxial strain, where the same column is constrained laterally (i.e., zero strain), the Poisson effect results in the induction of transverse stresses, and the shortening of the column is reduced as shown in Figure 32.(b). A rule of thumb for the Poisson's ratio of rocks is a value of approximately 0.25, whereas for Queensland coals it is commonly greater than 0.4. The upper bound of Poisson's ratio is 0.5, which means that the material is incompressible and any volumetric change due to shortening is accompanied by an equivalent volumetric change due to widening. Just like Young's modulus, it can be expected that the Poisson's ratio for coal and sedimentary rocks is anisotropic.

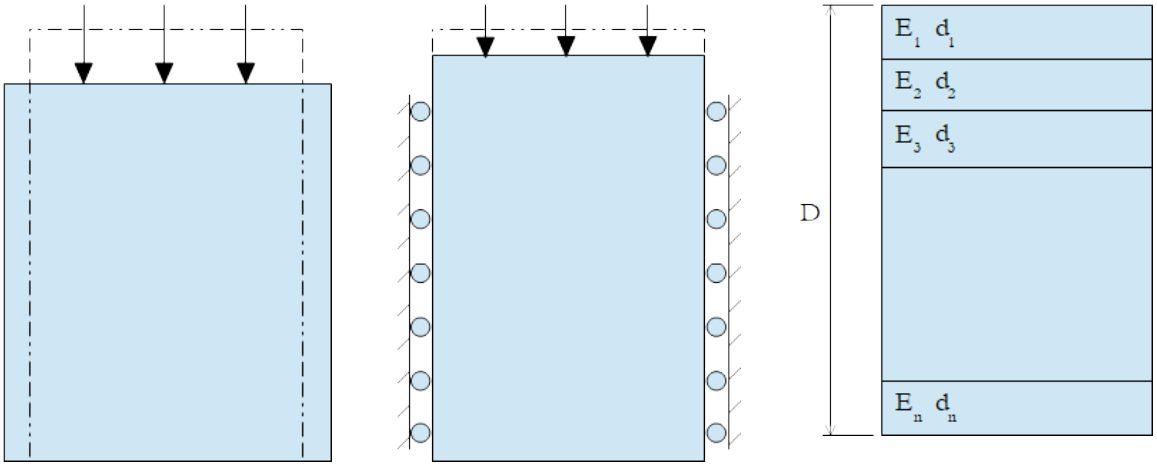

Figure 32. Aspects of linear elasticity, showing (a) the deformation of a column under uniaxial stress (i.e., laterally unconstrained), (b) the deformation of a column under uniaxial strain (i.e., laterally constrained), and (c) the different thickness s (d_1, d_2, d_3) and Young's modulus (E_1, E_2, E_3) of adjacent geological units, where $D = \sum_{i=1}^{n} d_i$

Representative values of Young's modulus for Australian coal and rocks can be sourced from the scientific literature, from research reports, or directly from industry. For example, Gale and Fabjanczyk (1993) presented an overview of the relationship between Young's modulus and unconfined compressive strengths (UCS) for a range of Australian rock types, such as coal, shale, siltstone and sandstone. This provides a crude approximation to one from the other.

Similarly, Young's modulus may also be calculated from UCS using the Hoek-Brown rock mass strength criterion and an assessment of the geological strength index (GSI),

$$E = \sqrt{\frac{UCS}{100}}\,10^{\frac{GSI-100}{40}}, \quad (18)$$

where E is in gigapascals and *UCS* is in megapascals (Galera et al. 2005).

In analytical and numerical calculations of compaction in the Surat CMA, it is usually necessary to upscale the properties of many thin adjacent geological units, as shown in Figure 32.(c). Based on the theory of elasticity, the equivalent Young's modulus of a horizontally layered unit with total thickness, D, undergoing vertical compression can be calculated in an analogous fashion to springs in series (resulting in an anisotropic equivalent elastic system),

$$\frac{D}{E} = \frac{d_1}{E_1} + \frac{d_2}{E_2} + \frac{d_3}{E_3} + \cdots + \frac{d_n}{E_n}, \quad (19)$$

where d_i and E_i are the thickness and Young's modulus, respectively, of each layer.

As the CSG industry has expanded in Queensland, the library of experimentally determined material properties has also grown. For example, Arrow Energy used data from unconfined compression tests of consolidated rock samples from four wells on the Condamine Alluvium in the Surat Basin to undertake analytical subsidence calculations (Coffey Services Australia 2021). A summary of the test results is presented in Table 4, where the Young's modulus is presented as the tangent value at the confining pressure rather than the secant value over the entire pressure range (recognising that the Young's modulus increases under increasing stress). The tangent value represents the slope (i.e., the instantaneous rate of change of stress with respect to strain) at the measurement point, whereas the secant value is calculated using the total change in stress and strain over the measurement range.

Table 4. Summary of Young's modulus values from four wells on the Condamine Alluvium

Well number	Depth range (m)	Confining pressure range (MPa)	Young's modulus range (GPa)
1	140.0–451.1	3.5–11.2	2.0–4.3
2	200.0–298.3	5.0–6.7	4.5–9.0
3	282.7–471.4	7.0–11.7	5.2–5.7
4	203.9–478.5	5.1–11.9	3.0–6.6

Data sourced from Coffey Services Australia (2021)

Data from wireline sonic logs, which include an estimate of dynamic Young's modulus, were also presented. The physical mechanical response of a material is dependent on the rate at which it is loaded and the applied stress-strain amplitude. Logging-based measurements are in the kilohertz range, whereas actual physical loading rates (such as those that occur in situ or in laboratory testing) are generally much slower (quasi-static). By performing laboratory testing for measurement of Young's modulus and Poisson's ratio, and simultaneously measuring the dynamic response of core samples, it is possible to calibrate estimates of static Young's modulus across the entire profile of a well log. Based on triaxial testing of 22 sandstone cores, Fei et al. (2016) presented an empirical correlation for converting dynamic Young's modulus, E_d, values to static Young's modulus, E_s,

$$E_s = 0.564E_d - 3.4941, \quad (20)$$

where both moduli are in gigapascals. This relationship, however, applies to sandstone and is not appropriate for coal. Eissa and Kazi (1988) presented an alternative correlation which takes into account the material density, γ, which is also available from logs,

$$\log_{10}(E_s) = 0.02 + 0.77 \log_{10}(\gamma E_d), \quad (21)$$

where both moduli are again in gigapascals, and the density is in tonnes per cubic metre.

Origin Energy has previously collated detailed mechanical properties of coal and rocks via laboratory experiments (Schlumberger Reservoir Laboratories 2017). Triaxial testing was employed to determine elastic properties (as well as anisotropic dynamic properties and Mohr-Coulomb failure properties) for a number of coal, shale and sandstone samples from three wells in the Surat Basin. A summary of the Young's modulus and Poisson's ratio for these samples, and the depth from which they were collected, is presented in Table 5. In the coal, shale and sandstone samples, no strong correlation between elastic properties and depth was observed. However, most of the samples showed a clear increase in Young's modulus and Poisson's ratio with increasing confining pressure (two of the three shale samples were exceptions to this rule). Although there is some variability, the coal data suggest that values of 3 GPa and 0.40 are good approximations of the Young's modulus and Poisson's ratio of the samples tested.

The uniaxial compressibility values in Table 5 were calculated from the elastic properties as per Equation 10. It can be seen that the large Poisson's ratio for the coal samples constrains the compressibility values, such that they are of similar magnitude to the shales and sandstones. Similarly, the low Poisson's ratio of the sandstones helps increase compressibility, even in the presence of relatively large Young's modulus.

Table 5. Elastic properties of samples from three Surat Basin wells determined using triaxial testing

Material	Depth (m)	Young's modulus (GPa)	Poisson's ratio (-)	Uniaxial compressibility (1/GPa)
Coal	509.19	2.963–3.240	0.40–0.41	0.133–0.158
Coal	579.52	3.019–3.351	0.41–0.43	0.116–0.132
Coal	621.21	3.182–3.487	0.42	0.112–0.123
Coal	641.67	3.219–3.433	0.40–0.41	0.125–0.145
Coal	651.61	3.030–3.227	0.43–0.45	0.085–0.116
Coal	656.29	3.110–3.396	0.41–0.44	0.091–0.138
Coal	727.73	3.028–3.389	0.41–0.43	0.104–0.142
Coal	732.64	2.840–2.941	0.43	0.119–0.124
Shale	370.05	4.413–4.817	0.39–0.47	0.035–0.114
Shale	502.60	6.587–7.612	0.20–0.23	0.118–0.131
Shale	636.36	2.541–3.591	0.38–0.39	0.140–0.210
Sandstone	385.14	4.012–4.547	0.21–0.22	0.195–0.221

Material	Depth (m)	Young's modulus (GPa)	Poisson's ratio (-)	Uniaxial compressibility (1/GPa)
Sandstone	530.36	5.822–6.977	0.23–0.24	0.123–0.148
Sandstone	607.12	6.887–8.743	0.24–0.26	0.097–0.119

Data sourced from Schlumberger Reservoir Laboratories (2017)

A recent report to the Australian Coal Association Research Program (ACARP) (Gray et al. 2019) investigated the anisotropy of coal and the dependence of elastic properties on confining stress. Triaxial testing was performed on 14 coal samples that had been collected from central Queensland (no further location information is available in the report). A summary of the data from one of these samples (classified as a heavily cleated, dull bright coal) is presented in Table 6. It can be seen that the vertical and horizontal Young's moduli, E_1 and E_2, increase to values of 3.78 GPa and 4.43 GPa, respectively, with increasing applied stress. The vertical and horizontal Poisson's ratios, ν_1 and ν_2, increase similarly. Anisotropy of the coal is most evident in the ratio of horizontal to vertical Young's modulus, which is 1.17:1 at the maximum confining pressure. The vertical and horizontal Poisson's ratio values remained quite similar.

A number of key points were summarised from this work. It reinforced the fact that the load response of coals is generally nonlinear within the elastic range, and that the tangent stiffness can increase by up to a factor of 10 with increasing confining stress. This results in values of Young's modulus which deviate significantly, both above and below, values that are widely accepted as standard. The elastic coal properties were sometimes found to be anisotropic. It was also concluded that the use of unconfined compressive testing is not the best approach for the measurement of the elastic properties of coal and other sedimentary rocks.

Table 6. Triaxial test data showing the anisotropy and stress dependence of a Queensland coal sample

Vertical stress (MPa)	Horizontal stress (MPa)	Vertical Young's modulus E_1 (GPa)	Vertical Poisson's ratio ν_{12} (-)	Vertical stress (MPa)	Horizontal stress (MPa)	Horizontal Young's modulus E_2 (GPa)	Horizontal Poisson's ratio ν_{21} (-)
2.17	0.07	0.46	0.18	2.15	1.80	0.78	0.12
4.20	1.83	1.67	0.13	4.18	3.61	2.20	0.17
6.21	3.67	2.47	0.17	6.26	5.40	3.00	0.23
8.23	5.49	2.93	0.21	8.25	7.21	3.52	0.25
10.24	7.33	3.22	0.24	10.27	9.01	3.86	0.24
12.26	9.12	3.53	0.25	12.28	10.81	4.00	0.26
14.31	10.91	3.50	0.25	14.33	12.61	4.17	0.27
16.30	12.71	3.71	0.27	16.33	14.42	4.34	0.29
18.44	14.54	3.78	0.28	18.46	16.25	4.43	0.29

Data sourced from Gray et al. (2019)

7.2 Elastic properties: compressibility

The coefficient of volume compressibility, C_m, is calculated from the Young's modulus and Poisson's ratio under the assumption of uniaxial strain (e.g., Figure 32.(b)), as per Equation 10. It can also be estimated in situ, given the relationship between specific storage, formation compressibility, and porosity (see Section 4.1). The evaluation of compressibility is necessary for analytical modelling of one-dimensional compaction; however, it is intrinsic in linear elastic numerical models that are subjected to uniaxial strain constraints.

The data for vertical Young's modulus and Poisson's ratio from Table 6 can be used with Equation 21 to highlight the effect of varying elastic properties on compressibility. Figure 33.(a) plots the calculated values against vertical stress, which can be interpreted here as a proxy for depth of burial. Note that the first data pair has been excluded from this plot as it would correspond to a depth of approximately 80 m, which is shallower than coal seams typically targeted for CSG production. It can be seen in the graph that the calculated compressibility decreases by a factor of nearly three over this range, which would significantly alter compaction estimates.

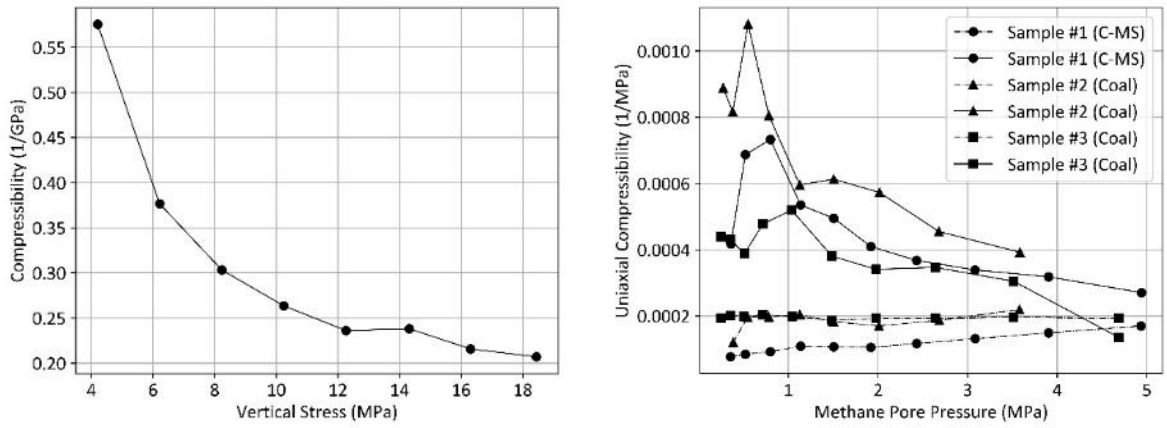

(a) *(b)*

Figure 33. Graphs of coal compressibility, showing (a) the variation in compressibility that stems from the stress-dependent interpretation of Young's modulus and Poisson's ratio in Gray et al. (2019), and (b) the variation in compressibility as a function of pore pressure when desorption-induced shrinkage is accounted for (reproduced from Dudley et al. 2019)

Attempts have been made (Coffey Services Australia 2021) to estimate compressibility of geological units in the Surat Basin using InSAR measurements of subsidence and observed drawdown. This assumed that all subsidence was attributed to the compaction of the geological units that comprise the Walloon Coal Measures, and that outside these there was negligible depressurisation. The thickness of units was informed by the OGIA groundwater model, and Poisson's ratio was assumed to be 0.25. Via inverse analysis, this resulted in Young's modulus estimates of 4.2 GPa and 23.2 GPa for the Taroom and Juandah coal measures, respectively. The former corresponded well with the data from UCS tests summarised in Table 4 but the latter was recognised to be improbably high.

7.3 Hydraulic conductivity, permeability and porosity

The ease with which a porous medium accommodates water flow is quantified as its hydraulic conductivity. For sedimentary rocks, this quantity can be anisotropic and vary by many orders of magnitude (e.g., between clays and sands). As a consequence of depositional bedding, hydraulic conductivity can end up being significantly smaller in the vertical direction than the horizontal direction. An example of its variability is that the hydraulic conductivity in the Condamine Alluvium can vary between 1.9 m/day and 40 m/day. The 2019 UWIR (OGIA 2019) provides a summary of calibrated horizontal and vertical hydraulic conductivities for a number of geological units in the Surat Basin, and a subset of these data (median, 5th percentile, 95th percentile) has been reproduced in Table 7. The vertical conductivity in these data is typically three orders of magnitude smaller than the horizontal conductivity.

Hydraulic conductivity, K, is linked to intrinsic permeability, k, which is a property of the porous medium and independent of the fluid, via

$$K = \frac{k\rho g}{\mu}, \quad (22)$$

where ρ is the fluid density, g is gravitational acceleration, and μ is the dynamic viscosity of the fluid. Intrinsic permeability is used as the basis for many relative permeability models, which determine the permeability to different fluids (e.g., water and gas), as the fraction of each fluid within a porous medium varies. Uncertainty in relative permeability, and its upscaling in simulators, propagates through to the prediction of gas and water production.

Porosity is commonly estimated from well log correlations as this approach enables estimation over the whole depth of a well, unlike laboratory testing of samples (e.g., porosimetry or computed tomographic imaging). As an alternative, formation permeability can be estimated in situ using techniques such as slug tests, pumping tests, response to mechanical loading, and analysis of natural pore-pressure fluctuations (van der Kamp 2001). Examples of the application of these techniques are widespread in the literature (e.g. Rau et al. (2022)).

Table 7. Calibrated horizontal and vertical hydraulic conductivity (median, 5th percentile, 95th percentile) of selected geological units (as modelled by OGIA) in the Surat Basin

Hydrogeological unit	Horizontal hydraulic conductivity (m/d)	Vertical hydraulic conductivity (m/d)
Gubberamunda Sandstone	2.23e-01 (5.00e-02–3.53e+00)	8.23e-05 (1.69e-05–1.31e-03)
Westbourne Formation	3.02e-04 (1.40e-04–1.02e-03)	3.14e- 07 (1.15e-07–1.20e-06)
Upper Springbok Sandstone	3.61e-04 (1.63e-04–4.46e-03)	1.40e-07 (5.07e-08–1.45e-06)
Lower Springbok Sandstone	5.85e-04 (3.34e-04–2.45e-03)	2.36e-06 (6.44e-07–2.33e-05)
Walloon Coal Measures NPZ	1.61e-04 (3.49e-07–8.19e-02)	2.05e-06 (6.18e-08–3.70e-04)
Upper Walloon Coal Measures	1.20e-04 (1.36e-05–1.95e-02)	5.78e-08 (1.17e-08–1.00e-06)
Middle 1 Walloon Coal Measures	6.34e-05 (2.50e-06–1.10e-02)	1.06e-08 (4.06e-09–2.56e-07)
Middle 2 Walloon Coal Measures	7.48e-05 (2.55e-06–1.32e-02)	1.17e-08 (4.19e-09–2.94e-07)
Middle 3 Walloon Coal Measures	9.77e-05 (2.63e-06–1.61e-02)	1.31e-08 (4.30e-09–3.94e-07)
Lower Walloon Coal Measures	1.01e-04 (1.41e-06–1.89e-02)	5.28e-09 (1.92e-09–6.44e-08)
Durabilla Formation	4.52e-05 (2.44e-05–1.31e-04)	2.33e-08 (8.43e-09–1.45e-07)
Upper Hutton Sandstone	3.32e-02 (1.08e-02–4.64e-01)	3.68e-06 (1.09e-06–1.08e-05)
Lower Hutton Sandstone	9.28e-03 (3.00e-03–4.70e-02)	1.00e-06 (2.60e-07–1.00e-06)
Upper Evergreen Formation	5.96e-05 (2.74e-05–1.73e-04)	1.62e-08 (6.12e-09–7.67e-08)
Boxvale Sandstone	3.11e-04 (1.54e-04–3.64e-03)	7.62e-08 (3.41e-08–1.00e-06)
Lower Evergreen Formation	6.27e-05 (2.66e-05–2.10e-04)	1.73e-08 (5.90e-09–1.11e-07)
Precipice Sandstone	7.47e-01 (5.00e-02–1.42e+01)	5.70e-04 (1.67e-05–1.24e-03)

Data sourced from OGIA (2019)

7.4 Langmuir properties

The incorporation of desorption-induced coal shrinkage in estimates of compaction and subsidence requires Langmuir properties of the coal. While many adsorption isotherms are publicly available, it is not usual that they contain the parameters relevant to shrinkage (i.e., Langmuir constant, b_L; and maximum volumetric swelling strain, ε_L^s). This is possibly due to the close relationship between these data and the constants that define the sorption isotherm of a coal, which is itself a measure of gas content (at a specific temperature and over a range of pressures) and thus a proxy for the economics of a field.

Connell et al. (2016) presented data for seven coal samples from the Bowen Basin which were taken from a range of depths between approximately 100 m and 600 m. Values for Langmuir and elastic properties are summarised in Table 8. It can be seen that the Poisson's ratio data are similar to those at maximum confining stress in Table 6, but the Young's modulus data are generally lower. Among other things, this study also presented correlations for the sorption strain with respect to gas content, and ε_L^s with respect to Langmuir volume.

Liu et al. (2017) conducted swelling experiments on small (4 mm) cylinders of medium volatile bituminous coal using methane at 40ºC and pressures up to 40 MPa. The data were used to calibrate models of gas diffusion and matrix swelling and showed that gas transport, adsorption/desorption, and time-dependent swelling/shrinking are controlled by the diffusion of free molecules and exhibit dependence on the state of stress.

The work of Dudley et al. (2019) presents the results of methane pore pressure depletion tests under approximate uniaxial strain and in situ stress conditions on whole core coal samples from a Queensland CSG reservoir (no more specific information was provided). The results clearly showed the influence of desorption-induced shrinkage on the compressibility of the samples. As pore pressure decreased (i.e., increasing depletion), the compressibility was found to increase. This is analogous to the steepening of the Langmuir shrinkage curve at decreasing pore pressure. The compressibility as a function of pore pressure for three samples is shown in Figure 33.(b). Data are presented both with and without desorption-induced shrinkage included. It can be seen that the results for the latter are largely independent of pore pressure. In describing the effect of shrinkage within a total compressibility coefficient, the data from this study could be applied in an iterative, analytical solution of uniaxial compaction. This is convenient from a computational efficiency point of view because the total compressibility coefficients could be included in large-scale models of compaction and subsidence based on one-dimensional consolidation theory.

Table 8. Langmuir shrinkage and elastic properties for seven coal samples from the Bowen Basin

Sample	Maximum swelling strain ε_L^s (%)	Langmuir constant P_{umax} (MPa)	Young's modulus E (GPa)	Poisson's ratio ν (-)
S1	1.13	5.06	3.771	0.279
S2	1.48	9.77	2.555	0.262
S3	1.28	4.73	3.517	0.320
S4	1.46	4.73	-	-
A1	1.55	6.51	2.278	0.298
A4	1.54	4.98	2.221	0.319
A5	1.21	6.93	2.645	0.284

Data sourced from Connell et al. (2016)

8. Prediction of CSG-induced subsidence

The depressurisation of coal seams is a key driver of both CSG production and CSG-induced subsidence. However, the route to effective depressurisation is complex and dependent on a number of interlinked physical processes, as discussed in Section 2. These complex relationships were also represented diagrammatically in Figure 10., which showed that coal permeability plays a fundamental role in gas and water flow. The extraction of these fluids from the subsurface results in formation depressurisation, which facilitates methane desorption and subsequent coal shrinkage. The methane liberated by desorption feeds back to the two-phase flow system, while formation depressurisation and coal shrinkage feed back to the coal permeability. The combination of depressurisation and shrinkage results in formation compaction which, after some attenuation by the overburden, is transmitted to the surface as subsidence. A further complication is that most of these processes vary with depth and coal type. There also exists significant variability in the stratigraphy throughout the Surat Basin, in particular, and interpolation of the stratigraphy between well locations is subject to a high degree of uncertainty. When attempting to predict CSG-induced subsidence it is, therefore, pertinent to consider how much of this detail is necessary and at what level of precision it should be included in the analysis.

A number of different approaches for predicting subsidence were discussed in Section 6, with the most appropriate technique dependent on the desired level of detail and the quality of the available input data. In this section, past subsidence predictions related to CSG production are compared and their differences discussed in the context of analysis choices. This review is then extended by using a synthetic case study to explore the influence of key parameter choices and assumptions on subsidence predictions using two different analysis techniques.

Depending on the scale, tools, data, and experience available, different analysts will approach the prediction of subsidence differently. However, if the key stratigraphic features are captured, material properties are well characterised, and appropriate assumptions are made, then this should not result in subsidence magnitudes that are too dissimilar.

8.1 Subsidence predictions related to Australian CSG production

Numerous predictions of CSG-induced subsidence have been made as the industry has progressed through the processes of environmental approval (e.g., water monitoring and management plans), field evaluation, and ongoing monitoring and compliance (e.g., UWIRs). These vary in their level of technical complexity, scale, and parameter assumptions. A summary of these most recent predictions is included in Table 9.

A wide range of subsidence magnitudes can be seen in the data summarised in Table 9. Some difference in these predictions is to be expected because the four operators listed produce gas from different locations in the Surat and Bowen basins, where there are differences in the lithology (e.g., coal seam thickness and continuity, depth of overburden), reservoir properties (e.g., pressure and permeability distribution) and mechanical properties of each geological unit (e.g. Young's modulus, Poisson's ratio). However, the differences in assumptions, input data, and approach to analysis will also have contributed to the variability in the estimates.

One of the most significant inputs to the prediction of compaction and subsidence is the final pressure distribution in the subsurface. This is best demonstrated by APLNG (2014), where the change from internal groundwater modelling to that in the 2012 UWIR reduced the maximum predicted subsidence from 900 mm to 500 mm. Based on observations since the commencement of production, these have both been demonstrated to be significant overpredictions, which is also attributable to the use of a simple compaction formula based on storage coefficient. Similarly, Golder Associates (2010) combined single-phase groundwater modelling with one-dimensional elastic

deformation (i.e. not the more conventional assumption of uniaxial strain) to predict subsidence. This work assumed that all 300 m of the coal measures (i.e., inclusive of all interburden) was depressurised during production, which again resulted in overestimation of compaction and subsidence.

Table 9. Summary of subsidence modelling predictions by CSG operators in Queensland

Company	Year	Prediction(s)	Comments
QGC Shell (Golder Associates 2010)	2012	Subsidence of 80 mm, 145 mm and 180 mm in the central, south-east and north-west development areas, respectively.	Single-phase groundwater modelling was used to inform an analytical subsidence model based on one-dimensional linear elasticity. Coal shrinkage was not incorporated.
Santos (Santos 2013)	2013	Subsidence of 280 mm near Roma and 150 mm at the Arcadia and Fairview fields.	Linear elastic theory (no further information could be found).
Australia Pacific LNG (APLNG 2014)	2014	Subsidence of 900 mm in high-risk areas and less than 50 mm in low-risk areas, with the maximum value reducing to 500 mm when using OGIA pressure data.	A simple compaction formula based on storage coefficient and change in pressure head was coupled to a numerical groundwater model (and the 2012 UWIR groundwater model for comparison). Coal shrinkage was not incorporated.
QGC Shell (Jacobs 2016)	2016	Subsidence up to 370 mm at the Kenya, Kenya East, Kate, Owen and Jammat fields (central) and Kathleen, Arthur, Philip, Cameron and Polaris (northern) fields. Results averaged over the 8 km × 8 km tenement scale.	Depressurisation predictions from the 2016 UWIR (OGIA 2016b) were used to inform axial compaction calculations (without assuming uniaxial strain). The key input, E, was estimated by combining information from laboratory tests, wellbore logs, and the literature. Coal shrinkage was not incorporated.
Arrow Energy (Coffey Environments 2018)	2018	Upper-bound subsidence of up to 100 mm by 2050 at the Daandine field when considering Arrow operations only, which increases to 120 mm when considering adjacent operations.	Depressurisation predictions from the 2016 UWIR (OGIA 2016b) were used to inform uniaxial elastic compaction. One of the key inputs, E', was evaluated from measured subsidence (InSAR) and pressure drawdown. An average shrinkage strain was applied to coal seams.

Company	Year	Prediction(s)	Comments
QGC Shell (Rai and Hummel 2019)	2019	Upper-bound subsidence of up to 200 mm (P50) or 250 mm (P90) by 2060 at the Lauren and Codie fields in the southern part of the Central Development Area (CDA).	Depressurisation predictions from reservoir simulation of the CDA were used to inform a 3D finite element model of compaction and subsidence. Numerical results were complemented by uniaxial compaction estimates. The coal compressibility, C_m, due to poroelasticity and shrinkage was determined experimentally.
OGIA (OGIA 2021)	2022	Maximum (P50) subsidence of 150 mm south of Miles and north of Cecil Plains. Highly localised predictions of 175 mm. Most locations predicted to undergo less than 100 mm of subsidence.	Depressurisation predictions from the 2021 UWIR (OGIA 2021) were used to inform 3D finite element modelling and large-scale uniaxial compaction. InSAR data were used to constrain compressibility parameters. The method used to represent coal shrinkage was not documented.

Data sourced from various industry reports

The comparison of these predictions is further complicated by the fact that only Coffey Environments (2018) and Rai and Hummel (2019) have directly accounted for desorption-induced coal shrinkage, which would add to the total amount of subsidence predicted. However, these more recent analyses have benefited from the continued evolution of stratigraphic understanding in the Surat and Bowen basins and the continuous improvement of reservoir simulations (e.g., that undertaken by OGIA in each successive UWIR; see below). In combination, these have resulted in more precise subsurface pressure predictions which in turn result in lower predictions of poroelastic compaction.

As discussed in Section 5.4, OGIA is required to report on the potential for subsidence impacts in its triennial UWIR process. The latest UWIR (OGIA 2021) included large-scale predictive modelling of subsidence based on analytical and numerical techniques. A three-dimensional finite element model was built using the VISAGE geomechanical analysis package from Schlumberger. The model was 130 km long and 50 km wide and oriented north-west–south-east over the towns of Cecil Plains, Dalby and Chinchilla. A total of 88 vertical layers were included with a cell size that ranged from 250 m × 250 m to 750 m × 750 m. The necessary geomechanical properties of each layer were calculated from sonic logs of the wells within the model domain. The subsurface pressure distribution applied to the geomechanical model was derived from the UWIR's updated groundwater model. The method used to represent coal shrinkage was not documented.

The application of finite element methods to the entire Surat CMA is not computationally tractable. To facilitate subsidence predictions at this scale, an analytical model based on uniaxial compaction was also constructed. Comparison of the analytical and numerical model results showed good correspondence of subsidence predictions. This provided the necessary confidence to apply the analytical model in stochastic analysis and history matching. A total of 1,000 realisations were analysed with the best 50, based on comparison to InSAR measurements of the same area, used in the assessment of subsidence and change in slope.

The large-scale analytical subsidence predictions showed a maximum (P50) of 150 mm in locations south of Miles and north of Cecil Plains. Highly localised predictions of 175 mm were also seen at the latter, but in general most locations were predicted to undergo less than 100 mm of subsidence. In terms of slope, which is of particular

importance in areas where flood irrigation is used, the results indicate a small region north of Cecil Plains where there is an approximately 80% probability of a 0.005% (i.e., 50 mm over 1 km) change in slope. This is attributed to the difference in depressurisation that occurs either side of the Horrane Fault in that location. In general, however, most locations were predicted to see a change in slope of 0.001%.

Interpretation of the modelling results was used to conclude that subsidence is dominated by linear elastic compaction of the Walloon Coal Measures, that the rate of subsidence is highest early in development (i.e., during initial dewatering), and that there is negligible arching of overburden to reduce the ratio between compaction of geological units and subsidence at the surface. The last conclusion is supported by geomechanical modelling commissioned by QGC Shell (Rai and Hummel 2019). However, the influence of desorption-induced shrinkage on the first two conclusions warrants further investigation. The characteristic shape of the Langmuir shrinkage strain curve suggests that the rate of shrinkage may increase with continued depletion (but not necessarily time), as has been observed in InSAR analysis undertaken by industry (Rai and Hummel 2019).

8.2 Surat Basin: synthetic case study

The comparison of past subsidence predictions highlighted the sensitivity of results to the depressurisation field and the approach to calculating compaction as a function of pressure change. Assumptions related to the extent of vertical depressurisation in the Walloon Coal Measures (i.e., how many of the non-coal geological units were depressurised and to what degree) were also shown to significantly affect the magnitude of predicted subsidence. One of the points discussed in Section 6 was that, in general, one-dimensional consolidation models are straightforward to apply but might yield overestimates of subsidence. Conversely, three-dimensional numerical analysis is too computationally and parameter intensive to be applied at the basin scale. Even sub-models of part of a single CSG tenement can become computationally intractable when sensitivity analyses are required (i.e., a number of repeat calculations). Therefore, the choice of analysis technique is a function of scale (i.e., single or multiple wells, entire field or basin), the amount of stratigraphic detail to be included, and the availability of data with which to parameterise a high-fidelity model.

Another factor in the prediction of subsidence is the variability of the key parameters, including permeability, Young's modulus, Poisson's ratio, Langmuir isotherm, and associated shrinkage behaviour. As highlighted in Section 7, some parameters can vary by orders of magnitude and exhibit little correlation with vertical or lateral proximity. This challenge can be partially overcome by stochastic analysis, in which a distribution of key inputs is used (as opposed to a single value) to generate a distribution of outputs, highlight sensitivity to different parameters, and help quantify uncertainty.

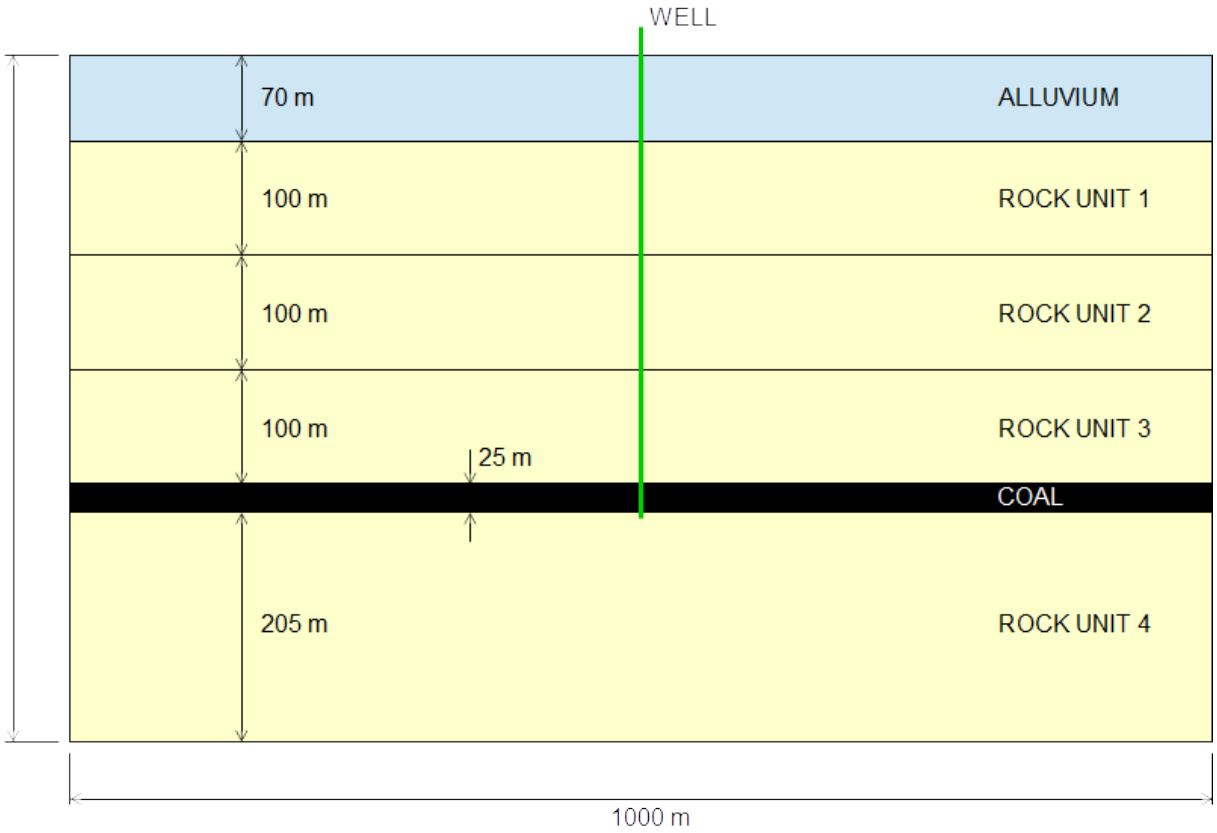

Figure 34. Schematic representation of the stratigraphy used in the subsidence case study

At the request of the IESC, a case study was developed to demonstrate how the various forms of complexity might be simplified to result in a tractable numerical model of subsidence around a single CSG well, and also to compare the predictions of two different numerical approaches. The case study is based on a synthetic Surat Basin well that is targeting the Walloon Coal Measures. It is not designed to replicate any particular location and should be interpreted as such. It was assumed that the multiple coal seams across the Walloon Coal Measures could be collapsed into a single, 25 m-thick coal layer (see Figure 34.) which had good hydraulic connectivity with the well, where the target bottom hole pressure was 300 kPa. The initial pore pressure profile was assumed to be hydrostatic from the ground surface. Material properties representative of the Walloon Coal Measures were chosen and are summarised in Table 10. The overburden (i.e., three rock units) and underburden (i.e., one rock unit) were assumed to have low permeability and thus not be prone to significant depressurisation. Note that this configuration has excluded the interburden that would exist between the aggregated coal seams and be prone to some degree of depressurisation. The simplified stratigraphy and low permeability of the overburden and underburden used in this case study mean that depressurisation is primarily confined to the coal. This is in contrast to the earlier predictions of Best et al. (2014), which assumed that all approximately 300 m of the Walloon Coal Measures were depressurised and, as such, represented an upper-bound conservative estimate of total compaction and subsidence.

The two modelling platforms used in this comparison were COMSOL Multiphysics and CMG-GEM. COMSOL is a generalised platform for finite element discretisation and analysis of partial differential equations related to solid mechanics, fluid mechanics, and other multiphysics problems. GEM, on the other hand, is an advanced equation-of-state (EOS) compositional and unconventional reservoir simulator, which also includes a geomechanics module. GEM is part of a suite of tools typically applied in reservoir engineering.

Table 10. Material parameters used in the subsidence case study

Property	Value	Property	Value
Coal properties		**Rock unit properties**	
Young's modulus, E	2 GPa	Young's modulus, E_{RU1}	4 GPa
Poisson's ratio, ν	0.40	Young's modulus, E_{RU2}	5 GPa
Fracture porosity, ϕ_0	0.01	Young's modulus, E_{RU3}	6 GPa
Initial permeability, k_0	100 mD	Young's modulus, E_{RU4}	8 GPa
Biot coefficient, α	1.0	Poisson's ratio, ν	0.25
Fracture compressibility, c_f	0.0002 kPa^{-1}	Fracture porosity, ϕ_0	0.20
Density, ρ	1,500 kg/m^3	Permeability, k_0	0.0001 mD
Maximum swelling strain, $\varepsilon_L{}^s$	0.013	Biot coefficient, α	1.0
Langmuir's constant, b_L	0.33 MPa^{-1}	Density, ρ	2,500 kg/m^3
Alluvium properties		**Modified rock unit properties**	
Young's modulus, E	0.2 GPa	Young's modulus, E_{RU1}	6 GPa
Poisson's ratio, ν	0.2	Young's modulus, E_{RU2}	8 GPa
Permeability, k_0	1 mD	Young's modulus, E_{RU3}	10 GPa
Density, ρ	2,000 kg/m^3	Young's modulus, E_{RU4}	20 GPa

The COMSOL model used an axisymmetric geometry around a single well, effectively resulting in a cylindrical domain. It included linear elastic solid mechanics, the Richards (Richards 1931) and van Genuchten (van Genuchten 1980) equations for the transport of water in an unsaturated medium (the other phase is gas), stress-dependent permeability (i.e. dynamic permeability) based on the Cui-Bustin model (Cui and Bustin 2005) listed in Equation 4, and shrinkage modelled analogously to thermal strain using Equation 12 in the solid mechanics model. The van Genuchten equation was calibrated to include the pressure-saturation data that was output from the GEM reservoir simulator. In terms of the modelling of flow, this approach is similar to that applied by OGIA (Herckenrath et al. 2015).

The GEM model used a three-dimensional, prismatic domain with the single well in the centre. It models the conservation of mass and momentum for multiple fluid phases in a reservoir and is iteratively coupled to a linear elastic solid mechanics module. The pressure-dependent Palmer-Mansoori model (Palmer and Mansoori 1998) was used to update the coal permeability as a function of drawdown.

Five different analyses were undertaken to contrast the sensitivity of predictions to methodology, coal seam permeability, overburden strength, and coal shrinkage. This is not intended to represent an exhaustive parameter study or sensitivity analysis, but rather an illustration of how results change with inputs. The input parameters used for this case study are summarised in Table 10. The five analysis scenarios are:

0. One-dimensional compaction based on uniaxial strain

1. Poroelastic with two phases modelled and static coal permeability

2. Poroelastic with two phases modelled and dynamic coal permeability

3. Poroelastic with two phases modelled, dynamic coal permeability, and 'strong' overburden

4. Poroelastic with two phases modelled, dynamic coal permeability, and isotropic coal shrinkage.

The result for Case 0 can be calculated using Equation 11 and the average pressure drop in the coal layer, 3.45 MPa, the coal's uniaxial compressibility, 0.233 GPa^{-1}, and the coal layer thickness, 25 m; and assuming that the coal's Biot coefficient is 1.0 (as is common in practice and in the absence of data to justify another value). This results in a coal layer compaction of 20.3 mm, which will be used as a basis for comparison for Cases 1 to 4. It is important to note that this value does not include any potential depressurisation of the rock units above or below the coal.

Figure 35 presents graphs from the comparison of the COMSOL (left column) and GEM (right column) models for Cases 1 and 2. COMSOL exports data from the coordinates of finite element nodes, whereas GEM exports averaged data from the centre of cells, meaning that the data presented herein are not sourced from exactly the same locations in the domain. However, this does not preclude meaningful comparison of the results from each model. Figure 35(a) and (b) plot the pressure profile with depth in the domain after 10, 20 and 30 years of drawdown for both Case 1 and Case 2 (i.e., static and dynamic permeability). The deviation from the initial hydrostatic profile is evident in both graphs, as is the propagation of pressure drop into the overburden and underburden as time progresses. The difference in data output is evident in these two graphs, as the GEM results do not show uniform depressurisation to 300 kPa of the coal layer at the well. However, some of this difference is a consequence of the different approaches to handling the gas and liquid phase in the models. Figure 35(c) and (d) plot the radial pressure profile in the coal with distance from the well, showing similar trends and pressure magnitudes from both models. In both COMSOL and GEM, the introduction of dynamic coal permeability reduced the magnitude of pressure drawdown in the coal layer. This is further explained in Figure 35(e) and (f), which plot the radial variation of coal permeability with distance from the well and how it changes with time. Both models show similar trends in permeability reduction as production (i.e., time) advances. In both modelling approaches, the use of a stress-dependent (COMSOL) and pressure-dependent (GEM) permeability model has resulted in a decrease in spatial depressurisation due to the reduction of coal permeability with drawdown. It is evident from both analyses that the permeability of the coal seam, and how it changes during dewatering and gas production, is a key parameter in the prediction of subsurface pressure distribution and resulting subsidence.

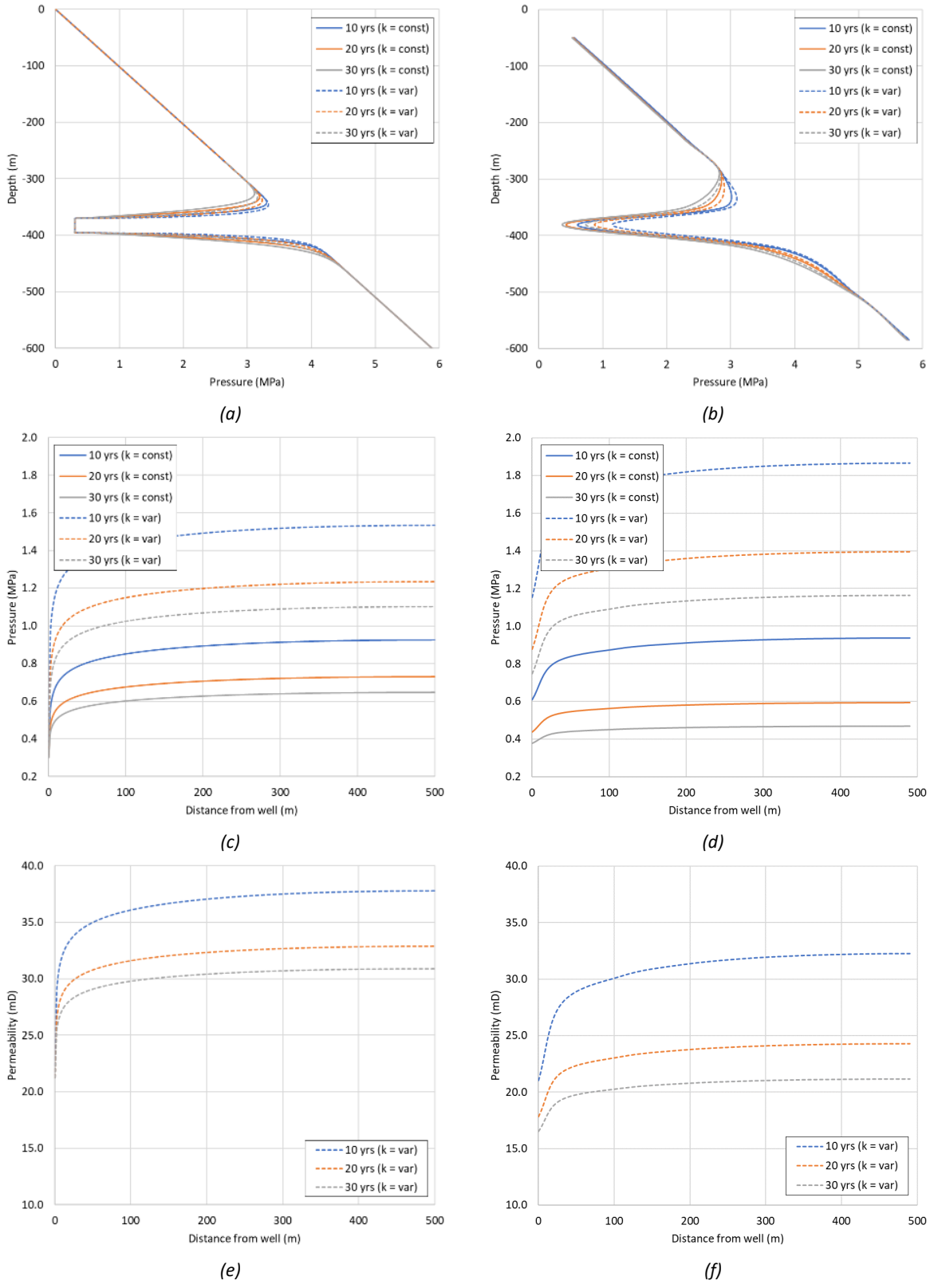

Figure 35. Results of the subsidence case study, showing (a, b) pressure profile with depth, (c, d) radial pressure profile in the coal with distance from the well, and (e, f) radial coal permeability with distance from the well

Note: Left column (a, c, e) produced with COMSOL; right column (b, d, f) produced with GEM.

Figure 36.(a) and (b) plot the cumulative compaction, or progressive subsidence, with depth in the domain for Case 1 (static permeability), Case 2 (dynamic permeability) and Case 3 (dynamic permeability and 'strong' overburden). After 30 years, the COMSOL model predicts 30 mm, 23 mm, and 20 mm subsidence above the well for each case, respectively. The reduced depressurisation caused by dynamic permeability change results in reduced subsidence, which is further reduced by the arching effect and reduction in compressibility when 'stronger' overburden is employed. All predictions are comparable to that calculated for Case 0, with the result for Case 3 almost identical to that calculated analytically. After 30 years, the GEM model predicts 34 mm, 27 mm, and 20 mm subsidence above the well for each case, respectively. The greater depressurisation predicted by GEM is borne out in greater subsidence magnitudes. However, the trend of subsidence reduction from Case 1 to Case 2 and then Case 3 is the same as that predicted by COMSOL. Figure 36.(c) and (d) plot the subsidence at the surface with distance from the well. Both results show effectively uniform subsidence, with no more than 2 mm difference between the location of the well and the model boundary. They also clearly show the similarity in predictions between the two modelling approaches. The absence of pronounced cones of subsidence around the well is representative of the surface movement observed in InSAR data adjacent to CSG wells.

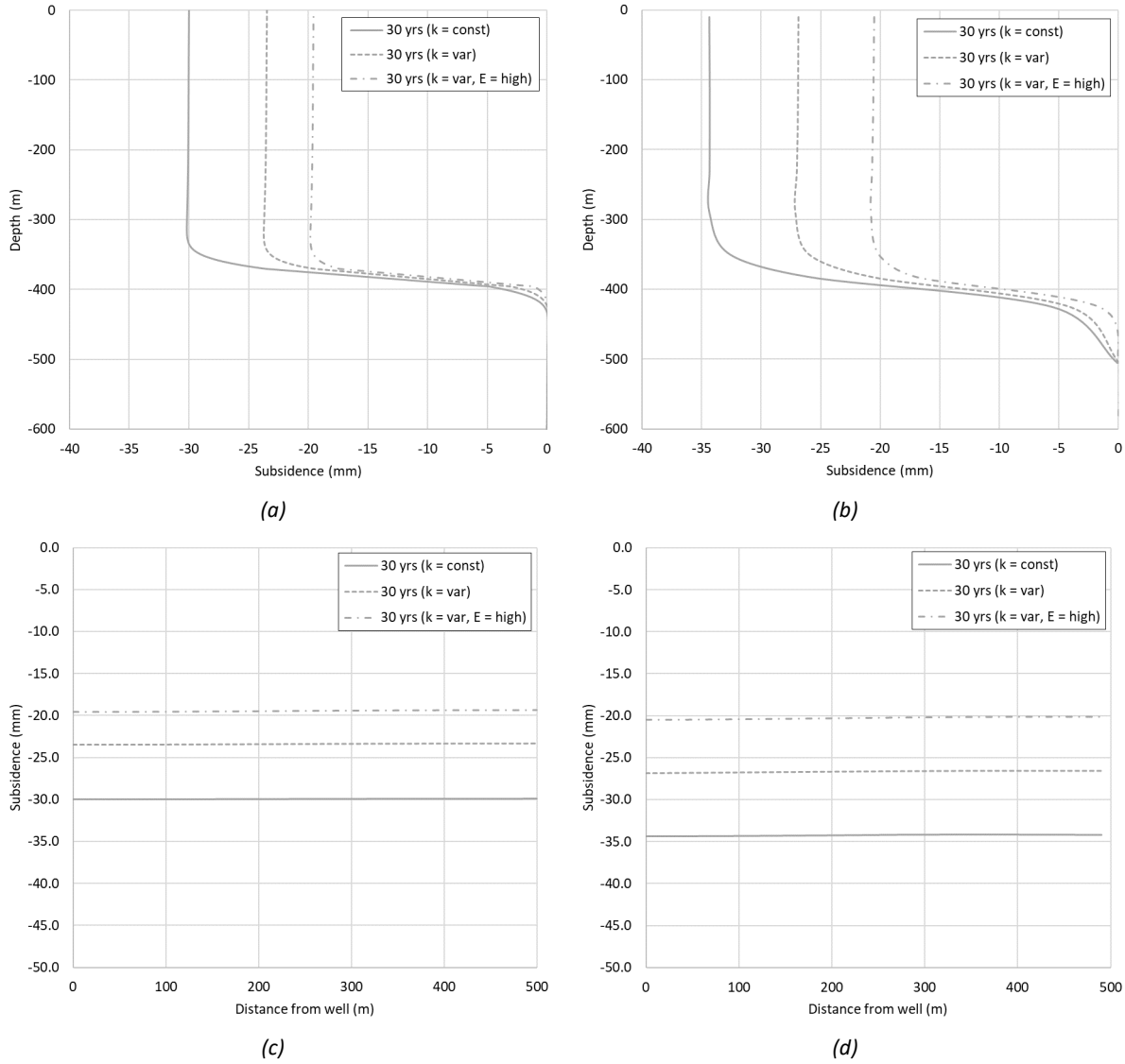

Figure 36. Results of the subsidence case study, showing (a, b) subsidence with depth, and (c, d) subsidence at the surface as a function of distance from the well

Note: Left column (a, c) produced with COMSOL; right column (b, d) produced with GEM.

The influence of shrinkage on the COMSOL predictions of subsidence is shown in Figure 37.(a) and (b). These graphs show approximately 115 mm of desorption-induced shrinkage within the coal layer, resulting in subsidence of 138 mm at the surface. It can also be seen that the rate of subsidence decreases significantly after approximately five years, regardless of whether shrinkage was included. These results are consistent with other predictions and some observations of subsidence in the Surat Basin, as reported by OGIA (2021), and provide evidence in support of the incorporation of shrinkage in analysis of CSG-induced subsidence. More widespread measurement of shrinkage strain, ε_L^s, from coals that are exploited for CSG, or might be in the future, would reduce uncertainty in predictions related to this key model parameter.

It is important to note the limitations in the approach to modelling desorption-induced shrinkage in this case study. The shrinkage strain defined by Equation 12 implies an immediate compaction and, therefore, subsidence response with change in pore pressure. In reality, though, change in gas adsorption pressure might not always occur synchronously with dewatering and pore pressure reduction. Reasons for this include the existence of coals in an undersaturated state or with low-conductivity connection to the source of depressurisation (i.e., the well), both of which would delay the temporal response of shrinkage. Further research on the time-dependent, rather than pressure-dependent, manifestation of desorption-induced coal shrinkage in situ is required.

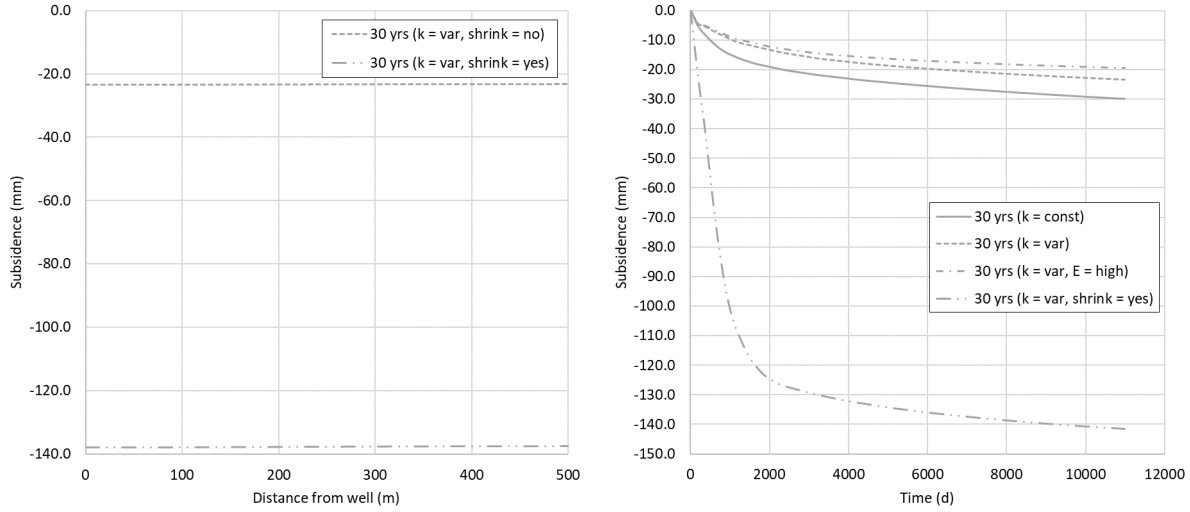

(a) *(b)*

Figure 37. Results of the subsidence case study when coal shrinkage is included, showing (a) subsidence at the surface as a function of distance from the well, and (b) subsidence as a function of time for Cases 1, 2, 3 and 4

Note: Produced with COMSOL, as desorption-induced shrinking and swelling is not available in GEM.

9. Concluding remarks

This Explanatory Note describes the subsurface flow and geomechanical processes by which CSG production induces subsidence, how the magnitude of CSG-induced subsidence can be predicted, and techniques for large-scale and high-precision monitoring of subsidence as it occurs. The information presented attempts to capture the state of the art in relation to these issues, so that it may be used to guide best practice in the assessment of CSG activities into the future. CSG-induced subsidence continues to be the focus of analysis, research and development from academic, industrial and regulatory perspectives, and these activities will contribute to greater understanding of the mechanics of CSG-induced subsidence, improved techniques for prediction and monitoring, and reduced uncertainty in the geometrical and material parameters that are input to analysis.

9.1 Ongoing monitoring and assessment activity

Proposals for new CSG projects, such as the Narrabri Gas Project in New South Wales, are typically assessed at both state and federal levels, including project-specific technical advice from the IESC. Experience from past and ongoing operations such as at Camden in New South Wales and in the Surat CMA, and the data that they generate, will help inform these assessments. Several organisations are involved in the monitoring, analysis and assessment of potential impacts of subsidence and surface movement. Some are focused on specific areas, while others work across New South Wales and Queensland. They include:

- OGIA, which will continue to analyse groundwater and subsidence measurements and iteratively update history-matched predictions of future subsidence across the Surat CMA
- Geoscience Australia, which has deployed infrastructure including InSAR corner reflectors and GNSS stations to monitor surface movement in Camden in New South Wales and in the Surat CMA and has reported data from both, and is well positioned to leverage this to provide ongoing large-scale assessment of surface movement in these locations and the nation more broadly
- the GasFields Commission Queensland, which in 2022 partnered with OGIA to better understand the potential impacts and risks to farming operations resulting from CSG-induced subsidence, and how these impacts may be assessed and managed should they occur
- CSG producers, each of which has its own management and monitoring program for subsidence and remote sensing (e.g., InSAR, LiDAR) of surface movement
- the Centre for Natural Gas at the University of Queensland, which works directly with three large CSG operators in the Surat CMA to address areas of research need, one of which is subsidence and surface movement.

9.2 Future research requirements

Predictions of subsurface phenomena continue to be challenged by uncertainty surrounding the stratigraphy (What is down there and where is it?), the properties of each geological unit (How do they behave from the perspectives of mechanics and fluid transport?), and the variability of these properties (What is an appropriate distribution?). In addition, as the continued collection of field data and improvements in analysis answer some of the outstanding

questions related to CSG-induced subsidence, they can also raise new questions. A non-exhaustive list of future research opportunities is as follows:

- Continued study of background (or baseline) trends of surface movement in non-production areas to assist with separating multiple contributions to net surface movement in areas of CSG production. This is particularly pertinent as recent climatic changes (i.e., the switch from an extended period of below-average rainfall to above-average rainfall) may manifest in observations such as changes to the long-term trends observed in the Surat CMA. The ability to better isolate the contribution of CSG-induced subsidence to observed surface movement would also facilitate inverse analysis of InSAR data aimed at, for example, quantifying reservoir depletion or history-matching reservoir properties.

- Further investigation of remote sensing tools (i.e., InSAR, GNSS, LiDAR) for surface movement measurement, including their respective strengths and limitations in the parts of Australia where they are required, and how they can be combined to result in a comprehensive monitoring strategy.

- Continued improvement in the description of the subsurface, including a better description of sequence stratigraphy and statistics on the correlation of strata between wells (as informed by data from logs). This would help inform the assumptions made in upscaling and simplifying the stratigraphy used in predictions of depressurisation and CSG-induced subsidence. It would also improve the statistical description of lithology and parameter distribution in stochastic analysis, such as that discussed in Section 6.4.

- Investigation of the influence of faults on subsidence and differential surface movement via the inclusion of discontinuities in geomechanical analysis. This would be of benefit where specific faults could influence surface gradient as the surrounding strata compact and subside. This would also be useful in studying the effect of coal seam, and therefore pressure, dislocation where faults act as a barrier to fluid flow.

- Investigation of how permeability, and particularly relative permeability, is upscaled from a single cleat to a coal block, a coal seam and then a coal-bearing unit; and investigation of how the uncertainty associated with this scaling can be better quantified using advanced computational models. Recalling that coal permeability is the foundation of gas production and surface subsidence (see Figure 10.), this has the potential to significantly improve subsidence predictions.

- Investigation of the transient nature of subsidence, recognising the cumulative impacts of poroelastic compaction (which should be greatest in the early stages of a well's life) and desorption-induced shrinkage (which might persist throughout a well's life). One aspect of this could be to employ small- to intermediate-scale modelling of the compaction of cleated coal blocks where diffusive transport in the coal matrix is coupled to two-phase Darcy flow in the cleat network.

- Understanding of how anisotropy and the stress dependence and pressure dependence of properties influence forward estimates of subsidence. Material properties of particular interest include the transverse isotropy of coal elastic and shrinkage properties, as well as the nonlinearity of the desorption-induced shrinkage of coal.

Glossary

This glossary is a modification of that published in Best et al. (2014).

Term	Description
Adsorption	The adhesion in an extremely thin layer of molecules (as of gases, solutes or liquids) to the surfaces of solid bodies or liquids with which they are in contact.
Anisotropy	The directional dependence of a material property (e.g., vertical and horizontal permeability may be different).
Aquifer	A water-bearing geological unit.
Aquitard	A relatively low hydraulic conductivity geological unit.
Associated water	Water that exists naturally within coal seams and is generally rich in salts and other minerals.
Biot coefficient	The ratio of the volume of the fluid change divided by the change in bulk volume under the constraint that pore pressure remains constant.
Cleats	Cleats are fractures in coal created during coalification. They usually occur in two sets that are perpendicular to one another and perpendicular to bedding. The cleats in one direction form first and exhibit a high level of continuity. These are called 'face cleats'. Cleats perpendicular to face cleats are called 'butt cleats'.
Coal measures	Geological formations composed of thin-bedded claystones, shales, siltstones, lithic and sublithic to feldspathic arenites, coal seams and partings and minor limestone.
Coal rank	A classification system that distinguishes the physical and chemical properties of different qualities of coal (from peat, through lignite and bituminous coal, to anthracite). Higher-rank coals possess a higher sorptive capacity for methane gas, and tend to have higher carbon content and decreased moisture content and volatile matter.
Coefficient of volume compressibility	A measure of the compressibility of a material.
Compaction	In a geological context, the process by which geological strata under pressure reduce in thickness and porosity, and increase in density (see Compression).
Compressibility	A parameter that determines the potential for compaction. Compressibility is typically high for soft clays, intermediate for sands, low (but variable) for coals, very low for consolidated sedimentary rocks such as sandstones and mudstone, and extremely low for competent rocks such as granites and other intrusions.

Term	Description
Compression	A system of geomechanical forces or stresses that tend to decrease the volume of or shorten a substance, or the change of volume produced by such a system of forces. In the context of this report, compression is a result of both the shrinkage of the coal due to gas desorbing from the coal matrix, and geomechanical compression due to depressurisations associated with gas and groundwater extraction.
Contingent resources (2c)	Potentially recoverable amounts of petroleum resources in known accumulations that are not yet considered commercially recoverable due to one or more technical, commercial or other factors.
Conventional	Conventional resources are concentrations of oil or gas that occur in discrete accumulations within rock formations that traditionally have high porosity and permeability and are found below impermeable rock formations. These resources are developed using vertical wellbores and minimal stimulation.
Darcy's law	A constitutive equation that describes the flow of a fluid through a porous medium (e.g., groundwater through an aquifer).
Depressurisation	Reduction in ground pressures due to the removal of groundwater.
Dewatering	The removal or draining of groundwater by pumping.
Drawdown	Groundwater drawdown is the fall in the groundwater pressure (or groundwater table) from a pre-existing level.
Dual porosity	A feature of soil/rock whereby fluids may be present within the open fractures (which possess a certain storage capacity or 'primary porosity') and within porous matrix blocks (which possess a different storage capacity or 'secondary porosity'). The secondary porosity is the principal conduit for flow and transport.
Elastic	The physical property of a material that returns to its original shape.
Fick's law	Typically referring to Fick's first law, a mathematical law that describes diffusion (the movement of a substance from regions of high concentration to regions of low concentration).
Gas resource	Defined by the internationally recognised Petroleum Resources Management System (PRMS) as those quantities of gas which are estimated, on a given date, to be potentially recoverable from known accumulations, but which are not currently considered to be commercially recoverable.
Gas reserve	Defined by the PRMS as those quantities of petroleum which are anticipated to be commercially recovered from known accumulations from a given date forward.
Geological unit	A volume of soil or rock of identifiable geological origin and age that is defined by distinctive and recognisable mineral and textural detail, physical characteristics, and (potentially) fossil content.
Geomechanical	Relating to the mechanics (movement/compression/expansion) of soils or rock.

Term	Description
Gilgai	From the Australian Aboriginal word meaning 'small water hole', a small, ephemeral lake formed from a depression in the soil surface in expanding clay soils. Additionally, the term gilgai is used to refer to the overall micro-relief in such areas.
Heterogeneous	Not uniform in composition or in a particular character.
History matching	The process of changing parameter values in a model such that the simulated values are closer to historical, observed values of the system. The term is often used interchangeably with calibration, inverse modelling or parameter inference.
Horizon	A geological bedding surface where there is a change in lithology, or a layer with a characteristic lithology within a sequence of layers.
Hydraulic conductivity	A measure of the rate or velocity of groundwater flow through a material (such as soil/rock).
Hydraulic fracturing	A technique used to increase the permeability of geological strata in the vicinity of a coal seam gas well by injecting a fluid slurry into a well under pressure.
Hydrogeological unit	A geological unit that bears groundwater.
Interbedded	Occurring between beds of rock. Geological beds (rock layers) of one lithology lie in alternating layers with beds of another lithology.
Knudsen number	A dimensionless number defined as the ratio of the molecular mean free path length to a representative physical length scale (e.g., pore throat diameter), used to determine whether continuum mechanics or statistical mechanics should be used to model transport.
Laminar flow	A water flow regime characterised by the flow of parallel streamlines with no disruption (such as eddies, cross flow, swirling or pulsing flow) between these streamlines.
Langmuir isotherm	A physical relationship describing the mass or volume of a substance covering by adsorption to a solid surface in relation to gas pressure or substance concentration.
Lithology	A description/characterisation of the physical characteristics of a rock mass.
Matrix (rock matrix)	The finer grained mass of rock material in which larger grains/crystals are embedded.
Modelling, analytical	The use of closed-form mathematical solutions to directly to calculate, for example, subsidence as a function of material properties, boundary conditions, and loading.
Modelling, numerical	The use of numerical methods (e.g., finite element method) to discretise a set of governing equations (e.g., coupled fluid in and compaction of porous rocks) and solve them on a computer to calculate, for example, subsidence in situations that are too complex for analytical models.
Overburden	In coal seam gas/coal mining, the soil/rock that lies above the coal seam.

Term	Description
Permeability	The measure of the ability of a rock, soil or sediment to yield or transmit a fluid. The magnitude of permeability depends largely on the porosity and the interconnectivity of pores and spaces in the ground.
Poisson's ratio	In solid mechanics, the measure of deformation of a material perpendicular to the direction of loading. Typically varies between 0 and 0.5.
Pore (water) pressure	The pressure of groundwater held within a soil or rock, in the space (pores) between soil/rock particles.
Preferential flow	Preferential flow refers to the uneven and often rapid and short-circuiting movement of water and solutes through porous media (typically soil) characterised by small regions of enhanced flux (such as faults, fractures or high permeability pathways) which contributes most of the flow, allowing much faster transport of a range of contaminants through that pathway.
Recharge	Groundwater recharge is the process whereby surface water (such as from rainfall runoff) percolates through the ground to the water table.
Saturated flow	Flow through a porous medium (such as soil or rock) in which the void space within the porous medium is entirely occupied by water (as opposed to water and gas).
Sedimentary rock	Rock formed by deposition of material at the Earth's surface and within water bodies.
Settlement	The vertical, downward displacement of strata in response to compaction or removal of underlying strata.
Sorption	Physical/chemical process whereby one substance becomes attached to another.
Strain	A proportional change in length or volume of a mass.
Stratum	A layer of sedimentary rock or soil with distinctive characteristics that distinguish it from other layers (plural: strata).
Subsidence	Usually refers to vertical displacement of a point at or below the ground surface. However, the subsidence process actually includes both vertical and horizontal displacements. Subsidence is usually expressed in units of millimetres (mm) or metres (m).
Two-phase flow	Fluid flow characterised by the flow of two fluid phases (e.g., a liquid and a gas).
Unconventional	Unconventional resources are oil- or gas-bearing units where the permeability and porosity are typically low and/or the target hydrocarbons still exist within the host formation.
Unsaturated flow	Flow through a porous medium (such as soil or rock) in which the void space within the porous medium is occupied by both water and gas (rather than water only).
Upstream operations	In the context of oil and gas, this typically refers to activities related to exploration and extraction, as opposed to transport, refinery and other value-adding processes.

Term	Description
Vertosol	A vertosol is a soil type in which there is a high content of expansive clay minerals, many of them known as montmorillonite, that form deep cracks in drier seasons or years.
Well	Borehole in which casing (e.g., steel piping) has been placed to restrict connection to specific ground horizons/depths.
Well field	The area over which wells are distributed to extract groundwater and coal seam gas.
Young's modulus	A measure of the stiffness of an elastic material. Also known as the elastic modulus.

References

Acar Yalcin B and El-Tahir A El-Tahir A 1986. Low strain dynamic properties of artificially cemented sand. *Journal of Geotechnical Engineering*, 112(11): 1001–1015. https://doi.org/10.1061/(ASCE)0733-9410(1986)112:11(1001)

Acworth RI, Halloran LJS, Rau GC, Cuthbert MO and Bernardi TL 2016. An objective frequency domain method for quantifying confined aquifer compressible storage using Earth and atmospheric tides. *Geophysical Research Letters*, 43(22): 11, 671–611, 678. https://doi.org/10.1002/2016GL071328

AGL 2022. *Camden Gas Project – safely supplying our share of NSW's gas needs since 2001*. https://www.agl.com.au/about-agl/how-we-source-energy/camden-gas-project

Al-Arouri KR, McKirdy DM and Boreham CJ 1998. Oil-source correlations as a tool in identifying the petroleum systems of the southern Taroom Trough, Australia. *Organic Geochemistry*, 29(1): 713–734. https://doi.org/10.1016/S0146-6380(98)00132-6

Ali A, Merrick NP, Williams RM, Mampitiya D, d'Hautefeuille F and Sinclair P 2004. Land settlement due to groundwater pumping in the Lower Namoi Valley of NSW, *9th Murray Darling Basin Groundwater Workshop*, Bendigo, Victoria, 17–20 February 2004.

Allen AS 1984. Types of land subsidence. *Studies and Reports in Hydrology*, 40: 133–142.

Alley WM, Healy RW, LaBaugh JW and Reilly TE 2002. Flow and storage in groundwater systems. *Science*, 296(5575): 1985–1990. https://doi.org/10.1126/science.1067123

Aminian K 2020. 4 – Gas storage in coal. In Thakur P, Schatzel SJ, Aminian K, Rodvelt G, Mosser MH and D'Amico JS (eds) *Coal bed methane*. 2nd edition. Elsevier, 115–131. https://doi.org/10.1016/B978-0-12-815997-2.00004-4

APLNG 2014. *Groundwater monitoring plan – Australia Pacific LNG upstream project* (Q-LNG-01-10-MP-0005).

Armstrong RT, Sun C, Mostaghimi P, Berg S, Rücker M, Luckham P, … McClure JE 2021. Multiscale characterization of wettability in porous media. *Transport in Porous Media*, 140(1): 215–240. https://doi.org/10.1007/s11242-021-01615-0

Arrow Energy unpublished 2022. *Draft Surat Gas Project – updated CSG water monitoring and management plan*.

Auvray R, Rosin-Paumier S, Abdallah A and Masrouri F 2014. Quantification of soft soil cracking during suction cycles by image processing. *European Journal of Environmental and Civil Engineering*, 18(1): 11–32. https://doi.org/10.1080/19648189.2013.840250

Bear J and Corapcioglu MY 1981. Mathematical model for regional land subsidence due to pumping: 2. Integrated aquifer subsidence equations for vertical and horizontal displacements. *Water Resources Research*, 17(4): 947–958.

Bell JS 2006. In-situ stress and coal bed methane potential in Western Canada. *Bulletin of Canadian Petroleum Geology*, 54(3): 197–220. https://doi.org/10.2113/gscpgbull.54.3.197

Benedek C, Majdik A, Nagy B, Rozsa Z and Sziranyi T 2021. Positioning and perception in LIDAR point clouds. *Digital Signal Processing*, 119: 103193. https://doi.org/10.1016/j.dsp.2021.103193

Berardino P, Fornaro G, Lanari R and Sansosti E 2002. A new algorithm for surface deformation monitoring based on small baseline differential SAR interferograms. *IEEE Transactions on Geoscience and Remote Sensing*, 40(11): 2375–2383. https://doi.org/10.1109/TGRS.2002.803792

Best R, Rotter B, Orton A, Geng I Zoorabadi M and Tammetta P 2014. *Monitoring and management of subsidence induced by coal seam gas extraction*. IESC.

Bhutto AW, Bazmi AA and Zahedi G 2013. Underground coal gasification: from fundamentals to applications. *Progress in Energy and Combustion Science*, 39(1): 189–214. https://doi.org/10.1016/j.pecs.2012.09.004

Biot MA 1941. General theory of 3-dimensional consolidation. *Journal of Applied Physics*, 12: 155–164.

Black DJ and Aziz NI 2009. Developments in coal mine methane drainage and utilisation in Australia. *Proceedings of the Ninth International Mine Ventilation Congress*, Dhanbad, India.

Booker JR and Carter JP 1986. Analysis of a point sink embedded in a porous elastic half space. *International Journal for Numerical and Analytical Methods in Geomechanics*, 10(2): 137–150. https://doi.org/10.1002/nag.1610100204

Booker JR and Carter JP 1987. Elastic consolidation around a point sink embedded in a half-space with anisotropic permeability. *International Journal for Numerical and Analytical Methods in Geomechanics*, 11(1): 61–77. https://doi.org/10.1002/nag.1610110106

Borchers JW and Carpenter M 2014. *Land subsidence from groundwater use in California*.

Bracegirdle A, Mair RJ, Nyren RJ and Taylor RN 1996. *A methodology for evaluating potential damage to cast iron pipes induced by tunnelling*. Technical Committee TC28 on Underground Construction in Soft Ground.

Briaud J-L, Zhang X and Moon S 2003. Shrink test-water content method for shrink and swell predictions. *Journal of Geotechnical and Geoenvironmental Engineering*, 129(7): 590–600. https://doi.org/10.1061/(ASCE)1090-0241(2003)129:7(590)

Brown N, Richardson C, Neufeld J and Woods A 2014. *Constraining surface deformation predictions resulting from coal seam gas extraction*. Geoscience Australia.

Budhu M, Ossai R and Adiyaman I 2014. Ground movements from aquifer recharge and recovery. Journal of *Hydrologic Engineering*, 19(4): 790–799.

Burbey TJ 2001a. Stress-strain analyses for aquifer-system characterization. *Groundwater*, 39(1): 128–136.

Burbey TJ 2001b. Storage coefficient revisited: is purely vertical strain a good assumption? *Groundwater*, 39(3): 458–464.

Burbey TJ 2002. The influence of faults in basin-fill deposits on land subsidence, Las Vegas Valley, Nevada, USA. *Hydrogeology Journal*, 10(5): 525–538.

Burbey TJ and Helm D C 1999. Modeling three-dimensional deformation in response to pumping of unconsolidated aquifers. *Environmental & Engineering Geoscience*, V(2): 199–212.

Busetti S and Flottmann T 2018. Modeling hydraulic fracturing in transitional stress regimes, Surat Basin, Australia. *2nd International Discrete Fracture Network Engineering Conference*.

Bustin RM 1997. Importance of fabric and composition on the stress sensitivity of permeability in some coals, northern Sydney basin, Australia: relevance to coalbed methane exploitation. *AAPG Bulletin*, 81(11): 1894–1908. https://www.osti.gov/biblio/563428

Calderhead A, Therrien R, Rivera A, Martel R and Garfias J 2011. Simulating pumping-induced regional land subsidence with the use of InSAR and field data in the Toluca Valley, Mexico. *Advances in Water Resources*, 34(1): 83–97.

Candela T, Chitu AG, Peters E, Pluymaekers M, Hegen D, Koster K and Fokker PA 2022. Subsidence induced by gas extraction: a data assimilation framework to constrain the driving rock compaction process at depth. *Frontiers in Earth Science*, 10. https://doi.org/10.3389/feart.2022.713273

Cardwell J 2018. Dynamic modelling of Walloon Coal Measures: an unsavoury cocktail of reservoir variability, mismatched resolutions, and unreasonable expectations. *SPE Asia Pacific Oil and Gas Conference and Exhibition*.

Case JC, Edgar TV and De Bruin RH 2000. *Subsidence potential related to water withdrawal in the Powder River basin: Wyoming State*. G. S. Wyoming.

Cassiani G and Zocatelli C 1998. Gas extraction and risk of subsidence: the case of the Northern Adriatic Gas Fields, technical issues. *SPE International Conference on Health, Safety, and Environment in Oil and Gas Exploration and Production*. https://doi.org/10.2118/46808-MS

Castellazzi P, Schmid W and Fu G 2023. Exploring the potential for groundwater-related ground deformation in Southern New South Wales, Australia. *Science of The Total Environment*, 895: 165167. https://doi.org/10.1016/j.scitotenv.2023.165167

Casu F, Manzo M and Lanari R 2006. A quantitative assessment of the SBAS algorithm performance for surface deformation retrieval from DInSAR data. *Remote Sensing of Environment*, 102(3): 195–210. https://doi.org/10.1016/j.rse.2006.01.023

Chaussard E, Wdowinski S, Cabral-Cano E and Amelung F 2014. Land subsidence in central Mexico detected by ALOS InSAR time-series. *Remote Sensing of Environment*, 140: 94–106. https://doi.org/10.1016/j.rse.2013.08.038

Chen J, Knight R, Zebker HA and Schreüder WA 2016. Confined aquifer head measurements and storage properties in the San Luis Valley, Colorado, from spaceborne InSAR observations. *Water Resources Research*, 52(5): 3623–3636. https://doi.org/10.1002/2015WR018466

Chen ZR 2011. Poroelastic model for induced stresses and deformations in hydrocarbon and geothermal reservoirs. *Journal of Petroleum Science and Engineering*, 80(1): 41–52. https://doi.org/10.1016/j.petrol.2011.10.004

Clarkson CR and Bustin RM 1999. The effect of pore structure and gas pressure upon the transport properties of coal: a laboratory and modeling study. 2. Adsorption rate modeling. *Fuel*, 78(11): 1345–1362. https://doi.org/10.1016/S0016-2361(99)00056-3

Coffey Environments 2018. *Surat gas project Stage 1 CSG water monitoring and management program – subsidence technical memorandum* (ENAUABTF20484AA).

Coffey Services Australia 2021. *Surat gas project – subsidence monitoring and prediction (prepared for Arrow Energy)* (754-MELENP268280-AA).

Colazas X and Olson L 1983. Subsidence monitoring methods and beach mark elevation response to water injection, Wilmington oil field, Long Beach, California. *Proceedings of the 1982 Forum on Subsidence due to Fluid Withdrawals*.

Commonwealth of Australia 2018. Bioregional Assessments.

Commonwealth of Australia (CoA) 2022. Independent Expert Scientific Committee on Unconventional Gas Development and Large Coal Mining Development (IESC). https://www.iesc.gov.au

Connell LD, Mazumder S, Sander R, Camilleri M, Pan Z and Heryanto D 2016. Laboratory characterisation of coal matrix shrinkage, cleat compressibility and the geomechanical properties determining reservoir permeability. *Fuel*, 165: 499–512. https://doi.org/10.1016/j.fuel.2015.10.055

Cook AGBSE and Draper JJ 2013. Post-orogenic Mesozoic basins and magmatism. In Jell PA (ed.) *Geology of Queensland*. Geological Survey of Queensland, 970.

Crilly MS and Driscoll RMC 2000. The behaviour of lightly loaded piles in swelling ground and implications for their design. *Proceedings of the Institution of Civil Engineers: Geotechnical Engineering*, 143(1): 3–16.

Crosdale PJ, Moore TA and Mares TE 2008. Influence of moisture content and temperature on methane adsorption isotherm analysis for coals from a low-rank, biogenically-sourced gas reservoir. *International Journal of Coal Geology*, 76(1): 166–174. https://doi.org/10.1016/j.coal.2008.04.004

Crosetto M, Monserrat O, Cuevas-González M, Devanthéry N and Crippa B 2016. Persistent scatterer interferometry: a review. *ISPRS Journal of Photogrammetry and Remote Sensing*, 115: 78–89. https://doi.org/10.1016/j.isprsjprs.2015.10.011

Cui X and Bustin RM 2005. Volumetric strain associated with methane desorption and its impact on coalbed gas production from deep coal seams. *AAPG Bulletin*, 89(9): 1181–1202. https://doi.org/10.1306/05110504114

David K, Timms WA, Barbour SL and Mitra R 2017. Tracking changes in the specific storage of overburden rock during longwall coal mining. *Journal of Hydrology*, 553: 304–320. https://doi.org/10.1016/j.jhydrol.2017.07.057

Day S, Fry R and Sakurovs R 2008. Swelling of Australian coals in supercritical CO_2. *International Journal of Coal Geology*, 74(1): 41–52. https://doi.org/10.1016/j.coal.2007.09.006

de Andrade Vieira Filh CL, Sobczak K, Holl H-G, Hurter S and Vasconcelos P 2021. Understanding the nature of the transition between Late Jurassic formations of the Surat Basin through borehole image logs using cumulative dip plots. *Australian Earth Sciences Convention 2021*, Virtual.

de Vallejo LG and Ferrer M 2011. *Geological engineering*. 1st edition. CRC Press.

Diaz JCF, Carter WE, Shrestha RL and Glennie CL 2017. LiDAR remote sensing. In Pelton J, Madry S and Camacho-Lara S (eds) *Handbook of satellite applications*. Springer, Cham, 929–980. https://doi.org/10.1007/978-3-319-23386-4_44

Doornhof D, Kristiansen TG, Nagel NB, Pattillo PD and Sayers C 2006. Compaction and subsidence. *Oilfield Review*, 18(3): 50–68.

Du Z, Ge L, Ng AH-M, Li X and Li L 2018. Monitoring of ground deformation in Liulin district, China using InSAR approaches. *International Journal of Digital Earth*, 11(3): 264–283. https://doi.org/10.1080/17538947.2017.1322151

Dudley JW, Deviney DB, Rai UB, Hol S, Hummel N, Sutton H and Gear I 2019. Methane pore pressure depletion experiments on coal seam gas reservoir rock. *53rd U.S. Rock Mechanics/Geomechanics Symposium*.

Dusseault M and Rothenburg L 2002. Analysis of deformation measurements for reservoir management. *Oil & Gas Science and Technology*, 57(5): 539–554. https://doi.org/10.2516/ogst:2002036

Dusseault MB, Yin S, Rothenburg L and Han H 2007. Seismic monitoring and geomechanics simulation. *Leading Edge*, 26(5): 610–620. https://doi.org/10.1190/1.2737119

Eissa EA and Kazi A 1988. Relation between static and dynamic Young's moduli of rocks. *International Journal of Rock Mechanics and Mining Sciences & Geomechanics Abstracts*, 25(6): 479–482. https://doi.org/10.1016/0148-9062(88)90987-4

Ellsworth WL, Giardini D, Townend J, Ge S and Shimamoto T 2019. Triggering of the Pohang, Korea, Earthquake (Mw 5.5) by enhanced geothermal system stimulation. *Seismological Research Letters*, 90(5): 1844–1858. https://doi.org/10.1785/0220190102

Enever J, Casey D and Bocking M 1999. The role of in-situ stress in coalbed methane exploration. In Mastalerz M, Glikson M and Golding SD (eds) *Coalbed methane: scientific, environmental and economic evaluation*. Springer, Dordrecht, 297–303. https://doi.org/10.1007/978-94-017-1062-6_18

Epstein VJ 1987. *Hydrologic and geologic factors affecting land subsidence near Eloy, Arizona* (Vol. 87). Department of the Interior, U.S. Geological Survey.

Erban LE, Gorelick SM and Zebker HA 2014. Groundwater extraction, land subsidence, and sea-level rise in the Mekong Delta, Vietnam. *Environmental Research Letters*, 9(8). https://doi.org/10.1088/1748-9326/9/8/084010

Escojido D 1981. Subsidence in the Bolivar Coast. In Meyer RF and Steele CT (eds) *Future of heavy crude and tar sands*. McGraw-Hill, 761–767.

Espinoza DN, Pereira JM, Vandamme M, Dangla P and Vidal-Gilbert S 2015. Desorption-induced shear failure of coal bed seams during gas depletion. *International Journal of Coal Geology*, 137: 142–151. https://doi.org/10.1016/j.coal.2014.10.016

Esterle JS, Williams R, Sliwa R and Malone M 2006. *Variability in gas reservoir parameters that impact on emissions estimations for Australian black coals*. ACARP.

Fakhri F and Kalliola R 2015. Monitoring ground deformation in the settlement of Larissa in Central Greece by implementing SAR interferometry. *Natural Hazards*, 78(2): 1429–1445. https://doi.org/10.1007/s11069-015-1779-6

Fei W, Huiyuan B, Jun Y and Yonghao Z 2016. Correlation of dynamic and static elastic parameters of rock. *Electronic Journal of Geotechnical Engineering*, 21: 1551–1560.

Ferguson W, Bere A, Rodriguez C, Félix L, Marsili M and Medeiros L 2016. Modelling of a deepwater Brazilian field to assess fault reactivation and the insitu stresses during production. *First Break*, 34(6). https://doi.org/10.3997/1365-2397.2016007

Ferretti A 2014. *Satellite InSAR data: reservoir monitoring from space*. EAGE Publications.

Ferretti A, Fumagalli A, Novali F, Prati C, Rocca F and Rucci A 2011. A new algorithm for processing interferometric data-stacks: SqueeSAR. *IEEE Transactions on Geoscience and Remote Sensing*, 49(9): 3460–3470. https://doi.org/10.1109/TGRS.2011.2124465

Ferretti A, Prati C and Rocca F 2001. Permanent scatterers in SAR interferometry. *IEEE Transactions on Geoscience and Remote Sensing*, 39(1): 8–20. https://doi.org/10.1109/36.898661

Finnegan NJ, Pritchard ME, Lohman RB and Lundgren PR 2008. Constraints on surface deformation in the Seattle, WA, urban corridor from satellite radar interferometry time-series analysis. *Geophysical Journal International*, 174(1): 29–41. https://doi.org/10.1111/j.1365-246X.2008.03822.x

Finol AS and Sancevic ZA 1995. Chapter 7 Subsidence in Venezuela. *Developments in Petroleum Science*, 41: 337–372. https://doi.org/10.1016/S0376-7361(06)80054-3

Fityus SG, Smith DW and Allman MA 2004. Expansive soil test site near Newcastle. *Journal of Geotechnical and Geoenvironmental Engineering*, 130(7): 686–695. https://doi.org/10.1061/(ASCE)1090-0241(2004)130:7(686)

Fokker PA 2002. Subsidence prediction and inversion of subsidence data. *SPE/ISRM Rock Mechanics Conference, Irving, Texas*.

Fokker PA, Gunnink JL, Koster K and de Lange G 2019. Disentangling and parameterizing shallow sources of subsidence: application to a reclaimed coastal area, Flevoland, the Netherlands. *Journal of Geophysical Research: Earth Surface*, 124(5): 1099–1117. https://doi.org/10.1029/2018JF004975

Fokker PA and Orlic B 2006. Semi-analytic modelling of subsidence. *Mathematical Geology*, 38(5): 565–589. https://doi.org/10.1007/s11004-006-9034-z

Freij-Ayoub R, Underschultz J, Li F, Trefry C, Hennih A, Otto C and McInnes K 2007. *Simulation of coastal subsidence and storm wave inundation risk in the Gippsland Basin* (Petroleum Report 07-003).

Fuhrmann T, Batchelor J, McCall T and Garthwaite MC 2020. *Positions and orientations for the Queensland corner reflector array, Australia: report on geodetic surveys conducted in May and June 2018*.

Fuhrmann T, Cuenca MC, Knopfler A, van Leijen FJ, Mayer M, Westerhaus M, … Heck B 2015. Estimation of small surface displacements in the Upper Rhine Graben area from a combined analysis of PS-InSAR, levelling and GNSS data. *Geophysical Journal International*, 203(1): 614–631.

Fuhrmann T and Garthwaite MC 2019. Resolving three-dimensional surface motion with InSAR: constraints from multi-geometry data fusion. *Remote Sensing*, 11(3). https://doi.org/10.3390/rs11030241

Gabrysch RK and Bonnett CW 1975. *Land-surface subsidence at Seabrook, Tex*. U.S. Geological Survey, Reston, VA.

Gale WJ and Fabjanczyk MW 1993. Design approach to assess coal mine roadway stability and support requirements. *Eighth Australian Tunnelling Conference: Finding Common Ground*. Parkville, VIC. Australasian Institute of Mining and Metallurgy, Parkville, VIC, 1993, 153–159. https://doi.org/10.3316/informit.835476555816231

Galera JM, Alvarez M and Bieniawski ZT 2005. Evaluation of the deformation modulus of rock masses: comparison of pressuremeter and dilatometer tests with RMR prediction. *Proceedings of the ISP5-PRESSIO 2005 international symposium, Madrid, Spain*.

Galloway DL, Hudnut KW, Ingebritsen SE, Phillips SP, Peltzer G, Rogez F and Rosen PA 1998. Detection of aquifer system compaction and land subsidence using interferometric synthetic aperture radar, Antelope Valley, Mojave Desert, California. *Water Resources Research*, 34(10): 2573–2585. https://doi.org/10.1029/98WR01285

Galloway DL, Jones DR and Ingebritsen SE 1999. *Land subsidence in the United States* (Vol. 1182). U.S. Geological Survey.

Gambolati G 1974. Second-order theory of flow in three-dimensional deforming media. *Water Resources Research*, 10(6): 1217–1228.

Gambolati G and Freeze RA 1973. Mathematical simulation of the subsidence of Venice: 1. Theory. *Water Resources Research*, 9(3): 721–733. https://doi.org/10.1029/WR009i003p00721

Gambolati G and Teatini P 2015. Geomechanics of subsurface water withdrawal and injection. *Water Resources Research*, 51(6): 3922–3955. https://doi.org/10.1002/2014wr016841

Gambolati G, Teatini P, Baú D and Ferronato M 2000. Importance of poroelastic coupling in dynamically active aquifers of the Po river basin, Italy. *Water Resources Research*, 36(9): 2443–2459.

Gan H, Nandi SP and Walker PL 1972. Nature of the porosity in American coals. *Fuel*, 51(4): 272–277. https://doi.org/10.1016/0016-2361(72)90003-8

Garthwaite MC and Fuhrmann T 2020. *Subsidence monitoring in the Sydney Basin, New South Wales: results of the Camden Environmental Monitoring Project* (Record 2020/16).

Garthwaite MC, Hazelwood M, Nancarrow S, Hislop A and Dawson JH 2015. A regional geodetic network to monitor ground surface response to resource extraction in the northern Surat Basin, Queensland. *Australian Journal of Earth Sciences*, 62(4): 469–477. https://doi.org/10.1080/08120099.2015.1040073

GasFields Commission Queensland 2021. *Industry snapshot – shared landscapes.*

GasFields Commission Queensland 2022. *Regulatory review of coal seam gas-induced subsidence.*

GasFields Commission Queensland 2023. *Potential consequences of CSG-induced subsidence for farming operations on the Condamine alluvial floodplain.*

Gash BW 1991. Measurement of 'rock properties' in coal for coalbed methane production. *SPE Annual Technical Conference and Exhibition.*

Gazzola L, Ferronato M, Frigo M, Janna C, Teatini P, Zoccarato C, … Mantica S 2021. A novel methodological approach for land subsidence prediction through data assimilation techniques. *Computational Geosciences*, 25(5): 1731–1750. https://doi.org/10.1007/s10596-021-10062-1

Geertsma J 1973. Land subsidence above compacting oil and gas reservoirs. *Journal of Petroleum Technology*, 25(6): 734–744. https://doi.org/10.2118/3730-PA

Geological Survey of Queensland 2012. *Queensland's coal seam gas overview*. Department of Employment, Economic Development and Innovation. http://www.landtrakcorp.com/wp-content/uploads/2012/01/coal-seam-gas-2012-facts.pdf

Geoscience Australia 2021. *Australia's Energy Commodity Resources*. http://pid.geoscience.gov.au/dataset/ga/130098

Geoscience Australia 2022a. *InSAR processing over the Great Artesian Basin and analysis over the western Eromanga Basin and northern Surat Basin* (eCat 146986). https://ecat.ga.gov.au/geonetwork/srv/eng/catalog.search#/metadata/146986

Geoscience Australia 2022b. Positioning Australia. *Geoscience Australia.* https://www.ga.gov.au/scientific-topics/positioning-navigation/positioning-australia

Geoscience Australia 2022c. Station coordinates and maps. *Geoscience Australia.* https://www.ga.gov.au/scientific-topics/positioning-navigation/geodesy/gnss-networks/station-coordinates-and-maps

Golder Associates 2010. *Queensland Gas Company – assessment of subsidence due to coal seam gas extraction.*

Golding SD, Boreham CJ and Esterle JS 2013. Stable isotope geochemistry of coal bed and shale gas and related production waters: a review. *International Journal of Coal Geology*, 120: 24–40. https://doi.org/10.1016/j.coal.2013.09.001

Gonthier GJ 2007. *A graphical method for estimation of barometric efficiency from continuous data; concepts and application to a site in the Piedmont, Air Force Plant 6, Marietta, Georgia*. U.S. Geological Survey, Reston, VA.

Gray I, Zhao X, Liu L and Wood J 2019. *The Young's moduli, Poisson's ratios and poroeleastic coefficients of coals* (ACARP Project C26061).

Grigg KM and Katzenstein KW 2013. Using InSAR and groundwater pumping data to model land subsidence from coalbed methane production in the Powder River Basin, Wyoming. *125th Anniversary Annual Meeting and Expo*, Denver, Colorado, 27–30 October 2013.

Gu F and Chalaturnyk RJ 2006. Numerical simulation of stress and strain due to gas sorption/desorption and their effects on in situ permeability of coalbeds. *Journal of Canadian Petroleum Technology*, 45(10). https://doi.org/10.2118/06-10-05

Hamilton SK, Golding SD, Baublys KA and Esterle JS 2014. Stable isotopic and molecular composition of desorbed coal seam gases from the Walloon Subgroup, eastern Surat Basin, Australia. *International Journal of Coal Geology*, 122: 21–36. https://doi.org/10.1016/j.coal.2013.12.003

Hanson RT 1988. *Aquifer-system compaction, Tucson Basin and Avra Valley, Arizona*. U.S. Geological Survey, Reston, VA.

Hanssen RF 2001. *Radar interferometry: data interpretation and error analysis* (Vol. 2). Springer, Dordrecht. https://doi.org/10.1007/0-306-47633-9

Hatton TJ, Otto C and Underschultz J 2004. *Falling water levels in the Latrobe Aquifer, Gippsland Basin – determination of cause and recommendations for future work*.

Hayes P, Nicol C, La Croix AD, Pearce J, Gonzalez S, Wang J, … Gornall D 2020. Enhancing geological and hydrogeological understanding of the Precipice Sandstone aquifer of the Surat Basin, Great Artesian Basin, Australia, through model inversion of managed aquifer recharge datasets. *Hydrogeology Journal*, 28(1): 175–192. https://doi.org/10.1007/s10040-019-02079-9

Hebblewhite BK 2023. *Subsidence associated with underground coal mining: information guidelines explanatory note*. Independent Expert Scientific Committee on Unconventional Gas Development and Large Coal Mining Development.

Helm D 1984. *Latrobe Valley subsidence predictions: the modeling of time-dependent ground movement due to groundwater withdrawal*. Joint report of Fuel Department and Design Engineering and Environment Department. State Electricity Commission of Victoria, Melbourne.

Helm DC 1976. One-dimensional simulation of aquifer system compaction near Pixley, California: 2. Stress-dependent parameters. *Water Resources Research*, 12(3): 375–391. https://doi.org/10.1029/WR012i003p00375

Helm DC 1978. Field verification of a one-dimensional mathematical model for transient compaction and expansion of a confined aquifer system. *Proceedings of the 26th Hydraulics Division Speciality Conference on Verification of Mathematical and Physical Models in Hydraulic Engineering*.

Herckenrath D, Doherty J and Panday S 2015. Incorporating the effect of gas in modelling the impact of CBM extraction on regional groundwater systems. *Journal of Hydrology*, 523: 587–601. https://doi.org/10.1016/j.jhydrol.2015.02.012

Hernandez-Marin M and Burbey TJ 2010. Controls on initiation and propagation of pumping-induced earth fissures: insights from numerical simulations. *Hydrogeology Journal*, 18(8): 1773–1785.

Hernandez-Marin M and Burbey TJ 2012. Fault-controlled deformation and stress from pumping-induced groundwater flow. *Journal of Hydrology*, 428: 80–93.

Hettema M, Papamichos E and Schutjens P 2002. Subsidence delay: field observations and analysis. *Oil & Gas Science and Technology*, 57(5): 443–458. https://doi.org/10.2516/ogst:2002029

Hocking JB 1980. *Definition and revision of tertiary stratigraphic units, onshore Gippsland Basin* (Geological Survey of Victoria Report 1976/1).

Hoerning S and Rodger I 2021. Key properties are not well represented by means: spatial asymmetry in coal seam gas reservoir modelling. *SPE/AAPG/SEG Asia Pacific Unconventional Resources Technology Conference*.

Hofmann-Wellenhof B, Lichtenegger H and Wasle E 2008. More on GNSS. *GNSS – global navigation satellite systems: GPS, GLONASS, Galileo, and more*. Springer, Vienna, 397–430. https://doi.org/10.1007/978-3-211-73017-1_12

Holdgate GR and Clarke JDA 2000. A review of tertiary brown coal deposits in Australia: their depositional factors and eustatic correlations. *AAPG Bulletin*, 84(8): 1129–1151.

Holdgate GR, Wallace MW, Gallagher SJ, Smith AJ, Keene JB, Moore D and Shafik S 2003. Plio-Pleistocene tectonics and eustasy in the Gippsland Basin, southeast Australia: evidence from magnetic imagery and marine geological data. *Australian Journal of Earth Sciences*, 50(3): 403–426. https://doi.org/10.1046/j.1440-0952.2003.01004.x

Holzer TL 1984. Ground failure induced by ground-water withdrawal from unconsolidated sediment. *Man-induced land subsidence*, 67–105. https://doi.org/10.1130/REG6-p67

Hooper A, Zebker H, Segall P and Kampes B 2004. A new method for measuring deformation on volcanoes and other natural terrains using InSAR persistent scatterers. *Geophysical Research Letters*, 31(23). https://doi.org/10.1029/2004GL021737

Hsieh PA 1996. Deformation-induced changes in hydraulic head during ground-water withdrawal. *Groundwater*, 34(6): 1082–1089.

Hu J, Li ZW, Ding XL, Zhu JJ, Zhang L and Sun Q 2014. Resolving three-dimensional surface displacements from InSAR measurements: a review. *Earth-Science Reviews*, 133: 1–17. https://doi.org/10.1016/j.earscirev.2014.02.005

Huang Y, Yang Y and Li J 2015. Numerical simulation of artificial groundwater recharge for controlling land subsidence. *KSCE Journal of Civil Engineering*, 19(2): 418–426. https://doi.org/10.1007/s12205-015-0505-y

IESC 2024. *Information guidelines for proponents preparing coal seam gas and large coal mining development proposals*. https://www.iesc.gov.au/publications/information-guidelines-independent-expert-scientific-committee-advice-coal-seam-gas

Ingebritsen SE and Galloway DL 2014. Coastal subsidence and relative sea level rise. *Environmental Research Letters*, 9(9). https://doi.org/10.1088/1748-9326/9/9/091002

Jacobs 2016. *Ground motion modelling using OGIA 2016 modelling results* (4500251750).

Jahangir E, Deck O and Masrouri F 2012. Estimation of ground settlement beneath foundations due to shrinkage of clayey soils. *Canadian Geotechnical Journal*, 49(7): 835–852. https://doi.org/10.1139/T2012-042

Jahr T, Jentzsch G, Gebauer A and Lau T 2008. Deformation, seismicity, and fluids: results of the 2004/2005 water injection experiment at the KTB/Germany. *Journal of Geophysical Research: Solid Earth*, 113(B11).

Jensen J 2000. *Remote sensing of the environment: an earth resource perspective*. Prentice-Hall.

Johnson RL, Cheong S and Farley A 2021. Characterising the application of horizontal wells and indirect hydraulic fracturing for improved coal seam gas drainage. *The APPEA Journal*, 61(1): 89–105. https://doi.org/10.1071/AJ20122

Jolivet R, Grandin R, Lasserre C, Doin M-P and Peltzer G 2011. Systematic InSAR tropospheric phase delay corrections from global meteorological reanalysis data. *Geophysical Research Letters*, 38(17). https://doi.org/10.1029/2011GL048757

Jung H and Frigaard IA 2022. Evaluation of common cementing practices affecting primary cementing quality. *Journal of Petroleum Science and Engineering*, 208, 109622. https://doi.org/10.1016/j.petrol.2021.109622

Kaplan ED 2017. Introduction. In Kaplan ED and Hegarty CJ (eds) *Understanding GPS/GNSS – principles and applications*. 3rd edition. Artech House, 1–18. https://app.knovel.com/hotlink/pdf/id:kt011M7GS2/understanding-gps-gnss/introduction

Kasmarek MC 2012. *Hydrogeology and simulation of groundwater flow and land-surface subsidence in the northern part of the Gulf Coast aquifer system, Texas, 1891–2009*. U.S. Geological Survey, Reston, VA.

Kasmarek MCR and James L 2004. *Hydrogeology and simulation of ground-water flow and land-surface subsidence in the northern part of the Gulf Coast aquifer system, Texas*. U.S. Geological Survey, Reston, VA.

Knutson TR, McBride JL, Chan J, Emanuel K, Holland G, Landsea C, … Sugi M 2010. Tropical cyclones and climate change. *Nature Geoscience*, 3(3): 157–163. https://doi.org/10.1038/ngeo779

Kolker AS, Allison MA and Hameed S 2011. An evaluation of subsidence rates and sea-level variability in the northern Gulf of Mexico. *Geophysical Research Letters*, 38(21). https://doi.org/10.1029/2011GL049458

Langmuir I 1916. The constitution and fundamental properties of solids and liquids. Part I. Solids. *Journal of the American Chemical Society*, 38(11): 2221–2295. https://doi.org/10.1021/ja02268a002

Larsen JW 2004. The effects of dissolved CO2 on coal structure and properties. *International Journal of Coal Geology*, 57(1): 63–70. https://doi.org/10.1016/j.coal.2003.08.001

Laubach SE, Marrett RA, Olson JE and Scott AR 1998. Characteristics and origins of coal cleat: a review. *International Journal of Coal Geology*, 35(1): 175–207. https://doi.org/10.1016/S0166-5162(97)00012-8

Lawrie S 2012. *Use of interferometric synthetic aperture radar (InSAR) to detect strain accumulation on the Sorong fault zone, West Papua, Indonesia*. Honours thesis, Australian National University.

Leonardi CR, Flottmann T, Pandey VJ and Johnson RJ 2019. Quantifying the influence of three dimensionality on hydraulic fracturing in coal seam gas wells. *SPE/AAPG/SEG Asia Pacific Unconventional Resources Technology Conference*.

Leonardi CR, Hurter S, Chen Z and Underschultz J 2017. *Surface movement and shallow processes*. Report Reference: 149345.

Lewis R and Schrefler B 1978. A fully coupled consolidation model of the subsidence of Venice. *Water Resources Research*, 14(2): 223–230.

Li C, Wang Z, Shi L and Feng R 2017. Analysis of analytical models developed under the uniaxial strain condition for predicting coal permeability during primary depletion. *Energies*, 10(11): 1849. https://www.mdpi.com/1996-1073/10/11/1849

Lin X, Sutherland G, Cumming D, Thomas B and Sani A 2018. Increasing coal seam gas field productivity with horizontal well technology: a case study. *SPE Asia Pacific Oil and Gas Conference and Exhibition*.

Ling HI, Smyth A and Betti R 2009. *Poromechanics IV*. DEStech Publications, Inc.

Liu J, Fokker PA and Spiers CJ 2017. Coupling of swelling, internal stress evolution, and diffusion in coal matrix material during exposure to methane. *Journal of Geophysical Research: Solid Earth*, 122(2): 844–865. https://doi.org/10.1002/2016JB013322

Liu S, Wang Y and Harpalani S 2016. Anisotropy characteristics of coal shrinkage/swelling and its impact on coal permeability evolution with CO2 injection. *Greenhouse Gases: Science and Technology*, 6(5): 615–632. https://doi.org/10.1002/ghg.1592

Liu Y and Helm DC 2008a. Inverse procedure for calibrating parameters that control land subsidence caused by subsurface fluid withdrawal: 1. Methods. *Water Resources Research*, 44(7).

Liu Y and Helm DC 2008b. Inverse procedure for calibrating parameters that control land subsidence caused by subsurface fluid withdrawal: 2. Field application. *Water Resources Research*, 44(7).

Mahoney SA, Rufford TE, Dmyterko AS, Rudolph V and Steel KM 2015. The effect of rank and lithotype on coal wettability and its application to coal relative permeability models. *SPE Asia Pacific Unconventional Resources Conference and Exhibition*.

Mares TE, Radliński AP, Moore TA, Cookson D, Thiyagarajan P, Ilavsky J and Klepp J 2009. Assessing the potential for CO2 adsorption in a subbituminous coal, Huntly Coalfield, New Zealand, using small angle scattering techniques. *International Journal of Coal Geology*, 77(1): 54–68. https://doi.org/10.1016/j.coal.2008.07.007

Masoudian MS 2016. Multiphysics of carbon dioxide sequestration in coalbeds: a review with a focus on geomechanical characteristics of coal. *Journal of Rock Mechanics and Geotechnical Engineering*, 8(1): 93–112. https://doi.org/10.1016/j.jrmge.2015.08.002

Masoudian MS, Airey DW and El-Zein A 2016. The role of coal seam properties on coupled processes during CO2 sequestration: a parametric study. *Greenhouse Gases: Science and Technology*, 6(4): 492–518. https://doi.org/10.1002/ghg.1575

Masoudian MS, Leonardi C, Chen Z and Underschultz J 2019a. The effect of sorption-induced shrinkage on the ground surface movement above gas-producing coalbeds. *53rd U.S. Rock Mechanics/Geomechanics Symposium*.

Masoudian MS, Leonardi C, Chen Z and Underschultz J 2019b. Towards the development of a baseline for surface movement in the Surat Cumulative Management Area. *The APPEA Journal*, 59(1): 95–114. https://doi.org/10.1071/AJ18181

Massarotto P, Rudolph V and Golding SD 2003. Anisotropic permeability characterisation of Permian coals. *International Coalbed Methane Symposium*, Alabama, USA, 7–8 May 2003.

Mastalerz M and Drobniak A 2020. 5 – Coalbed methane: reserves, production, and future outlook. In Letcher TM (ed.) *Future energy*. 3rd edition. Elsevier, 97–109. https://doi.org/10.1016/B978-0-08-102886-5.00005-0

Mastro P, Serio C, Masiello G and Pepe A 2020. The multiple aperture SAR interferometry (MAI) technique for the detection of large ground displacement dynamics: an overview. *Remote Sensing*, 12(7): 1189. https://www.mdpi.com/2072-4292/12/7/1189

Mathias SA, Nielsen S and Ward RL 2019. Storage coefficients and permeability functions for coal-bed methane production under uniaxial strain conditions. *Transport in Porous Media*, 130(2): 627–636. https://doi.org/10.1007/s11242-019-01331-w

Mavor MJ, Hartman C and Pratt TJ 2004. Uncertainty in sorption isotherm measurements. *2004 International Coalbed Methane Symposium*, University of Alabama, Tuscaloosa, Alabama.

Mayuga M and Allen D 1969. Subsidence in the Wilmington Oil Field, Long Beach, California, USA. *Proceedings of Tokyo Symposium on Land Subsidence.*

Mayuga MN 1970. Geology and development of California's Giant–Wilmington Oil Field. In MT Halbouty (ed.) *Geology of giant petroleum fields* (Vol. 14). American Association of Petroleum Geologists. https://doi.org/10.1306/M14368C7

Mayuga MN and Allen DR 1970. Subsidence in the Wilmington Oil Field, Long Beach, California, USA. In Tison LJ (ed.) *Land subsidence.* International Association of Scientific Hydrology, UNESCO, 66–79.

McClure JE, Berg S and Armstrong RT 2021. Capillary fluctuations and energy dynamics for flow in porous media. *Physics of Fluids*, 33(8): 083323. https://doi.org/10.1063/5.0057428

McIntyre DS, Watson CL and Loveday J 1982. Swelling of a clay soil profile under ponding. *Australian Journal of Soil Research*, 20(2): 71–79.

McKee CR and Bumb AC 1987. Flow-testing coalbed methane production wells in the presence of water and gas. *SPE Formation Evaluation*, 2(04): 599–608. https://doi.org/10.2118/14447-pa

McManamon P 2019. *LiDAR technologies and systems*. SPIE. https://app.knovel.com/hotlink/pdf/id:kt012EEJ02/lidar-technologies-systems/title-page

McMillan TC, Rau GC, Timms WA and Andersen MS 2019. Utilizing the impact of earth and atmospheric tides on groundwater systems: a review reveals the future potential. *Reviews of Geophysics*, 57(2): 281–315. https://doi.org/10.1029/2018RG000630

Merritt ML 2004. *Estimating hydraulic properties of the Floridan aquifer system by analysis of Earth-tide, ocean-tide, and barometric effects, Collier and Hendry Counties, Florida.* U.S. Geological Survey, Reston, VA.

Michael K, Bunch M and Varma S 2013. Simulation of the cumulative impacts of CO2 geological storage and petroleum production on aquifer pressures in the offshore Gippsland Basin. *International Journal of Greenhouse Gas Control*, 19(Supplement C): 310–321. https://doi.org/10.1016/j.ijggc.2013.09.009

MIT Energy Initiative 2011. *The future of natural gas – an interdisciplinary MIT study*.

Moore TA 2012. Coalbed methane: a review. *International Journal of Coal Geology*, 101: 36–81. https://doi.org/10.1016/j.coal.2012.05.011

Moreira A, Prats-Iraola P, Younis M, Krieger G, Hajnsek I and Papathanassiou KP 2013. A tutorial on synthetic aperture radar. *IEEE Geoscience and Remote Sensing Magazine*, 1(1): 6–43.

Müller N 2011. Supercritical CO2-brine relative permeability experiments in reservoir rocks—literature review and recommendations. *Transport in Porous Media*, 87(2): 367–383. https://doi.org/10.1007/s11242-010-9689-2

Muntendam-Bos AG, Kroon IC and Fokker PA 2008. Time-dependent inversion of surface subsidence due to dynamic reservoir compaction. *Mathematical Geosciences*, 40(2): 159–177. https://doi.org/10.1007/s11004-007-9135-3

Nagel NB 2001. Compaction and subsidence issues within the petroleum industry: from Wilmington to Ekofisk and beyond. *Physics and Chemistry of the Earth, Part A: Solid Earth and Geodesy*, 26(1): 3–14. https://doi.org/10.1016/S1464-1895(01)00015-1

Ng AH-M, Ge L and Li X 2015. Assessments of land subsidence in the Gippsland Basin of Australia using ALOS PALSAR data. *Remote Sensing of Environment*, 159(Supplement C): 86–101. https://doi.org/10.1016/j.rse.2014.12.003

Ng AH-M, Ge L, Li X, Abidin HZ, Andreas H and Zhang K 2012. Mapping land subsidence in Jakarta, Indonesia using persistent scatterer interferometry (PSI) technique with ALOS PALSAR. *International Journal of Applied Earth Observation and Geoinformation*, 18: 232–242. https://doi.org/10.1016/j.jag.2012.01.018

Nicot J-P and Scanlon BR 2012. Water use for shale-gas production in Texas, U.S. *Environmental Science & Technology*, 46(6): 3580–3586. https://doi.org/10.1021/es204602t

Nowamooz H 2014. Effective stress concept on multi-scale swelling soils. *Applied Clay Science*, 101: 205–214. https://doi.org/10.1016/j.clay.2014.07.036

OGIA 2016a. *Hydrogeological conceptualisation report for the Surat Cumulative Management Area.*

OGIA 2016b. *Underground Water Impact Report for the Surat Cumulative Management Area.*

OGIA. (2019. *Underground Water Impact Report for the Surat Cumulative Management Area.*

OGIA 2021. *Underground Water Impact Report for the Surat Cumulative Management Area.*

Ortiz-Zamora D and Ortega-Guerrero A 2010. Evolution of long-term land subsidence near Mexico City: review, field investigations, and predictive simulations. *Water Resources Research*, 46(1). https://doi.org/10.1029/2008WR007398

Osmanoğlu B, Sunar F, Wdowinski S and Cabral-Cano E 2016. Time series analysis of InSAR data: methods and trends. *ISPRS Journal of Photogrammetry and Remote Sensing*, 115: 90–102. https://doi.org/10.1016/j.isprsjprs.2015.10.003

Otott GE and Clarke DD 1996. *History of the Wilmington Field: 1986–1996*.

Ozawa T and Ueda H 2011. Advanced interferometric synthetic aperture radar (InSAR) time series analysis using interferograms of multiple-orbit tracks: a case study on Miyake-jima. *Journal of Geophysical Research: Solid Earth*, 116(B12). https://doi.org/10.1029/2011JB008489

Palmer I 2009. Permeability changes in coal: analytical modeling. *International Journal of Coal Geology*, 77(1): 119–126. https://doi.org/10.1016/j.coal.2008.09.006

Palmer I and Mansoori J 1998. How permeability depends on stress and pore pressure in coalbeds: a new model. *SPE Reservoir Evaluation & Engineering*, 1(06): 539–544. https://doi.org/10.2118/52607-pa

Pan Z and Connell LD 2011. Modelling of anisotropic coal swelling and its impact on permeability behaviour for primary and enhanced coalbed methane recovery. *International Journal of Coal Geology*, 85(3): 257–267. https://doi.org/10.1016/j.coal.2010.12.003

Pandey VJ, Flottman T and Zwarich NR 2017. Applications of geomechanics to hydraulic fracturing: case studies from coal stimulations. *SPE Production & Operations*, 32(04): 404–422. https://doi.org/10.2118/173378-pa

Parker AL, Pigois JP, Filmer MS, Featherstone WE, Timms NE and Penna NT 2021. Land uplift linked to managed aquifer recharge in the Perth Basin, Australia. *International Journal of Applied Earth Observation and Geoinformation*, 105: 102637. https://doi.org/10.1016/j.jag.2021.102637

Pepe A and Calò F 2017. A review of interferometric synthetic aperture RADAR (InSAR) multi-track approaches for the retrieval of Earth's surface displacements. *Applied Sciences*, 7(12): 1264. https://www.mdpi.com/2076-3417/7/12/1264

Pineda JA and Sheng D 2013. *Subsidence – an overview of causes, risks and future developments for coal seam gas production.* Report submitted to the Office of the NSW Chief Scientist and Engineer as part of the Review of Coal Seam Gas Activities in NSW.

Poland JF 1984. *Guidebook to studies of land subsidence due to ground-water withdrawal* (Vol. 40). UNESCO, Paris.

Pope JP and Burbey TJ 2003. Characterization and modeling of land subsidence due to groundwater withdrawals from the confined aquifers of the Virginia Coastal Plain. In Prince KR and Galloway DL (eds) U.S. Geological Survey Subsidence Interest Group Conference, *Proceedings of the Technical Meeting, Galveston, Texas, November 27–29, 2001.*

Pope JP and Burbey T J 2004. Multiple-aquifer characterization from single borehole extensometer records. *Groundwater*, 42(1): 45–58.

Pratt WE and Johnson DW 1926. Local subsidence of the Goose Creek Oil Field. *The Journal of Geology*, 34(7): 577–590. http://www.jstor.org/stable/30056838

Prokopovich NP 1986. Classification of land subsidence by origin. *Land subsidence: Proceedings of the Third International Symposium on Land Subsidence held in Venice, Italy, 19–25 March 1984*, 281–290.

Purcell J 2012. Developing a surface irrigation system. In Wiggington D (ed) *WATERpak – a guide for irrigation management in cotton and grain farming systems*. 3rd edition. Cotton Research and Development Corporation.

Queensland Building and Construction Commission 2022. *A guide to preventing structural damage*. https://www.qbcc.qld.gov.au/sites/default/files/2021-10/guide-preventing-structural-damage.pdf

Radlinski AP, Mastalerz M, Hinde AL, Hainbuchner M, Rauch H, Baron M, … Thiyagarajan P 2004. Application of SAXS and SANS in evaluation of porosity, pore size distribution and surface area of coal. *International Journal of Coal Geology*, 59(3): 245–271. https://doi.org/10.1016/j.coal.2004.03.002

Rai UB and Hummel ND 2019. *Prediction of compaction and subsidence due to gas production from coal seams in the Surat Basin, Australia (report prepared for QGC Shell)*. Report Reference: SR.19.00168.

Rajora A, Sharma V, Oberhardt M, Lukyanov M, Lim E and Mazumder S 2019. Deviated pad wells in Surat: journey so far. *SPE/AAPG/SEG Asia Pacific Unconventional Resources Technology Conference*.

Rau GC, McMillan TC, Andersen MS and Timms WA 2022. In situ estimation of subsurface hydro-geomechanical properties using the groundwater response to semi-diurnal Earth and atmospheric tides. *Hydrology and Earth System Sciences*, 26(16): 4301–4321. https://doi.org/10.5194/hess-26-4301-2022

Reeves JA, Knight R, Zebker HA, Kitanidis PK and Schreüder WA 2014. Estimating temporal changes in hydraulic head using InSAR data in the San Luis Valley, Colorado. *Water Resources Research*, 50(5): 4459–4473. https://doi.org/10.1002/2013WR014938

Richards LA 1931. Capillary conduction of liquids through porous mediums. *Physics*, 1(5): 318–333. https://doi.org/10.1063/1.1745010

Roberts R 1992. *Silver Springs/Renlim Field – Australia, Bowen Basin, Queensland. AAPG treatise of petroleum geology – atlas of oil and gas fields*. 219–236. https://www.scopus.com/inward/record.uri?eid=2-s2.0-84961718730&partnerID=40&md5=dfb74b550c63829cd5d72536b0857a3b

Robertson EP and Christiansen RL 2008. A permeability model for coal and other fractured, sorptive-elastic media. *SPE Journal*, 13(03): 314–324. https://doi.org/10.2118/104380-pa

Roscoe KH and Burland J 1968. *On the generalized stress-strain behaviour of wet clay*.

Ross J and Jeffrey L 1991. *Ground subsidence and bore collapse associated with groundwater withdrawals – Namoi Valley, NSW*.

Sadek S, Ghanimeh S and El-Fadel M 2007. Predicted performance of clay-barrier landfill covers in arid and semi-arid environments. *Waste Management*, 27(4): 572–583. https://doi.org/10.1016/j.wasman.2006.06.008

Safai NM and Pinder GF 1979. Vertical and horizontal land deformation in a desaturating porous medium. *Advances in Water Resources*, 2: 19–25.

Safai NM and Pinder GF 1980. Vertical and horizontal land deformation due to fluid withdrawal. International *Journal for Numerical and Analytical Methods in Geomechanics*, 4(2): 131–142.

Saghafi A, Faiz M and Roberts D 2007. CO2 storage and gas diffusivity properties of coals from Sydney Basin, Australia. *International Journal of Coal Geology*, 70(1): 240–254. https://doi.org/10.1016/j.coal.2006.03.006

Sandhu RS 1979. Modeling land subsidence. In Saxena SK (ed.) *Evaluation and prediction of subsidence*. ASCE, 565–579.

Santos 2013. *Santos GLNG Project – CSG water monitoring and management plan – Summary plan Stage 2* (Revision 2).

Saurabh S and Harpalani S 2019. Anisotropy of coal at various scales and its variation with sorption. International *Journal of Coal Geology*, 201: 14–25. https://doi.org/10.1016/j.coal.2018.11.008

Schlumberger Reservoir Laboratories 2017. *Geomechanics characterization of selected core material (prepared for Origin Energy)*. Report Reference: 16-015.

Schoonbeek JB 1976. *Land subsidence as a result of natural gas extraction in the province of Groningen*. SPE European Spring Meeting. https://doi.org/10.2118/5751-MS

Schultz H, Hayes P, McIntyre N and Miraldo-Ordens C 2021. *Resetting our understanding of the Surat Part of the Great Artesian Basin*. University of Queensland, Brisbane.

Seidle JP, Jeansonne MW and Erickson DJ 1992. Application of matchstick geometry to stress dependent permeability in coals. *SPE Rocky Mountain Regional Meeting*.

Şenel İG, Gürüz AG, Yücel H, Kandas AW and Sarofim AF 2001. Characterization of pore structure of Turkish coals. *Energy & Fuels*, 15(2): 331–338. https://doi.org/10.1021/ef000081k

Shaw D, Mostaghimi P and Armstrong RT 2019. The dynamic behaviour of coal relative permeability curves. *Fuel*, 253, 293–304. https://doi.org/10.1016/j.fuel.2019.04.107

Shi J-Q and Durucan S 2005. A model for changes in coalbed permeability during primary and enhanced methane recovery. *SPE Reservoir Evaluation & Engineering*, 8(04): 291–299. https://doi.org/10.2118/87230-pa

Shi J-Q, Pan Z and Durucan S 2014. Analytical models for coal permeability changes during coalbed methane recovery: model comparison and performance evaluation. *International Journal of Coal Geology*, 136, 17–24. https://doi.org/10.1016/j.coal.2014.10.004

Shi JQ and Durucan S 2004. Drawdown induced changes in permeability of coalbeds: a new interpretation of the reservoir response to primary recovery. *Transport in Porous Media*, 56(1): 1–16. https://doi.org/10.1023/B:TIPM.0000018398.19928.5a

Smerdon BD and Ransley TR 2012. *Water resource assessment for the Surat region. A report to the Australian Government from the CSIRO Great Artesian Basin Water Resource Assessment*.

Smith DJ 1988. Project management of subsidence and Ekofisk jacking project. *Offshore Technology Conference*, Houston, Texas, May 1988. https://doi.org/10.4043/5655-MS

Sobczak K, Holl H-G and Garnett A 2021. Estimating porosity and permeability in the Springbok Sandstone, Surat Basin (Queensland), using new wireline log-based workflow. *The APPEA Journal*, 61(2): 720–725. https://doi.org/10.1071/AJ20201

Somerton WH, Söylemezoğlu IM and Dudley RC 1975. Effect of stress on permeability of coal. *International Journal of Rock Mechanics and Mining Sciences & Geomechanics Abstracts*, 12(5): 129–145. https://doi.org/10.1016/0148-9062(75)91244-9

Sparks DP, McLendon TH, Saulsberry JL and Lambert SW 1995. The effects of stress on coalbed reservoir performance, Black Warrior Basin U.S.A. *SPE Annual Technical Conference and Exhibition*, Dallas, Texas.

Standards Australia 2011. *AS 2870 Residential slabs and footings*.

Sulak RM, Thomas LK and Boade RR 1991. 3D reservoir simulation of Ekofisk compaction drive (includes associated papers 24317 and 24400). *Journal of Petroleum Technology*, 43(10): 1272–1278. https://doi.org/10.2118/19802-PA

Sun C, McClure JE, Mostaghimi P, Herring AL, Berg S and Armstrong RT 2020a. Probing effective wetting in subsurface systems. *Geophysical Research Letters*, 47(5): e2019GL086151. https://doi.org/10.1029/2019GL086151

Sun C, McClure JE, Mostaghimi P, Herring AL, Shabaninejad M, Berg S and Armstrong RT 2020b. Linking continuum-scale state of wetting to pore-scale contact angles in porous media. *Journal of Colloid and Interface Science*, 561: 173–180. https://doi.org/10.1016/j.jcis.2019.11.105

Taigbenu AE 1999. Unsaturated flow (Richards equation). *The Green Element Method*. Springer, New York. https://doi.org/10.1007/978-1-4757-6738-4_8

Teatini P, Gambolati G, Ferronato M, Settari AT and Walters D 2011. Land uplift due to subsurface fluid injection. *Journal of Geodynamics*, 51(1): 1–16.

Teatini P, Tosi L and Strozzi T 2012. Comment on "Recent subsidence of the Venice Lagoon from continuous GPS and interferometric synthetic aperture radar" by Y. Bock, S. Wdowinski, A. Ferretti, F. Novali, and A. Fumagalli. *Geochemistry, Geophysics, Geosystems*, 13(7). https://doi.org/10.1029/2012GC004191

Tenthorey E, Vidal-Gilbert S, Backé G, Puspitasari R, Pallikathekathil ZJ, Maney B and Dewhurst D 2013. Modelling the geomechanics of gas storage: a case study from the Iona gas field, Australia. *International Journal of Greenhouse Gas Control*, 13: 138–148.

Thakur P, Schatzel SJ, Aminian K, Rodvelt G, Mosser MH and D'Amico JS (eds) 2020. *Coal bed methane: theory and applications*. 2nd edition. Elsevier. https://doi.org/10.1016/C2017-0-02178-X

Thompson BR and Walker GM 1982. Coal resources – origin and utilisation in Australia – the geology of the Seaspray Depression: Gippsland Basin. Coal Group, *Geological Society of Australia Symposium*, Melbourne, 15–19 November.

TNO 2021. *Reservoir pressure and subsidence – Groningen field update for production profile GTS*. https://www.rvo.nl/sites/default/files/2021/04/Appendix-A-Pressure-and-Subsidence-March-GTS-raming-2021.pdf

Tomás R, Romero R, Mulas J, Marturià JJ, Mallorquí JJ, Lopez-Sanchez JM., … Blanco P 2014. Radar interferometry techniques for the study of ground subsidence phenomena: a review of practical issues through cases in Spain. *Environmental Earth Sciences*, 71(1): 163–181. https://doi.org/10.1007/s12665-013-2422-z

Tosi L, Teatini P, Carbognin L and Brancolini G 2009. Using high resolution data to reveal depth-dependent mechanisms that drive land subsidence: the Venice coast, Italy. *Tectonophysics*, 474(1-2): 271–284. https://doi.org/10.1016/j.tecto.2009.02.026

Towler B, Firouzi M, Underschultz J, Rifkin W, Garnett A, Schultz H, … Witt K 2016. An overview of the coal seam gas developments in Queensland. *Journal of Natural Gas Science and Engineering*, 31: 249–271. https://doi.org/10.1016/j.jngse.2016.02.040

Ulaby F and Long D 2014. *Microwave radar and radiometric remote sensing*. University of Michigan Press.

Underschultz JR, Vink S and Garnett A 2018. Coal seam gas associated water production in Queensland: actual vs predicted. *Journal of Natural Gas Science and Engineering*, 52: 410–422. https://doi.org/10.1016/j.jngse.2018.02.010

van der Kamp G 2001. Methods for determining the in situ hydraulic conductivity of shallow aquitards – an overview. *Hydrogeology Journal*, 9(1): 5–16. https://doi.org/10.1007/s100400000118

van Elk J, Doornhof D, Bommer JJ, Bourne SJ, Oates SJ, Pinho R and Crowley H 2017. Hazard and risk assessments for induced seismicity in Groningen. *Netherlands Journal of Geosciences*, 96(5): s259–s269. https://doi.org/10.1017/njg.2017.37

van Genuchten MT 1980. A closed-form equation for predicting the hydraulic conductivity of unsaturated soils. *Soil Science Society of America Journal*, 44(5): 892–898. https://doi.org/10.2136/sssaj1980.03615995004400050002x

Walker GR and Mallants D 2014. *Methodologies for investigating gas in water bores and links to coal seam gas development*. CSIRO.

Wang K, Zang J, Wang G and Zhou A 2014. Anisotropic permeability evolution of coal with effective stress variation and gas sorption: model development and analysis. *International Journal of Coal Geology*, 130: 53–65. https://doi.org/10.1016/j.coal.2014.05.006

Webb SW 2006. Two-phase gas transport. In Ho CK and Webb SW (eds) *Gas transport in porous media*. Springer, Dordrecht, 55–70. https://doi.org/10.1007/1-4020-3962-x_5

Wegmüller U and Werner C 1997. Gamma SAR processor and interferometry software. *3rd ERS Symposium*, Florence, Italy, 14–21 March. https://earth.esa.int/eogateway/events/the-3rd-ers-symposium

Wei Y-n., Fan W and Cao Y 2017. Experimental study on the vertical deformation of aquifer soils under conditions of withdrawing and recharging of groundwater in Tongchuan region, China. *Hydrogeology Journal*, 25(2): 297–309. https://doi.org/10.1007/s10040-016-1498-4

Werner C, Wegmuller U, Strozzi T and Wiesmann A 2003. Interferometric point target analysis for deformation mapping. IGARSS 2003. *2003 IEEE International Geoscience and Remote Sensing Symposium: Proceedings* (IEEE Cat. No. 03CH37477).

Wolff RG 1970. Relationship between horizontal strain near a well and reverse water level fluctuation. *Water Resources Research*, 6(6): 1721–1728.

Woodhouse I 2006. *Introduction to microwave remote sensing*. CRC Press.

Wright TJ, Parsons BE and Lu Z 2004. Toward mapping surface deformation in three dimensions using InSAR. *Geophysical Research Letters*, 31(1). https://doi.org/10.1029/2003GL018827

Wu G, Jia S and Wu B 2019. Comparison of a novel coupled hydro-mechanical model with typical analytical models in subsidence of coal seam gas extraction. *International Journal of Oil, Gas and Coal Technology*, 22(2): 246–268. https://doi.org/10.1504/ijogct.2019.102783

Wu G, Jia S, Wu B and Yang D 2018. A discussion on analytical and numerical modelling of the land subsidence induced by coal seam gas extraction. *Environmental Earth Sciences*, 77(9): 353. https://doi.org/10.1007/s12665-018-7526-z

Xue F, Lv X, Dou F and Yun Y 2020. A review of time-series interferometric SAR techniques: a tutorial for surface deformation analysis. *IEEE Geoscience and Remote Sensing Magazine*, 8(1): 22–42. https://doi.org/10.1109/MGRS.2019.2956165

Yao Y, Liu D, Tang D, Tang S and Huang W 2008. Fractal characterization of adsorption-pores of coals from North China: an investigation on CH_4 adsorption capacity of coals. *International Journal of Coal Geology*, 73(1): 27–42. https://doi.org/10.1016/j.coal.2007.07.003

Yeh A and O'Sullivan M 2007. Modelling subsidence in geothermal fields. *Proceedings 29th New Zealand Geothermal Workshop*.

Yesiller N, Miller CJ, Inci G and Yaldo K 2000. Desiccation and cracking behavior of three compacted landfill liner soils. Engineering Geology, 57(1): 105–121. https://doi.org/10.1016/S0013-7952(00)00022-3

Zang A, Oye V, Jousset P, Deichmann N, Gritto R, McGarr A, … Bruhn D 2014. Analysis of induced seismicity in geothermal reservoirs – an overview. *Geothermics*, 52: 6–21. https://doi.org/10.1016/j.geothermics.2014.06.005

Zang J, Wang K and Zhao Y 2015. Evaluation of gas sorption-induced internal swelling in coal. *Fuel*, 143: 165–172. https://doi.org/10.1016/j.fuel.2014.11.007

Zare Reisabadi M, Haghighi M, Salmachi A, Sayyafzadeh M and Khaksar A 2020. Analytical modelling of coal failure in coal seam gas reservoirs in different stress regimes. *International Journal of Rock Mechanics and Mining Sciences*, 128: 104259. https://doi.org/10.1016/j.ijrmms.2020.104259

Zeng Q and Wang Z 2017. A new cleat volume compressibility determination method and corresponding modification to coal permeability model. *Transport in Porous Media*, 119(3): 689–706. https://doi.org/10.1007/s11242-017-0906-0

Zhang J, Feng Q, Zhang X, Wen S and Zhai Y 2015. Relative permeability of coal: a review. *Transport in Porous Media*, 106(3): 563–594. https://doi.org/10.1007/s11242-014-0414-4

Zhang J, Zhang B, Xu S, Feng Q, Zhang X and Elsworth D 2021. Interpretation of gas/water relative permeability of coal using the hybrid Bayesian-assisted history matching: new insights. *Energies*, 14(3): 626. https://www.mdpi.com/1996-1073/14/3/626

Zhong R, Mitchell T, Johnson R and Leonardi C 2022. Efficient implicit methods for wellbore shear failure analysis during drilling and production in coalbeds. *International Journal of Rock Mechanics and Mining Sciences*, 155: 105129. https://doi.org/10.1016/j.ijrmms.2022.105129

Zhou X, Chang N-B and Li S 2009. Applications of SAR interferometry in earth and environmental science research. *Sensors*, 9(3): 1876–1912. https://www.mdpi.com/1424-8220/9/3/1876

Zimmerman RW 2017. Pore volume and porosity changes under uniaxial strain conditions. *Transport in Porous Media*, 119(2): 481–498. https://doi.org/10.1007/s11242-017-0894-0

Zoback MD 2007. *Reservoir geomechanics*. Cambridge University Press. https://doi.org/10.1017/CBO9780511586477

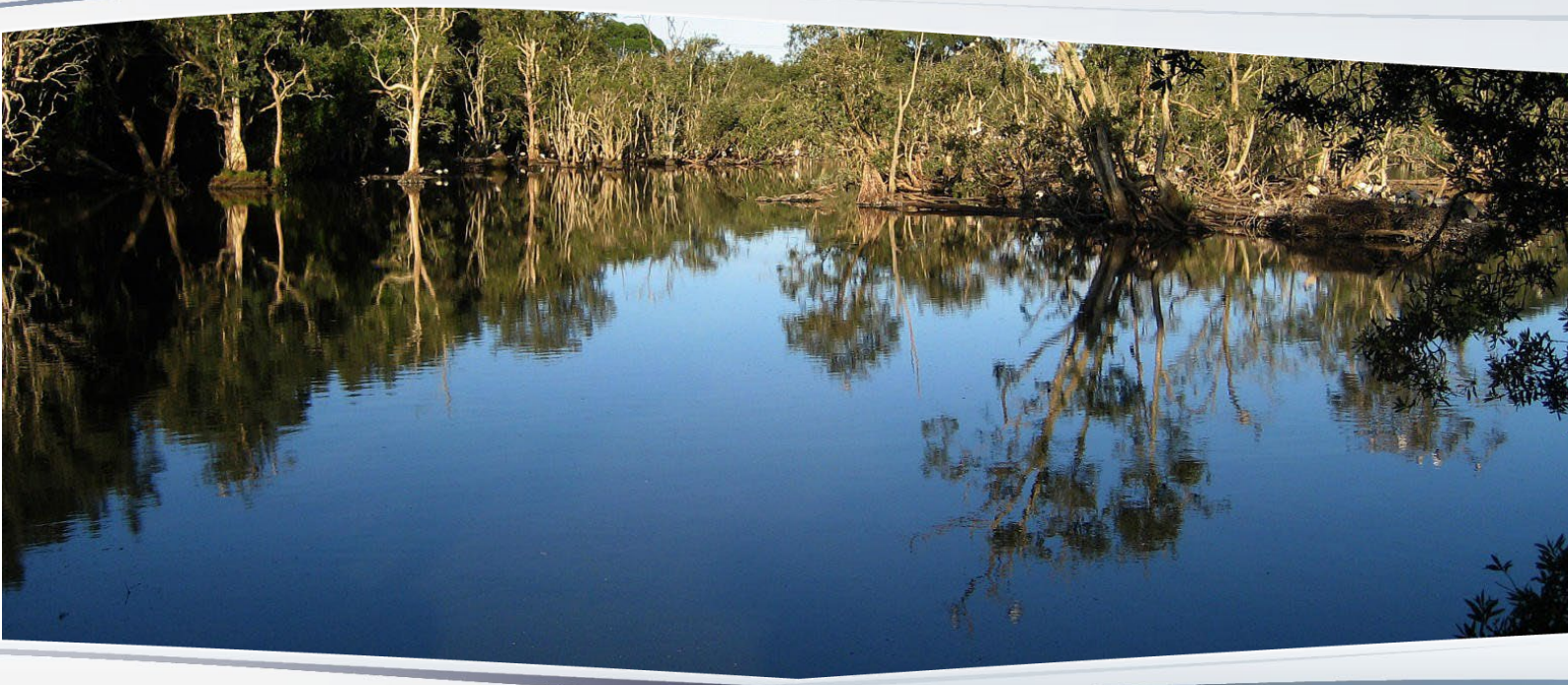

Australian Government | This initiative is funded by the Australian Government